



Lawrence Berkeley Laboratory

UNIVERSITY OF CALIFORNIA

EARTH SCIENCES DIVISION

RECEIVED
LAWRENCE
BERKELEY LABORATORY

NOV 18 1988

LIBRARY AND
DOCUMENTS SECTION

**Geotechnical Support and Topical Studies for
Nuclear Waste Geologic Repositories:
Annual Report, Fiscal Year 1987**

January 1988



LBL-24758
c.2

DISCLAIMER

This document was prepared as an account of work sponsored by the United States Government. While this document is believed to contain correct information, neither the United States Government nor any agency thereof, nor the Regents of the University of California, nor any of their employees, makes any warranty, express or implied, or assumes any legal responsibility for the accuracy, completeness, or usefulness of any information, apparatus, product, or process disclosed, or represents that its use would not infringe privately owned rights. Reference herein to any specific commercial product, process, or service by its trade name, trademark, manufacturer, or otherwise, does not necessarily constitute or imply its endorsement, recommendation, or favoring by the United States Government or any agency thereof, or the Regents of the University of California. The views and opinions of authors expressed herein do not necessarily state or reflect those of the United States Government or any agency thereof or the Regents of the University of California.

**GEOTECHNICAL SUPPORT AND TOPICAL STUDIES
FOR NUCLEAR WASTE GEOLOGIC REPOSITORIES**

Annual Report, Fiscal Year 1987

**Earth Sciences Division
Lawrence Berkeley Laboratory
1 Cyclotron Road
Berkeley, California 94720**

Prepared for

**Engineering and Geotechnology Division
Office of Geologic Repositories
Office of Civilian Radioactive Waste Management
U.S. Department of Energy**

January 1988

This work was prepared for the U.S. Department of Energy under Contract No. DE-AC03-76SF00098.

Table of Contents

EXECUTIVE SUMMARY, <i>C.F. Tsang</i>	1
GEOSCIENCE TECHNICAL SUPPORT FOR NUCLEAR WASTE GEOLOGIC REPOSITORIES, <i>D.C. Mangold and C.F. Tsang</i>	8
FRACTURE STUDIES	
Geochemical and Geomechanical Investigations of Fractured, Heated Rock, <i>H.A. Wollenberg, L.R. Myer, S. Flexser, and J. Scheiner</i>	17
Fracture Stiffness and Aperture as a Function of Applied Stress, <i>D.L. Hopkins, L.R. Myer, and N.G.W. Cook</i>	37
Channeling Characteristics of Flow and Solute Transport through a Rough-Surfaced Fracture, <i>Y.W. Tsang, C.F. Tsang, F.V. Hale, L. Moreno, and I. Neretnieks</i>	52
Tracer Transport in Fractured Media—A Variable-Aperture Channel Approach, <i>Y.W. Tsang and C.F. Tsang</i>	61
A Scheme for Calculating Flow in Fractures Using Numerical Grid Generation in Three-Dimensional Domains of Complex Shapes, <i>J.C.S. Long, P.A. Witherspoon, and K. Muralidhar</i>	69
Studies Relating to the Stress Corrosion of Minerals in Radioactive Waste Repositories, <i>J.A. Apps and A. Meike</i>	76
Investigation of Seismic Imaging for Fracture Characterization, <i>E.L. Majer and T.V. McEvilly</i>	95
Wellbore Breakout and Applications, <i>Z. Zheng and N.G.W. Cook</i>	108
Deformation, Fracture and Failure around Single Underground Openings, <i>R.T. Ewy, N.G.W. Cook, and L.R. Myer</i>	126
Fracture Mechanics Applied to Faulting and Earthquake Rupture, <i>J.M. Kemeny and N.G.W. Cook</i>	137

Executive Summary

Chin-Fu Tsang

This multidisciplinary project was initiated in fiscal year 1986. It comprises two major interrelated tasks:

1. **Technical Assistance.** This part of the project includes: (a) reviewing the progress of the major projects in the DOE Office of Civilian Radioactive Waste Management (OCRWM) Program and advising the Engineering and Geotechnology Division on significant technical issues facing each project; (b) analyzing geotechnical data, reports, tests, surveys and plans for the different projects; (c) reviewing and commenting on major technical reports and other program documents such as Site Characterization Plans (SCP) and Study Plans; and (d) providing scientific and technical input at technical meetings.
2. **Topical Studies.** This activity comprises studies on scientific and technical topics, and issues of significance to in-situ testing, test analysis methods, and site characterization of nuclear waste geologic repositories. The subjects of study were selected based on discussions with DOE staff. One minor topic is a preliminary consideration and planning exercise for postclosure monitoring studies. The major task, with subtasks involving various geoscience disciplines, is a study of the mechanical, hydraulic, geophysical and geochemical properties of fractures in geologic rock masses.

Two important features of this project should be pointed out here. First, this project is multidisciplinary, involving LBL staff with expertise in a broad range of earth science disciplines. As seen from the list of LBL personnel below all major geoscience disciplines are represented. This group of scientists has many years of combined experience in the nuclear waste geologic isolation problem. Many times, the major issues and results presented to DOE have undergone multidisciplinary discussions and the scrutiny by the whole LBL team.

<i>Name</i>	<i>Principal Expertise</i>
Chalon L. Carnahan	Geochemistry
Steven Flexser	Geology
Harold A. Wollenberg	Geology
Neville G. W. Cook	Geomechanics
John Kemeny	Geomechanics
Larry R. Myer	Geomechanics
Ernest L. Majer	Geophysics
Thomas V. McEvilly	Geophysics
H. Frank Morrison	Geophysics
Iraj Javandel	Hydrogeology
Marcelo J. Lippmann	Hydrogeology
Chin-Fu Tsang	Hydrogeology
Paul A. Witherspoon	Hydrogeology

Second, both parts of the project, the technical assistance and the topical studies, are largely performed by the same personnel (with additional LBL staff participating in some of the topical studies). This ensures the participation of highly respected researchers working at the forefront of the state-of-the-art in

providing DOE with comments and results relevant to the geotechnical aspects of nuclear waste geologic repositories. Often, technical reviews influence the direction and emphasis of topical studies, and topical studies provide inputs to the reviews.

The present report lists the technical reviews and comments made during the fiscal year and summarizes the technical progress of the topical studies.

In the area of technical assistance, there were numerous activities detailed in the next section. These included 45 geotechnical support activities, including reviews of 25 SCP Chapters, 3 whole document SCP reviews, participation in 13 SCP Review Workshops, 4 reviews of dispositions of former comments; the hosting of a DOE program review and a DOE-sponsored workshop on hydrologic behavior of rock discontinuities; 12 trips to technical and planning meetings; reviews related to 2 Study Plans, review of 2 NRC Generic Technical Position (GTP) papers, review of 2 unsolicited proposals to DOE, 2 other kinds of reviews, and one instance of technical assistance by giving answers to technical questions. These activities are described in a Table in the following section entitled "Geoscience Technical Support for Nuclear Waste Geologic Repositories."

The project also included the consideration of postclosure monitoring studies. The objective of these studies was to give a preliminary evaluation of key parameters and issues in postclosure monitoring, and to prepare appropriate plans and proposals for detailed investigations. A number of in-house meetings were held and many ideas were discussed and incorporated into a draft report for DOE. After its review by OCRWM it was revised based on their comments. A draft final report entitled "Critical Parameters and Measurement Methods for Postclosure Monitoring" was prepared and sent to DOE in May 1987. It provides a summary of the available literature on postclosure monitoring, with attention to special problems, critical parameters, measurement methods and suggestions

for the development of new monitoring methods using seismic, electrical and electromagnetic geophysical techniques. One key point that emerges from this study is that it is important to begin postclosure monitoring planning and execution at an early stage of repository design and construction. Some of the monitoring methods may require special built-in features in the repository and all the monitoring methods require a properly established data baseline.

The subject of fracture studies forms the main part of the topical studies. The problem was approached from many directions:

Solid Mechanics,
Fluid Dynamics,
Geology,
Geophysics, and
Geochemistry.

The progress of our fracture studies is described in this report, with the article titles and authors listed in the Table of Contents. This multidisciplinary program included laboratory experiments and theoretical analyses as well as numerical simulations. Some of the studies are of a fundamental nature, which we expect will provide the basis for important practical geotechnical issues to be addressed, clarified or resolved in the next two or three years. Other studies have already yielded results that provide new insights and analysis techniques for understanding the physics and chemistry of fractured repository rock systems.

The major accomplishments of the second year of this project may be summarized as follows:

- The mobility of uranium in response to fracturing and fluid movement in the near field of the heater was studied in the laboratory with cores from close to and away from a heater simulating a waste canister in granitic rock.

Results indicate preponderance of U in the zone within ≈ 2 mm of the fracture and evidence of disequilibrium in the U decay series. These imply a potential for U mobilization in mineral-filled fractures which may reopen in response to thermally induced stresses in the near field (page 17).

- Seismic velocity and attenuation characteristics of heated rock were measured in the laboratory on cores from varying distance from a heater in granitic rock. Results indicate a degradation of mechanical properties in response to long term high temperature heating as evidenced by low values of seismic velocities, amplitudes and Q factors. However this effect may not be significant for temperatures below 300° C (page 17).
- An analytic study was performed to determine the important parameters that control the mechanical stiffness of fractures. It is found that the spatial geometry of the asperities and their dimension affect both the shape and magnitude of the stress-stiffness curve. The analytic model developed yielded results that are consistent with those observed in the laboratory for single fractures in natural rock (page 37).
- A detailed analysis was made of fluid flow and tracer transport through a two-dimensional fracture with variable apertures. The results show that transport is expected to occur in preferred paths or channels so that point measurements give very uncertain results depending on whether the point is in a flow channel or not. It seems that line-averaged measurements are required to overcome this problem. This may have important implications in site characterization studies (page 52).
- A new channel model was developed to describe tracer transport through a fractured medium. It considers such transport to occur through a set of statistically generated variable-aperture channels between points. New parameters to be measured that are important to characterize the transport

properties of the fractured medium are identified and discussed (page 61).

- A numerical method was developed to calculate fluid flow in a system of irregular geometry, such as a fracture with a non-uniform distribution of asperities. The numerical method consists of a three-dimensional grid generation procedure that transforms the complex geometry onto the interior of a rectangular parallelepiped and a numerical solution method for solving the flow equations in both 2-D and 3-D. Selected test cases were calculated (page 69).
- An experimental study was conducted to measure the enhanced dissolution kinetics due to stress-induced defect formation in selected minerals. A critical review of the literature was made to determine the rate controlling mechanisms involved in the dissolution and transport of chemical constituents away from stressed asperities (page 76).
- Two codes for ray tracing in fractured anisotropic media were developed. The first code was an adaptation of BEAM87, a code developed by V. Cervený. This 2-D code calculates refractions, reflections full amplitudes at any source receiver configuration. The second code, also developed by V. Cervený is a full anisotropic ray-calculation (3-D) the seismic response. Both codes are very useful for forward modeling of fractured anisotropic rocks for tomographic VSP and crosshole applications (page 95).
- Using an approach based on the micro-mechanics of rock in combination with the displacement discontinuity numerical method, the generation and growth of breakouts around boreholes and underground excavations was studied. The method was successful in predicting the generation of stable excavation shapes resulting from breakouts. A correlation between breakout angle and breakout depth was observed (page 108).

- Laboratory experiments were performed on thick-walled hollow cylinders of rock to simulate and observe deformation, fracture and failure around underground openings. A metal injection technique was used to preserve the fracture geometry under load. Results showed that opening geometry, stresspath, and strain rate affect the strength, deformation and failure processes of rock around underground openings (page 126).
- The application of fracture mechanics to the mechanics of faulting and earthquake rupture. Theoretical and numerical models have been developed to take into account heterogeneity of strength and stress along fault surfaces. These models predict seismic and aseismic behavior associated with fault slip and also some new relationships between the source parameters (moment, stress drop, energy release) for unstable events (page 137).

**Geoscience Technical Support
for Nuclear Waste Geologic Repositories**

D. C. Mangold and C. F. Tsang

During FY87 the Geoscience Technical Support activities in the Geologic Repository Project (GRP) at LBL covered a broad range of reports and reviews, with particular emphasis on the review of Site Characterization Plans (SCP) of the three potential repository sites and participating in their associated Review Workshops. They also included hosting, at DOE's request, a two-day workshop on the Hydrologic Behavior of Rock Discontinuities. The accompanying table, "Geotechnical Support Activities: Fiscal Year 1987," listing the type of technical review or other activities, the date when a report was sent to DOE, and a brief description of the material reviewed or meeting attended.

The reviews were performed by a group of respected research scientists, expert in a broad range of disciplines in the earth sciences. The individuals and their specialities are listed in the table below. The diversity of backgrounds of the participating scientists is representative of the multidisciplinary teamwork that has characterized LBL's effort in this project. The participants have developed a close working relationship in carrying out the topical studies (reported in subsequent parts of this report) and thus were able to perform the many different technical support tasks given by DOE in a timely and effective manner.

<i>Name</i>	<i>Principal Expertise</i>
Chalon L. Carnahan	Geochemistry
Steven Flexser	Geology
Harold A. Wollenberg	Geology
Neville G. W. Cook	Geomechanics
John Kemeny	Geomechanics
Larry R. Myer	Geomechanics
Ernest L. Majer	Geophysics
Thomas V. McEvelly	Geophysics
H. Frank Morrison	Geophysics
Iraj Javandel	Hydrogeology
Marcelo J. Lippmann	Hydrogeology
Chin-Fu Tsang	Hydrogeology
Paul A. Witherspoon	Hydrogeology

In total, under this task there were 45 geotechnical support activities, described in Table at the end of this section. A brief summary of the various activities is given below.

Site Characterization Plan (SCP) Reviews

Selected chapters of the Site Characterization Plan Reviews for NNWSI (Nevada Nuclear Waste Storage Investigations Project), BWIP (Basalt Waste Isolation Project) and SRP (Salt Repository Project) were reviewed by LBL scientists expert in the areas of geology, geomechanics, geophysics, hydrology and geochemistry. In general, the reviews were carried out by a few specialists in each

area in order to cover the technical aspects in each chapter. Those who review particular chapters or sections also participated in the overall review discussions held at LBL. Many of the same scientists attended the SCP Review Workshops where all comments on a given chapter were considered. There they worked with the authors and DOE review leaders to suggest changes or revisions to improve the technical content of the documents, particularly by helping to clarify technical points in the plans. Later they also dealt with the dispositions of their comments by others, so that a well-balanced review could be achieved.

Hosting DOE Workshops

LBL hosted two gatherings at DOE's request. The first on April 21, 1987, was a program review of this particular project and two other OCRWM-sponsored LBL research projects on high-level waste management. The second was the Workshop on Hydrologic Behavior of Rock Discontinuities held on April 22-23, chaired by Dr. C. Voss of DOE/HQ and attended by 38 persons. There were representatives from DOE, the three project offices (NNWSI, BWIP, SRPO), five other national laboratories (INEL, LANL, LLNL, PNL, SNL), other institutions (Battelle/ONWI, USGS) and engineering consulting companies (Golder Associates, SAIC). At this workshop LBL scientists gave four presentations describing their research on laboratory studies of fracture properties and behavior, fracture network modeling, multi-phase flow in fractured media, and geophysical detection of fractures. Abstracts of these presentations were sent to Dr. Voss for inclusion in the meeting proceedings being prepared by him.

Reviews of Study Plans, NRC Papers, and Other Reviews

In July 1987, LBL scientists attended the Study Plans Briefing/Review Coordination Training held at DOE/HQ for reviewers of the draft SCP's. These plans

summarize the proposed investigations of the past and present conditions of the site with regard to its geology, hydrology, geochemistry, geomechanics, etc.; the expected effects of site characterization activities; the regional and local effects of locating a repository at the site; and an evaluation of the suitability of the site for site characterization and for development as a repository. Two such reviews were performed in a timely way as required by DOE.

Under this project LBL also reviewed the Generic Technical Position papers of the US Nuclear Regulatory Commission. These documents establish generic guidelines on topics of technical interest related to nuclear waste storage. The topics were concerning the extent of the disturbed zone around a repository and ground water travel time. To provide comments on these documents LBL personnel expert in different fields often reviewed the same paper, bringing together different perspectives to the review process.

From time to time, DOE received proposals from researchers to conduct studies on various aspects of the potential sites or on the methodology used to evaluate the technical aspects of the sites. A proposal on the isotopic and geochronologic study of the Palo Duro Basin bedded evaporites was reviewed by LBL. Also reviewed was methodology investigation proposal that addressed the stochastic analysis of flow through fractured media and associated monitoring network design as applied to a high-level waste repository.

Other technical assistance was rendered to DOE, such as answering technical questions posed to DOE concerning the hydrological aspects of nuclear waste disposal, and evaluating miscellaneous technical documents.

Other Meetings Attended

One of LBL's hydrologists was asked to participate in the BWIP Hydrology Task Group to assist BWIP in planning their well-testing program for the

Hanford site. He attended meetings almost every month at either DOE/HQ or Richland, Washington, and reviewed BWIP documents on the hydrology of the site.

At DOE's request another LBL staff member attended the October 7-9, 1986 NRC Symposium on Seismic and Geologic Siting Criteria for Nuclear Power Plants at Rockville, Maryland. The purpose was to keep DOE up to date with recent developments in NRC's consideration of these criteria for siting, a nuclear waste repository. Two representatives from LBL also participated in the DOE/OCRWM Geosciences Coordination Committee held in Washington, DC on January 14, 1987 to review the progress of this project and to make a presentation of proposed studies on postclosure monitoring of a nuclear waste repository.

Conclusion

LBL has been very active in meeting DOE's need for technical review as part of the geoscience technical support for nuclear waste repositories. The ability of LBL scientists to work as a multidisciplinary team was an important asset that allowed LBL to provide timely, and balanced technical comments to meet DOE's requirements.

GEOTECHNICAL SUPPORT ACTIVITIES

FISCAL YEAR 1987

Activity	Delivery	Description
Review	10/1/86	NRC Generic Technical Position (GTP) "Interpretation and Identification of the Extent of the Disturbed Zone in the High-Level Waste Rule (10 CFR 60)"
SCP Review	10/7/86	BWIP Chapter 8.3.1.3 (Site Characterization Program, Hydrology)
SCP Review	10/7-8/86	BWIP Chapter 3 (Hydrology)
Trip	10/7-9/86	NRC Symposium on Seismic and Geologic Siting Criteria for Nuclear Power Plants, held in Rockville, MD (no trip report required; recorded in monthly report)
SCP Review	10/13/86	BWIP Chapter 2 (Geomechanics)
SCP Review	10/13/86	BWIP Chapter 8.3.3 (Repository Seals)
Review	10/23/86	NRC GTP "Ground Water Travel Time"
SCP Review	10/24/86	BWIP Chapter 8.3.2 (Repository Program)
SCP Review	10/29/86	BWIP Chapter 6 (Design of Repository)
SCP Review	11/4/86	Dispositions of LBL's earlier comments on BWIP Chapter 2 (Geomechanics) reviewed and signed
SCP Review	11/6/86	BWIP Chapter 4 (Geochemistry)
SCP Review	11/6/86	Dispositions of LBL's earlier comments on BWIP Chapter 4 (Geochemistry) reviewed and signed
Review	11/13/86	BWIP "Plan for Multiple-Well Hydraulic Testing of Selected Hydrogeologic Units at the RRL-2 Site"
SCP Review	11/24/86	Dispositions of LBL's earlier comments on BWIP Chapter 1 (Geology) reviewed and signed
SCP Review	11/24/86	BWIP Chapter 1 (Geology)
SCP Review	12/2/86	BWIP Chapter 2 (Geomechanics)
Review	12/24/86	Unsolicited proposal to DOE by Brookins, "Strontium Isotopic and Rubidium-Strontium Geochronologic Study of Palo Duro Basin Bedded Evaporites"
Trip	1/14/87	DOE/OCRWM Geosciences Coordination Committee meeting held in Washington, DC

GEOTECHNICAL SUPPORT ACTIVITIES

FISCAL YEAR 1987 (Continued)

Activity	Delivery	Description
Review	1/21/87	Unsolicited proposal to DOE by Borgman et al., "Stochastic Analysis of Flow through Fractured Media and Associated Monitoring Network Design Applied to a High Level Waste Repository"
SCP Review	1/23/87	BWIP Chapter 3 (Hydrology)
Assembled Document Review	2/10/87	Review of the NNWSI SCP, 23 portions by 9 technical reviewers in the areas of Geology, Tectonics, Geoengineering, Postclosure Performance Assessment, Hydrology, and Geochemistry
Trip Report	3/9/87	BWIP hydrology characterization program meetings on proposed well-testing, held November 24 and December 8 in Washington, DC and December 15-18 in Richland, WA
SCP Review	3/13/87	Dispositions of LBL's earlier comments on BWIP Chapter 6 (Design of Repository) reviewed and signed
Trip	3/31/87 4/1/87	BWIP hydrology characterization program for well-testing, meetings held in Washington, DC
Review	4/87	Participation in BWIP License Assurance Review of Chapter 2 (Geoengineering), Chapter 6 (Design of Repository), and Chapter 8 (Site Characterization Program) under an arrangement with BWIP with approval of GRP program manager
Trip	4/7-9/87	BWIP hydrology characterization program meeting held in Richland, WA (no trip report required; LBL input was recorded in the BWIP Hydrology Task Group report)
Hosted DOE Program Review	4/21/87	At DOE's request, LBL hosted a one-day program review of the GRP project and two other OCRWM-supported research projects on high-level waste repositories
Hosted DOE Workshop	4/22-23/87	At DOE's request, LBL hosted a two-day Workshop on Hydrologic Behavior of Rock Discontinuities attended by 38 persons from DOE, the three project offices, and a number of national laboratories and engineering consulting firms; LBL scientists gave four presentations of their research

GEOTECHNICAL SUPPORT ACTIVITIES

FISCAL YEAR 1987 (Continued)

Activity	Delivery	Description
SCP Review	4/26-30/87 5/4-7/87	Review of the BWIP SCP document by 6 technical reviewers and participation in BWIP SCP Review workshops held in Washington, DC
Trip	6/2-4/87	BWIP Hydrology Task Group meeting held in Richland, WA
Technical Assistance	6/5/87	A series of questions on various aspects of hydrogeology in nuclear waste disposal were received and answers were sent the same day by telecopy
SCP Review	6/19/87	Review of the whole document of the NNWSI SCP by LBL technical reviewers
Trip	6/24-26/87	BWIP Hydrology Task Group meeting held in Richland, WA
Trip	7/7/87	Study Plans Briefing/Review Coordination Training held at DOE/HQ in Washington, DC
Trip	7/21-22/87	BWIP Hydrology Task Group meeting held in Richland, WA
SP Review	7/29/87	SRP Study Plans for Water Resources and Land Use
SCP Review	8/87	SRP SCP Chapters 1 (Geology), 2 (Geoengineering), 3 (Hydrology), 4 (Geochemistry), 6 (Design of Repository), and 8 (Site Characterization Program) by 14 technical reviewers
SCP Review Workshops	8/3-7/87	SRP SCP Review Workshops on Chapters 1 (Geology), 2 (Geoengineering), and 4 (Geochemistry) held in Hereford, TX
SCP Review Workshop	8/9-12/87	SRP SCP Review Workshop on Chapter 6 (Design of Repository) held in Hereford, TX
Trip	8/19-21/87	BWIP Hydrology Task Group meeting held in Richland, WA
SCP Review Workshop	8/24-27/87	SRP SCP Review Workshop on Chapter 3 (Hydrology) held in Hereford, TX

GEOTECHNICAL SUPPORT ACTIVITIES

FISCAL YEAR 1987 (Continued)

Activity	Delivery	Description
SCP Review	9/87	BWIP SCP Chapters 1 (Geology), 2 (Geoengineering), 3 (Hydrology), 4 (Geochemistry), 6 (Design of Repository), and 8 (Site Characterization Program), and Issues 1.5 (Release Rate), 1.8 (Siting Criteria), and 1.11 (Repository) by 14 technical reviewers
SCP Review Workshops	9/20-25/87	BWIP SCP Review Workshops on Chapter 1 (Geology), and various sections of Chapter 8 (Site Characterization Program) held in Washington, DC
SCP Review Workshops	9/22-28/87	BWIP SCP Review Workshops on Chapters 2 (Geoengineering), 6 (Design Workshops of Repository), and various sections of Chapter 8 (Site Characterization Program) held in Washington, DC
SCP Review Workshops	9/27-30/87	SRP SCP Review Workshops on Chapters 1 (Geology), 3 (Hydrology), and 4 (Geochemistry) held in Amarillo, TX

Geochemical and Geomechanical Investigations of Fractured, Heated Rock

H. Wollenberg, L. Myer, S. Flexser, and J. Scheiner

INTRODUCTION

In the near field of a nuclear waste canister, high temperatures will affect the local geochemical - hydrological regime. It is important that these hydro-geochemical processes be understood if the transport of radionuclides away from a breached canister is to be modeled and predicted. The objective of these investigations, then, is to develop an understanding of the interaction under elevated temperatures, of radionuclides in the fracture-fluid system with the material lining the fractures. To accomplish this, samples of core from holes that have penetrated high-temperature zones are examined petrologically, geochemically, and geomechanically. Emphasis to date has been on core samples of quartz monzonite, obtained by drilling back into rock previously subjected to a year-long heater experiment simulating high-level radioactive waste, conducted at Stripa, Sweden (Chan et al., 1980 and Flexser, et al., 1982). Recently, work has begun on core from a hole penetrating a fractured hydrothermal system in rhyolitic tuff (Wollenberg et al., 1987). In both cases, properties of rock in elevated temperature zones are compared with those of zones of lower and near-ambient temperature. In this report we describe radioelement and geomechanical investigations of core from the Stripa heater experiment and preliminary work on samples of tuff.

A. RADIOELEMENT INVESTIGATIONS

The large-scale distribution of uranium, its daughter products and thorium in the Stripa quartz monzonite and its fracture-controlled groundwater system has been described by Wollenberg and Flexser (1985). At Stripa, U and Th, each at 30-40 ppm, are concentrated considerably higher than in most granitic rocks, and contrary to most granitics, the abundances of U and Th are nearly equal. Uranium is strongly associated with fracture-filling material, predominantly chlorite, but in some cases epidote and sphene, enhancing the availability of U to the groundwater. Uranium is in relatively high concentrations (up to 20 ppb) in groundwater in the upper portion of the quartz monzonite, where Eh is also high (+200 to 500 mv), while considerably lower concentrations (~ 1 to 5 ppb) occur at lower Eh (0 to +200 mv) at depths below 400 m. Whole-rock gamma spectrometric measurements of U and Th in the heater drill-back core show U concentrations of ~ 40 ppm within ~ 1m of the heater axis, decreasing to 33 to 36 ppm in core more distant from the heater. There is no corresponding change in Th over the same span. Initial alpha-track radiography suggested that U was added to fracture-lining material in rock near the heater. This, together with the whole-rock data suggested mobility of U in response to fracturing and fluid movement in the near field of the heater.

Subsequently, detailed alpha- and fission-track radiographic examinations have been made in core within 1 m of the heater where distributions of radioelements in and adjacent to filled and open fractures have been measured. The zone of core investigated is shown in the photograph, Figure 1, with the prominent open fracture located 5 to 7 cm from the edge of the heater hole. The position of the open fracture near the edge of the heater hole, in comparison with closed fractures farther away from the heater, suggest that the fracture opened in response to heating (several kg of rock spalled from the wall of the heater hole, 0.3 m in diameter, 2.6 m long, during heating). Nelson et al. (1981) reported that water flowed readily into the hole in the early

stages of heating. Flow into monitoring holes within several decimeters of the heater hole continued, but lessened throughout the experiment.

Both alpha- and fission-track densities were measured, because alpha tracks are from members of both the U and Th decay series, while fission tracks are essentially from ^{235}U . Fission tracks are generated by bombarding rock thin sections, covered with track detectors, by a flux of thermal neutrons that cause essentially only ^{235}U to fission. The resulting fission fragments impinge on the detectors, and their subsequent etching reveals the damage pits or "tracks" that show the distribution and abundance of U. Exposure of standards along with the thin sections permits determination of U concentration.

By comparing alpha- and fission-track patterns and track densities, we differentiate between contributions from the U and the Th decay series, because U fission-track densities are directly quantifiable into U concentrations (Table 1). In Figure 2 alpha-track densities and U concentrations in fracture-lining minerals are plotted with distance from the edge of the open fracture. Alpha track densities and U concentrations decrease in similar patterns away from the sides of the fracture. The similarity in the profiles and the relatively high U concentrations (~ 0.2 to 1.6%) of the lining material compared to 0.1 to 0.2% in filled fractures away from the heater and 0.003% in the rock indicate that in this case U is the principal contributor to the alpha tracks. The pattern of decreasing U and alpha tracks away from the open fracture was not observed in a nearby fracture completely filled with similar minerals, where track densities are uniform and U concentrations ~ 0.2%.

The measured track densities and U concentration patterns associated with the open fracture lead to consideration of evidence for mobility of U in response to prolonged heating of the rock. The U distribution pattern and evidence for disequilibrium in the U decay series are examined in this respect. The relatively high concentrations of U adjacent to the open fracture and its gradient in the lining material over the

Table 1. Track Densities and Uranium Concentrations of Fracture-Filling Material and Material Lining an Open Fracture

Distance from Edge of heater Hole (m)		Alpha Track Density (T/mm ²)	Fission Track Density (T/mm ²)	Uranium (%)
0.005 ^a	Open-Fracture Lining	Mean 1560 (Range 550 to 2250)	Mean 1449 (Range 254 to 2807)	Mean 0.88 (Range 0.15 to 1.71)
0.15		438 ± 36 ^b	273 ± 33	0.17 ± 0.02
0.39		574 ± 16		0.22 ^c
1.40	Filling of Closed Fractures	562 ± 20		0.22
1.68		501 ± 20		0.19

^aThis population illustrated on Figure 2.

^b± values represent counting statistics.

^cEstimated by applying the observed to calculated alpha-track ratio of 1.7, based on the 0.15 m position data.

adjacent 1.2 mm, in contrast to lower concentrations and no apparent gradients in filled fractures of similar mineralogy, suggest that U was deposited from fluid moving through the fracture. The higher concentrations of U on the right side of the fracture and lower concentrations on the left side (Figure 2) might reflect a small offset along the fracture.

Evidence for disequilibrium in the U decay series was examined by calculating the alpha-track densities that would result from the U concentrations (based on track densities of a U standard) observed from fission tracks, and comparing these calculated track densities with observed alpha-track densities. This is illustrated in Figure 3, where the ratio of observed to calculated track densities is plotted with distance from the fracture's edge. A ratio of 1 represents secular equilibrium and a ratio less than 1 represents the absence of some alpha-emitting daughters of the U decay series (disequilibrium). Uncertainties in spatial resolution of alpha and fission-track populations, abundances of U in standards, and track counting statistics cause uncertainties in the determination of the ratios, perhaps by 10 to 20%. However, there is still strong indication of disequilibrium in that there are several values less than 0.8. These could represent the recent addition of U to the fracture lining material, or the removal of one or more U daughter elements. The excess of alpha tracks at sites of relatively low U concentration where the ratios are well above 1 might be due the presence of thorium and its daughters in significant abundance. This may also be the case in the filled fracture ~ 15 cm from the heater hole, where U (by fission tracks) averages 0.17% and the ratio of observed to calculated alpha tracks is 1.7. As shown in Table 1, alpha track densities associated with filled-fracture material farther from the heater are somewhat greater than at the 15 cm position. Assuming that the ratio 1.7 holds for these populations, their U concentrations are also of the order of 0.2%.

Independent evidence of the preponderance of U in the zone within ~ 2 mm of the fracture was provided by secondary-ion mass spectrometric (SIMS) measurements. Even though the resolution of SIMS is not high enough for direct comparison with the sub-millimeter resolution of the track-radiographic methods, SIMS is capable of determining element ratios over relatively small zones. The concentration ratio U/Th by this method is ~ 3, in contrast to approximate parity of U and Th in the rock matrix.

At this juncture the pattern of uranium distribution and evidence of disequilibrium in the U-decay series suggest that U was mobilized and deposited in the localized vapor-dominated fluid system in fractures adjacent to the heater. This implies that in a repository environment close to the waste canisters, fractures that had been mineral-filled might reopen in response to the thermally-induced stress caused by the introduction and long-term presence of the waste. The open fractures would permit a vapor-dominated near-field thermal system to mobilize uranium leaking from a canister, but, depending on fracture-lining mineralogy, a significant portion of the uranium could be deposited on material lining the fractures in the near field of the canister.

When instrumentation becomes available in the new Center for Isotope Geosciences, micron-scale analytical methods can be used independently to determine U concentrations, U-series isotope ratios, and oxygen-isotope ratios to provide the detail necessary for more definitive examination of U mobility.

B. Studies of Tuff

To begin investigations of the effects of heating on tuff, core has been collected from DOE hole RDO-8, penetrating rhyolitic tuff of the Long Valley caldera (Wollenberg et al., 1987). Samples covering the temperature range 60 to 200°C were selected from megascopic examination of the core and from examination of the natural gamma-ray log of the hole. The samples were analyzed preliminarily by gamma-ray spectrometry to determine their uranium, thorium, and potassium concentrations and

to screen them for more detailed study. Areas of primary interest are anomalous zones where high-resolution gamma spectral measurements indicate that U is the predominant radioelement and that there is indication of disequilibrium in the U decay series. Figure 4 is a composite diagram of the alteration mineralogy, temperature profile, and gamma log of the hole, with U anomalies delineated. A principal zone for examination is at 915 - 950 ft., where temperatures are in the range 130 to 150°C, calcite first appears, rhyolitic tuffaceous sediments in a fault zone are cemented by calcite, and disequilibrium is indicated in the U decay series. Oxygen isotope ratios will be measured on the calcite and adjacent rhyolite, and the detailed distribution of U and Th will be examined by radiography. Depending on downhole accessibility, an attempt will be made to perforate the hole to obtain fluid samples from this zone for analyses of their major- and radio-element concentrations and isotope ratios. These will be compared with results of similar analyses of calcite and rhyolite of the core to determine the extent of rock - fluid interaction.

Another suite of core with good potential for studies in unsaturated conditions is that from DOE hole VC-2A, drilled through the vapor-dominated zone in tuff of the Valles caldera, New Mexico (Goff et al., 1987). The gamma-ray log of this hole shows anomalies in the upper 400 ft. of the hole, over the temperature range 40 - 120°C, that indicate core intervals for investigation of U concentrations, distribution, and possible U-series disequilibrium.

SEISMIC VELOCITY AND ATTENUATION MEASUREMENTS

The seismic velocity and attenuation characteristics of heated rock were investigated in core from the vicinity of the Stripa heater experiment. In this experiment a 5 KW heater was operated for 200 days. Peripheral heaters were then turned on and all heaters operated for an additional 200 days. Figure 5 shows the measured and calculated temperature distribution in the rock surrounding the horizontal midplane of the

heater in the A-10 area. Agreement was very good between calculations and actual temperatures measured at various locations in the vicinity of the heater.

Figure 6 shows the configuration of the drillback holes through the heater experiment and the general position of the core samples; Figure 7 shows the sample positions in greater detail. Though no temperature measurements were made at positions corresponding to the exact sample locations, calculations show that the peak temperatures at the locations were about 375°C, 325°C, and 200°C, from the sample closest to the heater to the one farthest away.

The velocity and attenuation of compressional (P) and shear (S) waves through the samples were measured in the laboratory by the pulse transmission method under axial loads ranging from 4.1 to 62 MPa. The maximum axial stress was less than 1/3 the unconfined compressive strength of unheated intact Stripa quartz monzonite (Swan, 1978). The center frequency of the transmitted P and S waves was about 600 Hz. For attenuation analysis and calculation of the seismic quality factor (Q), an aluminum reference standard of the same configuration as the core samples was subjected to similar experimental conditions.

As expected, the velocity, peak to peak amplitude, and Q for both P- and S-waves increased with pressure in all samples. Figures 8 and 9 show the P- and S-wave amplitude data. The rate of change in amplitudes and velocities with increasing pressure was also similar, in that the most rapid change was observed at low axial stresses, followed by a more gradual increase at higher stresses. The observed trends reflect the closure of microfractures as the axial stress is increased. The increase in velocity reflects the increase in effective modulus in response to this microcrack closure. Microcrack closure also reduces energy loss in the traveling wave and hence results in the observed increases in amplitude.

The rate of change in Q with pressure differed from that of the other parameters: in most cases Q increased with increased pressure in nearly a linear manner. However, sample 3, of intermediate distance from the heater showed a nearly exponential increase in Q with pressure. It is not clear why the trend of Q with pressure should be different for the one sample.

The effect of proximity of the heater to sample locations is clear in the P wave data. The sample closest to the heater (2) had the lowest P- wave velocity, amplitude, and Q ; the calculated maximum temperature at this location was approximately 375°C. P-wave parameter values for samples 1 and 3, farther from the heater, were similar even though the maximum temperatures were quite different (calculated ~ 325°C vs ~ 200°C). Paulsson (1983) measured P-wave velocities and Q values from unheated core in the H-10 area and found values similar to those obtained for samples 1 and 3. It is believed that the observed behavior of the sample closest to the heater was due to increased microcracking in response to long term heating at high temperatures. Results also indicate, however, that changes in properties are minimal below about 300°C.

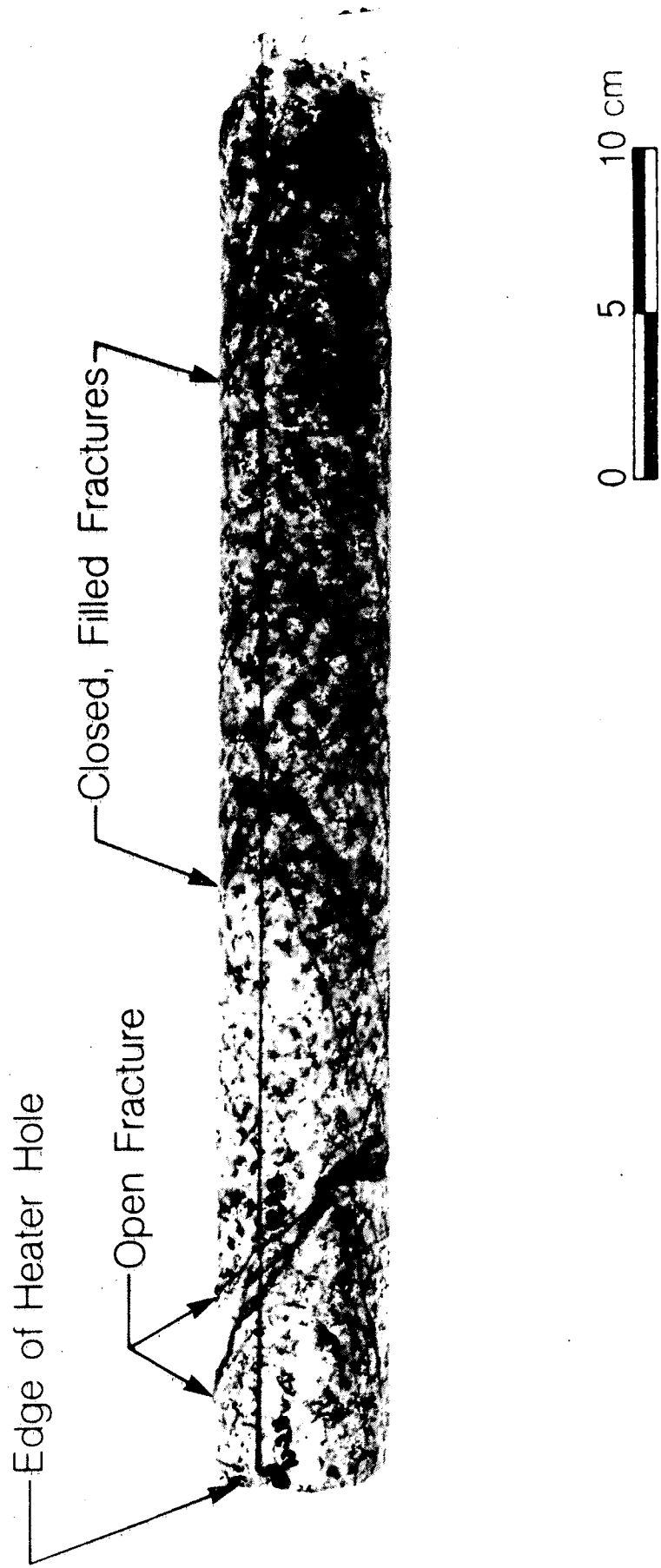
Results of the S-wave measurements also indicated that close proximity to the heater resulted in low S-wave parameter values. However, in contrast to the P-wave results, the amplitude and Q values for the sample experiencing the intermediate temperature (3) were similar to those of the hottest sample (see Fig. 9). Surprisingly, the S-wave velocity of the coolest sample was low (similar to that of the hottest sample) while its S-wave amplitude and Q were high. Results of S-wave velocity measurements on unheated core from the H-10 area and elsewhere (Paulsson 1983) exhibited a range with minimum values similar to those of the hottest sample (2). One possible reason for this variability is the presence of a preferred orientation of the microcracks. The experimental configuration of polarized shear waves propagating along the axis of the core is sensitive to anisotropy induced by microcracks oriented in planes parallel to

the drill core axis. If such a preferred microcrack orientation is present, polarized shear waves will have different velocities and amplitudes depending upon the angle between the direction of particle motion of the wave and the plane of preferred orientation.

In summary, degradations of mechanical properties in response to long term high temperature heating was indicated by low values of seismic wave velocities, amplitudes and Q factors. Significant degradation may not have occurred at temperatures below 300°C. At higher temperatures the heating apparently caused increases in microcracking. Detailed microscopic studies of the samples tested are in progress to evaluate microcrack densities and possible anisotropy in microcrack orientations.

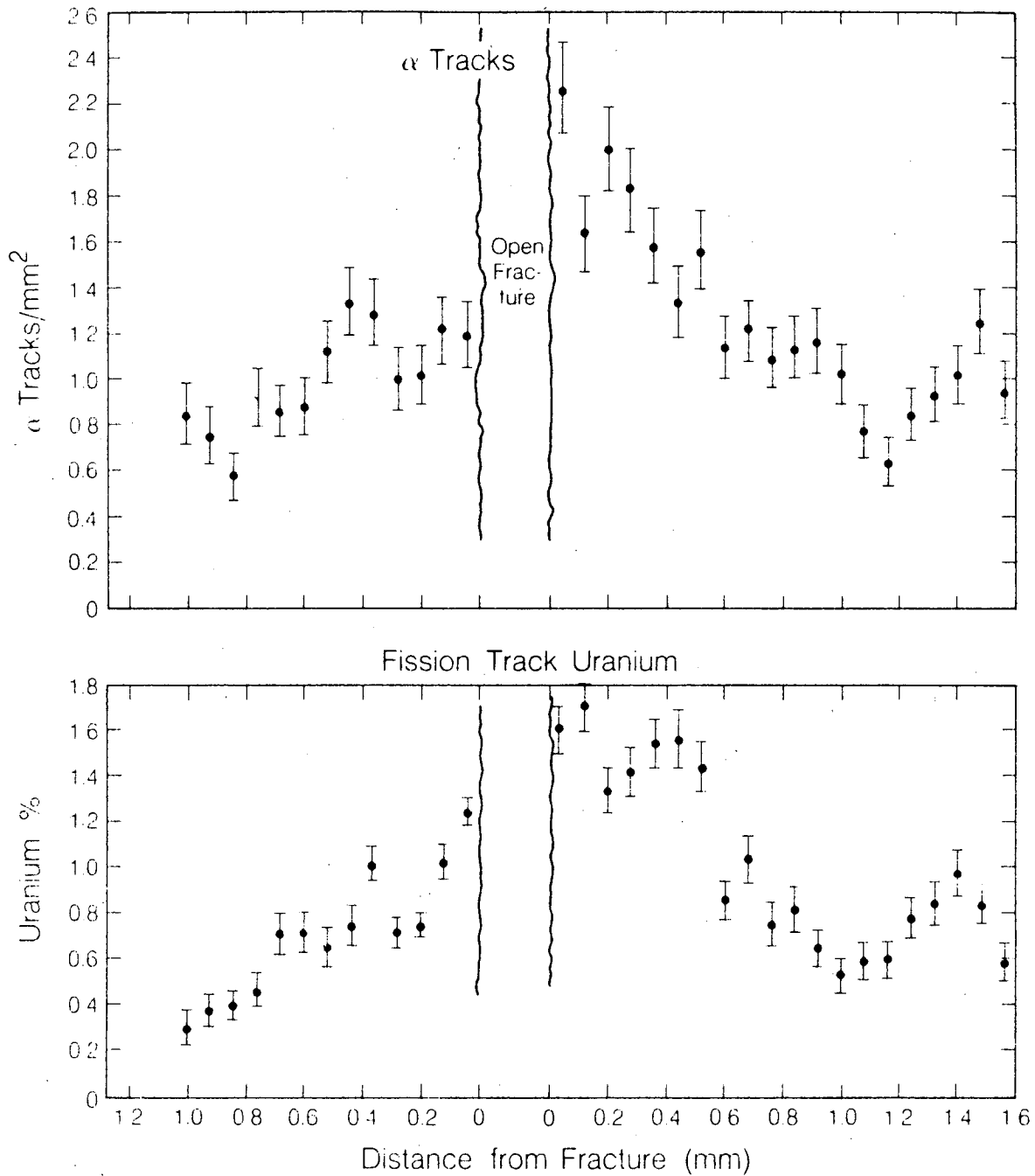
References

- Chan, T., Littlestone, N., and Wan, O., 1980. Thermomechanical modeling and data analysis for heating experiments at Stripa, Sweden; Proc., 21st Rock Mechanics Symp., Rolla Missouri.
- Flexser, S., Wollenberg, H., and Wedge, D., 1982. Petrologic changes and damage in the Stripa quartz monzonite in response to heater tests; Lawrence Berkeley Lab. Rept. LBL 14929.
- Goff, F., Nielson, D., Gardner, J., Hulen, J., Lysne, P., Shevenell, L., and Rowley, J., 1987. Scientific drilling at Sulphur Springs, Valles Caldera, New Mexico: Core Hole VC 2A; EOS, v. 68, no. 30, p. 649.
- Javandel, I., and Witherspoon, P., 1981. Thermal analysis of the Stripa heater test data; Lawrence Berkeley Lab. Rep., LBL-13217.
- Nelson, P., Rachiele, R., Remer, J., and Carlsson, H., 1981. Water inflow into boreholes during the Stripa heater experiments; Lawrence Berkeley Lab. Rept., LBL-12574.
- Paulsson, B. N. P., Seismic velocities and attenuation in a heated underground granitic repository; Lawrence Berkeley Laboratory Report LBL-16346, 1983.
- Swan, G., 1978. The Mechanical Properties of Stripa Granite; Lawrence Berkeley Laboratory Report LBL-7074, 1978.
- Wollenberg, H., and Flexser, S., 1985. The distribution of uranium and thorium in the Stripa quartz monzonite, Sweden; Uranium, v. 2, p. 155 - 167.
- Wollenberg, H., Sorey, M., Farrar, C., White, A., Flexser, S., and Bartel, L., 1987. A core hole in the southwestern moat of the Long Valley caldera: early results; EOS, v. 68, no. 20.



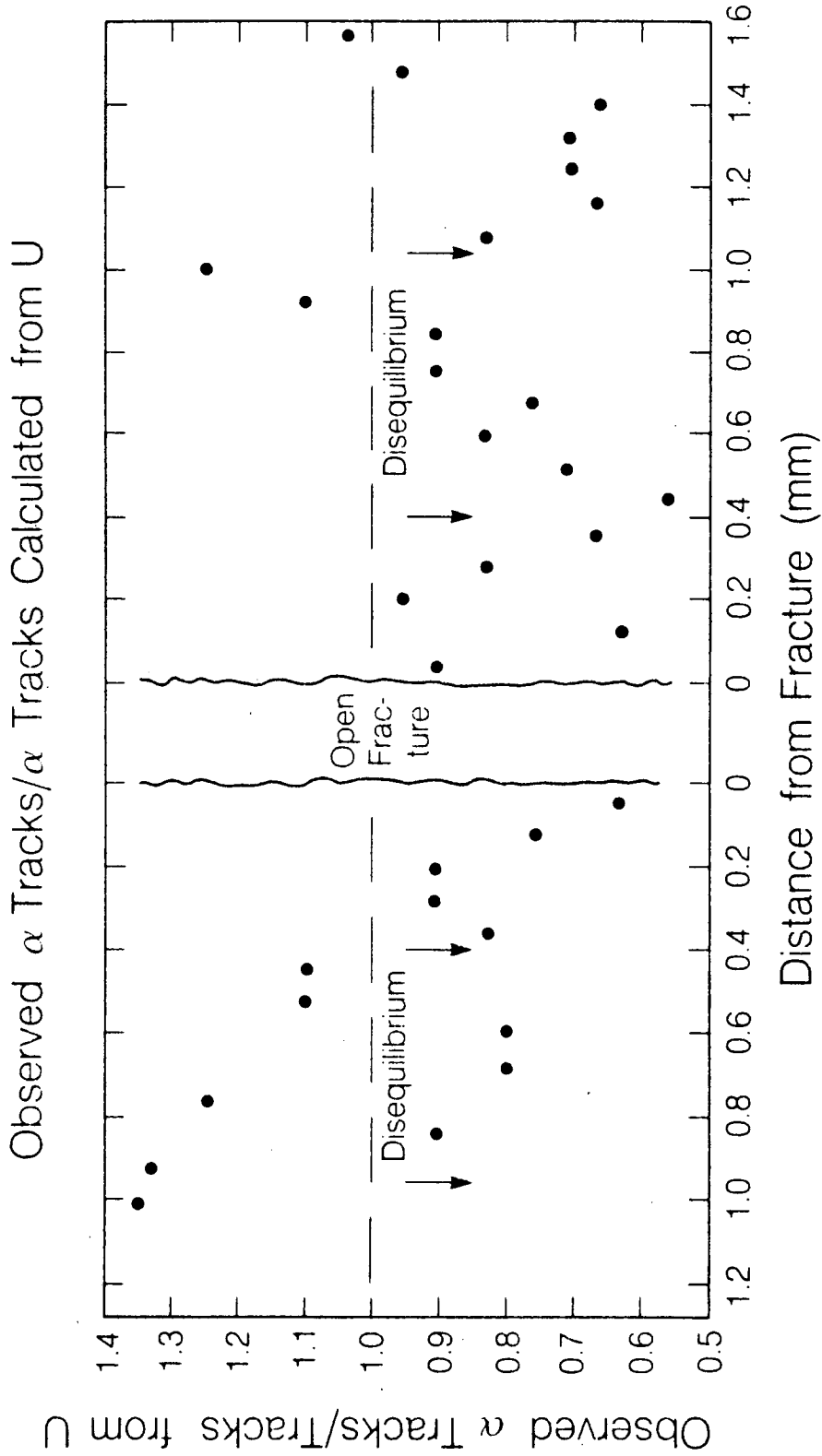
CBB 809-10887A

Figure 1. Core from Stripa drillback hole, showing locations of fractures examined for uranium.



AD-6710-10411

Figure 2. Alpha-track densities and U concentrations (by fission tracks) in filling material lining an open fracture in drillback core near the heater hole, Stripa experiment. Error bars reflect counting statistics.



XBL 8710 10412

Figure 3. Ratios of observed alpha track densities to those calculated from concentrations, in filling material lining an open fracture in drillback core near the heater hole, Stripa experiment. Ratios less than 1 suggest disequilibrium in the U decay series.

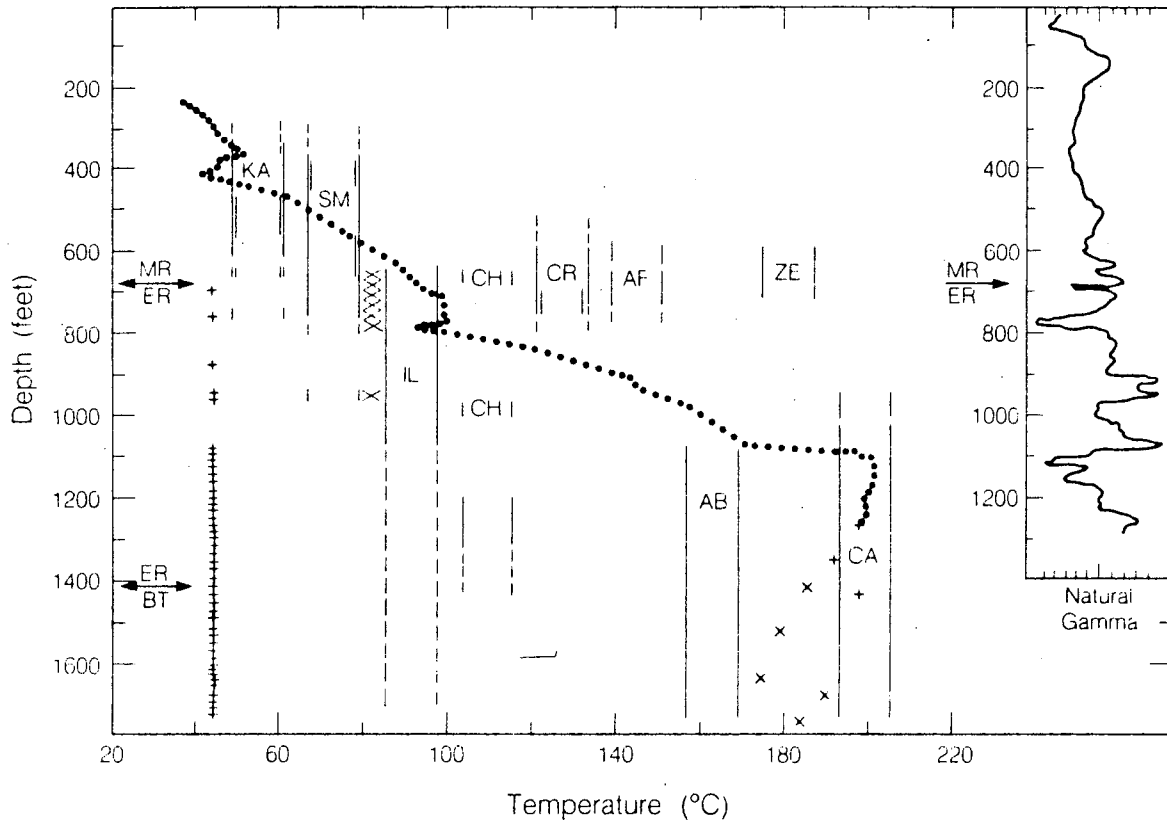
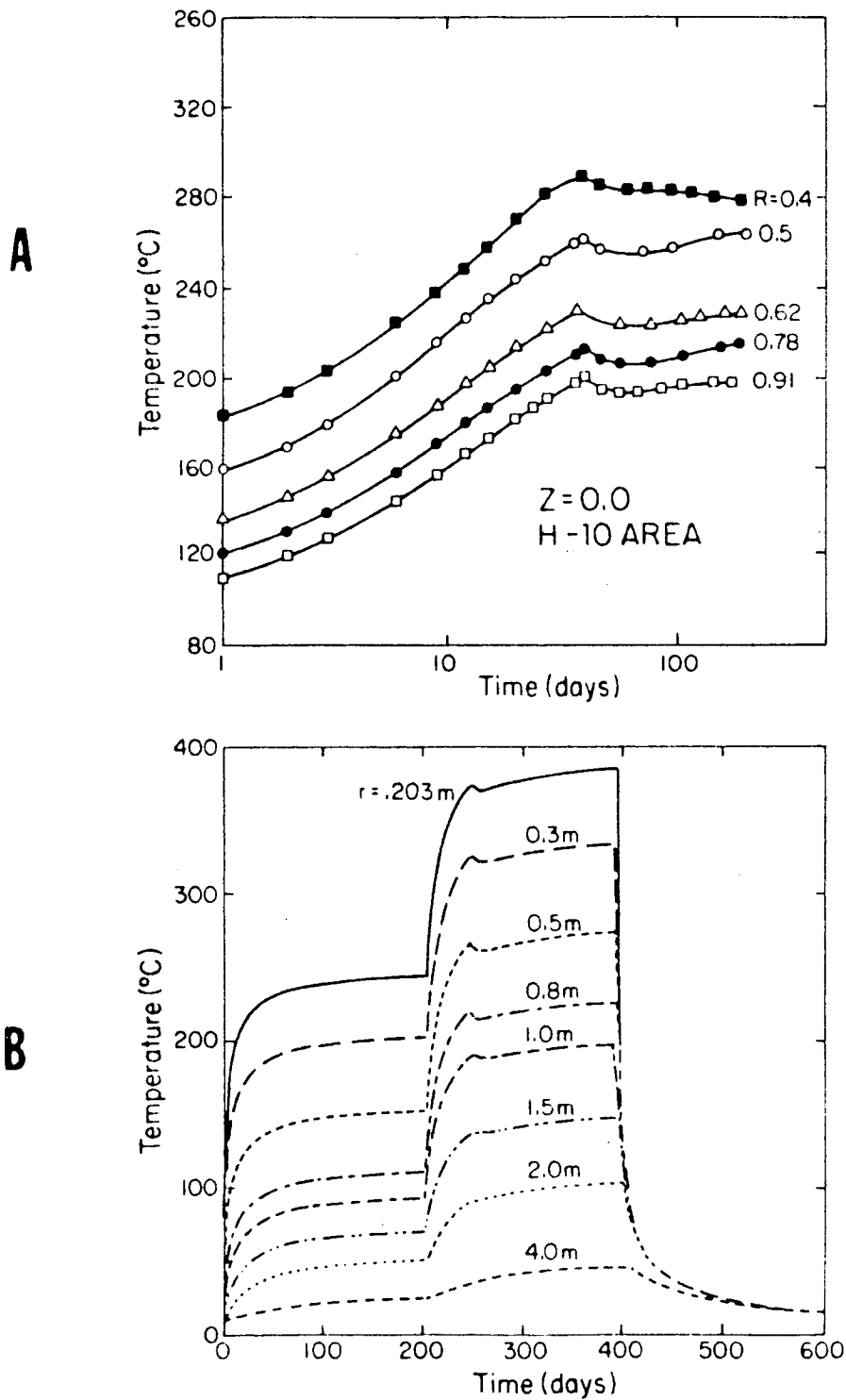


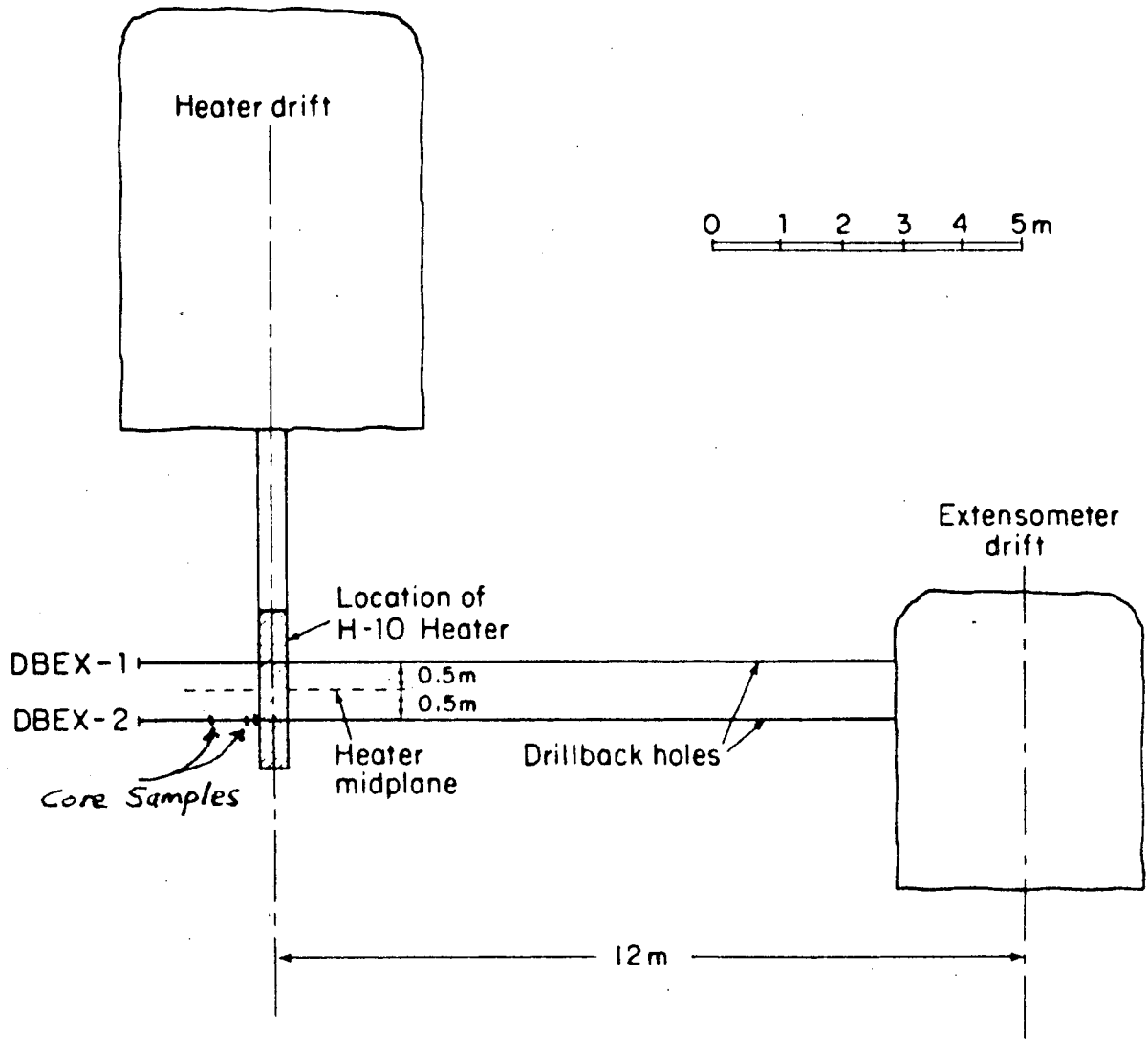
Fig. 8-11. 14.

Figure 4. Alteration mineralogy, temperature profile, and natural gamma-ray log of DOE hole RDO-8 in tuff. Double vertical lines indicate the strong presence of a mineral, single lines a moderate presence, and dashed lines a weak presence. KA = kaolinite, SM = smectite, IL = illite, CH = chlorite, CR = cristobalite/tridymite, AF = alkali feldspar, ZE = zeolites, and CA = calcite. Lithologic units: MR = moat rhyolite, ER = early rhyolite, BT = Bishop Tuff. The cross pattern on the left margin indicates the intensity of fracturing. The hatched pattern between portions of the SM and IL columns indicate the presence of both minerals.



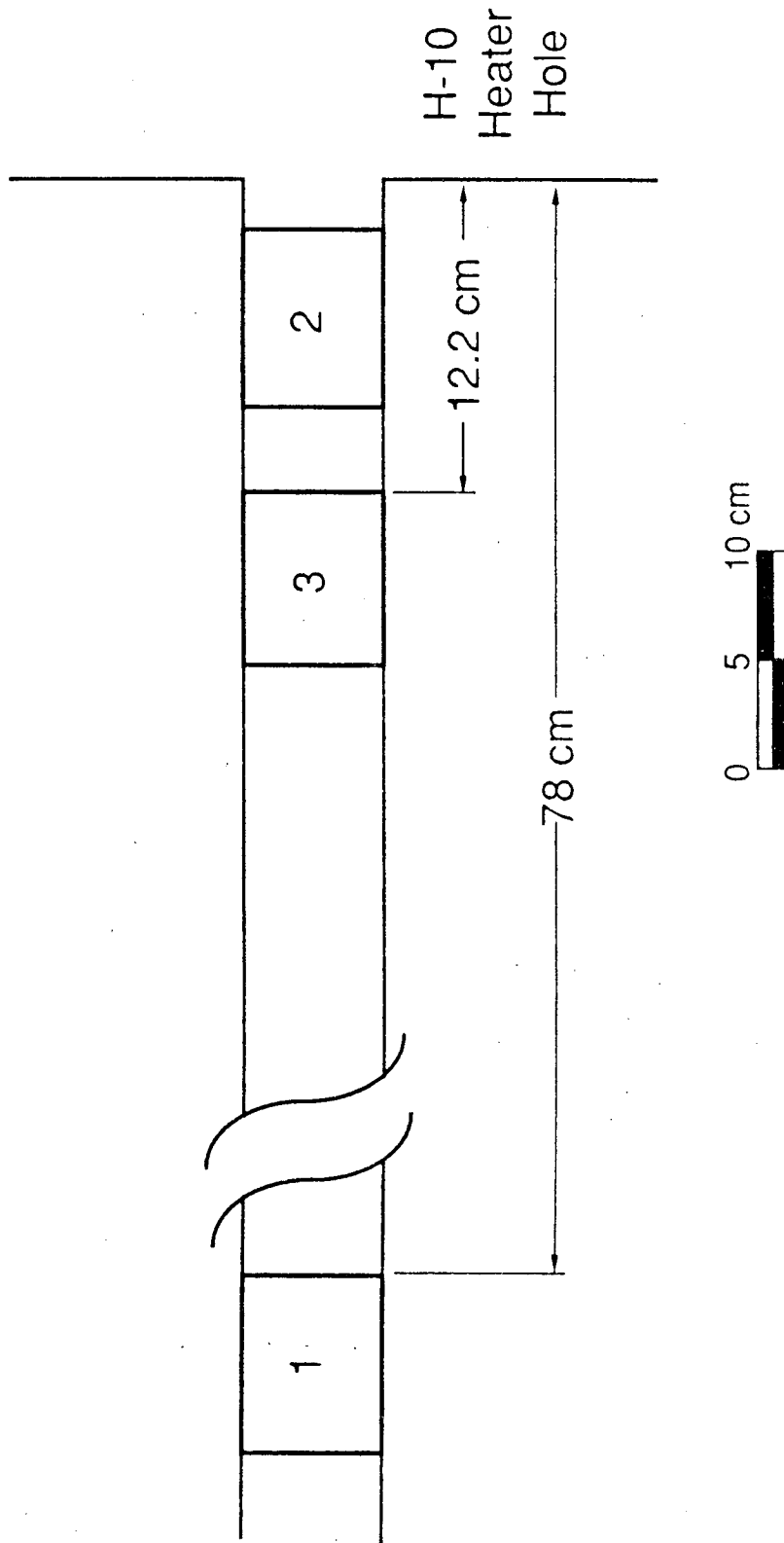
XBL 829-2389

Figure 5. (A) Measured temperatures following turn-on of the peripheral heaters, at varying distances from the H-10 heater hole along heater midplane (from Javandel and Witherspoon, 1981). (B) Projected temperature fields in rock surrounding the H-10 heater array along heater midplane (from Chan et al., 1980).



XBL 829-2391

Figure 6. Vertical cross-section through the H-10 heater hole and the heater and extensometer drifts, showing the location of drillback holes and core samples for seismic studies.



XBL 8711-10452

Figure 7. Detail of locations of drillback core samples for seismic studies.

P-AMPLITUDE vs. PRESSURE

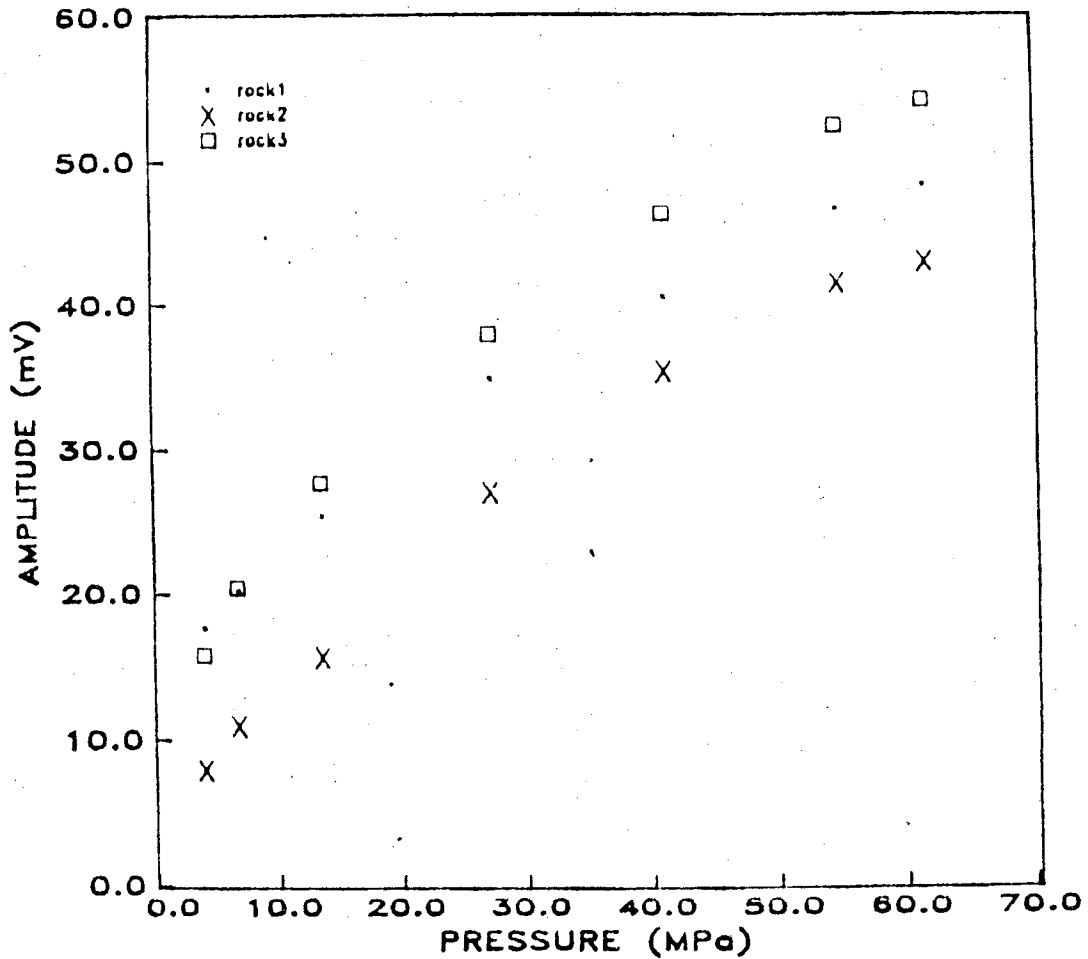


Figure 8. Variation of peak-to-peak amplitude of P-wave signals through the core samples as a function of pressure. Sample 2 was nearest the heater, sample 3 the furthest.

S-AMPLITUDE vs. PRESSURE

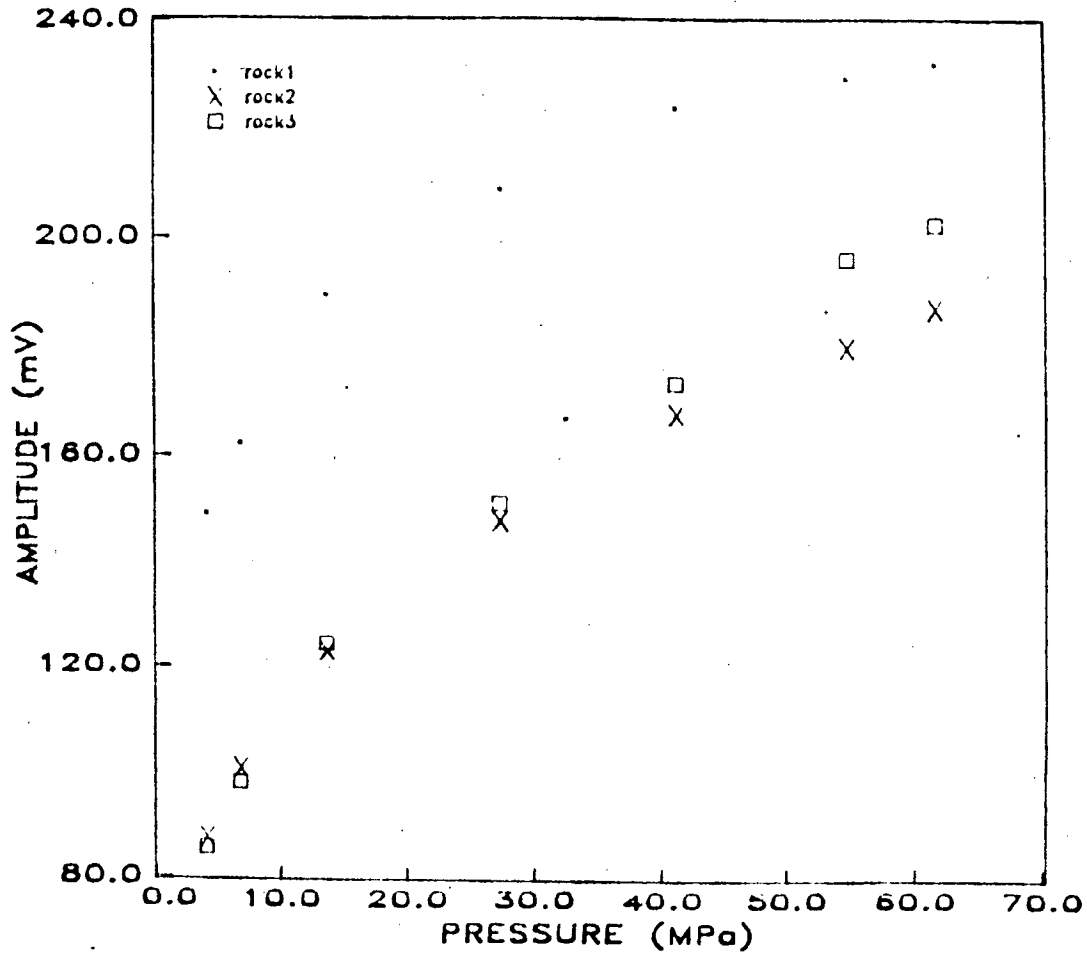


Figure 9. Variation of peak-to-peak amplitude of S-wave signals through the core samples as a function of pressure. Sample 2 was nearest the heater, sample 3 the furthest.

Fracture Stiffness and Aperture as a Function of Applied Stress

D.L. Hopkins, L.R. Myer, and N.G.W. Cook

Understanding how single fractures deform under stress has important applications in a number of fields. For example, being able to predict how fluids move through rock is a fundamental concern in ensuring the stability of underground engineering structures, maximizing petroleum and geothermal energy recovery, and controlling toxic wastes. Since fractures are the major conduits of fluid flow in many rocks, it is necessary to be able to describe changes in fracture aperture with changes in stress to predict fluid flow through fractured rock.

Another area of application is geophysics where it is important to understand how fractures influence the physical quantities being measured. One property of a single fracture of particular interest is specific stiffness which defines the relationship between applied stress and fracture deformation. A theory has been developed which completely specifies the reflection, refraction, and transmission of seismic waves incident upon a fracture based on its stiffness (Schoenberg, 1980).

Most laboratory experiments provide information about the average response of a fracture; e.g. average displacement as a function of stress. However, to understand phenomena such as fluid flow and seismic wave transmission through fractured rock requires more detailed information about such attributes as contact area and aperture and knowledge of how they change under load. To that end, an analytical model has been developed and implemented numerically to study the deformation of a single fracture subjected to a normal stress. The model has been used to calculate aperture profiles and specific stiffness for specified fracture

geometries.

THE MODEL

A typical rock fracture can be envisioned as a number of areas of contact surrounded by voids. The geometry of the voids and the aperture are likely to be quite variable. A common approach to modeling the mechanical deformation of fractures has been to represent the fracture surfaces as parallel planes separated by asperities of varying height. Greenwood and Williamson (1966) modeled the contact between a plane and a nominally flat surface covered by a large number of asperities with heights described by a specified statistical distribution. The asperity tips were taken to be spherical and their deformation calculated from the Hertzian solution for an elastic sphere in contact with a plane. Their model was extended by Greenwood and Tripp (1971) to the case of two rough surfaces in contact. Gangi (1978) used what he termed a *bed of nails* model to describe the permeability of a fractured porous rock as a function of confining pressure. The asperities were modeled as rods with equal spring constants and heights following a power law distribution. Brown and Scholz (1985, 1986), like Greenwood and Williamson, assumed the asperity tips to be spherical and modeled their deformation using the Hertzian solution. However, they also included a term for tangential stresses arising from the oblique contact of spheres so that the stresses at the contacts are not restricted to be normal. Implicit in all the asperity models discussed above is the assumption that the contacts are sufficiently far apart so that they do not interact mechanically. Further, the closure of the fracture is based solely on the deformation of the asperities between the opposing fracture surfaces.

The model developed for the studies discussed here is also an asperity model but differs from those described above in two important ways. First, the constraint that the deformation at a contact point is independent of the other asperi-

ties is removed. Secondly, the deformation of the half-spaces defining the fracture is accounted for in addition to the deformation of the asperities. This formulation can lead to significant changes in void geometry with increasing stress that are not observed when only the deformation of the asperities is considered. An accurate description of the void geometry is important in predicting fluid flow through the fractures because of the highly nonlinear relationship between fluid flow and aperture (Iwai, 1976; Witherspoon, et al., 1980; and Pyrak-Nolte et al., 1987).

For the results presented here, the asperities are modeled as circular disks of varying height. The model was originally developed to calculate the specific stiffness of idealized fractures created in the laboratory to study seismic wave propagation. The model has been extended so that a distribution of heights can be assigned to the asperities (Hopkins et al., 1987). The asperities are not assumed to be mechanically independent. Rather, the force carried by each asperity depends on its height and the heights and proximity of neighboring asperities. The deformation of the asperities is calculated from the elastic compression of the disks. The deformation of the half-spaces defining the fracture is calculated using the Boussinesq solution for displacement beneath a loaded circle assuming a constant stress boundary condition. The deformation at any point on the half-planes is assumed to be a linear combination of the displacements caused by the forces acting on all asperities in the region. The calculation of specific stiffness is based on the average deformation of the fracture surfaces and asperities.

CHANGES IN FRACTURE APERTURE WITH STRESS

An important area of research in recent years has been the investigation of the conditions under which flow through a fracture can be described by the cubic law for laminar flow; i.e. flow is proportional to the cube of the fracture aperture. If the adjacent sides of a fracture are not in contact, experiments indicate that the

cubic relationship holds (e.g. Snow, 1965 and Iwai, 1976). In reality, rock fractures are not usually open; rather, they are better described as two rough surfaces in contact at a number of asperities. The number of contact points increases with increasing normal stress across the fracture (Goodman, 1976 and Pyrak-Nolte et al., 1987). However, fractures in rock are sufficiently rough so that even under high stresses, the area of contact between the fracture surfaces may be less than 60 percent (Pyrak-Nolte et al., 1987). Thus, even deep below the Earth's surface, fractures may be important conduits for fluid flow.

Deviations from the cubic law have been observed by a number of researchers who have analyzed data from laboratory experiments using both induced and natural fractures (e.g. Iwai, 1976; Witherspoon et al., 1980; Engelder and Scholz, 1981; and Raven and Gale, 1985). For natural fractures, departures from the cubic law are seen even at relatively low stress levels on the order of 10 MPa. The divergence increases with increasing stress.

A possible explanation for the divergence from the cubic law is the change in fracture topography that occurs with increasing stress. The change in aperture geometry can be illustrated in two-dimensions. Figure 1a shows a two-dimensional slice through an idealized fracture with the dotted lines representing reference planes. If only the deformation of the asperities is considered, and a normal stress is applied, the reference lines remain parallel and come together by an amount that depends on the deformation of the contacts. For the case of a simple interpenetration model, the surfaces come together in a manner equivalent to allowing the top and bottom fracture surfaces to overlap as illustrated in Figures 1b-1d. If instead, the asperity tips are modeled as spheres and the Hertzian solution is used to calculate the deformation of the tips, the reference planes still remain parallel and come together an amount equal to the deformation of the asperities. For both cases, the dimensions of the asperities themselves are impor-

tant, but their spatial location on the fracture surface is not.

For comparison, the model described herein was used to calculate the displacement across the same idealized fracture pictured in Figure 1a. To apply the model, the fracture surface is first discretized as shown in Figure 2a. When a normal force is applied, the reference lines no longer remain parallel because the asperities indent the half-spaces defining the fracture. This is illustrated in Figures 2c and 2d where the dashed lines show the calculated deformation of the reference planes.

Adding in the deformation of the half-plane results in much greater changes in fracture aperture than would occur if just the deformation of the asperities were considered. To see this, compare Figure 2d to Figure 1c. In 1c, the reference lines have come together 22.6% compared to their original position under zero load. In 2d, the average displacement of the two reference planes is 25.7%. Even though the displacement of the reference planes is roughly equal, Figure 2d shows a greater reduction in aperture and appreciable changes in void geometry.

This change in geometry has important implications for fluid flow through the fracture. The asperities have the effect of propping the fracture open while more than average closure occurs in open areas. To illustrate, consider the idealized case of a single circular asperity between two parallel fracture surfaces as pictured in cross-section in Figure 3a. Under zero load, the fracture aperture b is everywhere equal and fluid flow is proportional to b^3 (Snow, 1965). As the load is increased, the fracture surfaces deform as illustrated in Figure 3b. The aperture at the asperity is $b - \delta$ where δ is the deformation of the asperity. The high aperture pockets formed around the asperity are everywhere surrounded by a region of smaller aperture (a). Under stress, the large voids formed around asperities will affect the storativity of the fracture whereas the permeability will be largely controlled by the smaller aperture regions adjacent to the voids.

The change in fracture topography that occurs can be seen by looking at aperture contours for a three-dimensional array of disks. Figure 4 shows aperture contours and the displacement of the fracture surface for an array of 10 disks for two different stress levels. Under low stress, the aperture is relatively uniform as shown in Figure 4a. At higher stresses, the asperities begin to indent the fracture surfaces creating high aperture pockets and steep gradients as indicated in Figure 4b. Work will continue to study the relationship between this change in fracture geometry and fluid flow. Deviations from the cubic law that are observed in laboratory experiments are likely due, at least in part, to these changes in fracture topography with increasing stress.

SPECIFIC STIFFNESS

Specific stiffness is a property that defines the relationship between applied stress and fracture deformation. More formally, specific stiffness is defined as the average applied stress divided by the average displacement across the fracture interface in excess of the displacement that would occur if the fracture were not present. Laboratory experiments on single fractures in rock indicate that specific stiffness is initially a sharply rising function with stress that levels off and approaches a constant value (e.g., Goodman, 1976; Bandis et al., 1983; and Pyrak-Nolte et al., 1987).

To begin to understand what properties of the fracture surface are important in determining specific stiffness, the model described previously was used to perform a parameter sensitivity study. In particular, the effect of the asperity height distribution was studied. It is the distribution of heights that determines the rate at which asperities come into contact with increasing stress. The values of specific stiffness calculated using the model were compared with laboratory measurements.

In developing realistic fracture models, it is important to consider the spatial

correlation of the asperity locations and heights. Nonetheless, as a first step in demonstrating the model, we have considered disks of equal diameter (1 mm) distributed randomly across a planar surface. In reality, fracture surfaces are irregular rather than planar and parallel. However, the deformations calculated for the idealized parallel surfaces can be superposed on the actual irregular surfaces to obtain the true profile.

Curves of specific stiffness were generated using 100 disks distributed in an area of 3.14 cm^2 as shown in Figure 5. The maximum contact area in this case is 25% when all disks are in contact. Using this spatial distribution, specific stiffness as a function of applied stress was calculated for a variety of height distributions. The resulting curves, and histograms of the height densities, are plotted in Figure 6. The results show that for a fixed spatial geometry, a wide range of behavior can be obtained by varying the distribution of heights of the asperities. In all cases, the stiffness curve rises sharply as increasing numbers of asperities come into contact and then begins to level off as the rate at which asperities come into contact diminishes. Eventually, the curve will asymptote when there is no increase in contact area with increasing stress.

For comparison, the specific stiffnesses calculated using the model are compared to a curve obtained by L. Pyrak-Nolte et al. (1987) in the laboratory for a granite core sample with a fracture oriented perpendicular to the axis of the core. In making the model calculations, a Young's Modulus of 50.0 GPa and a Poisson's ratio of 0.2 was used to coincide with the values of the granite used in the laboratory experiment. For the laboratory data, specific stiffness was calculated by taking the inverse of the tangent slope to the stress vs. displacement curve. The curve obtained from the laboratory data is plotted in Figure 6 as the bold line. As can be seen from the figure, the curves obtained using the model, assuming a maximum contact area of 25% and asperity heights distributed

between zero and 100 microns, bracket the results obtained in the laboratory for this particular specimen. The best matches are with curves 3 and 4 which have height distributions that are more tightly clustered than those used to generate curves 1 and 2.

The horizontal lines in Figure 6 show the maximum stiffness that can be achieved using the particular spatial configuration shown in Figure 5. The curves represent the limiting case that occurs when all asperities are of equal height. Curves 5, 6, and 7 correspond to asperity heights of 30, 50, and 80 microns, respectively. The difference between the lines is due to the difference in the compressibility of the asperities; the shorter asperities are less compressible and thus create a stiffer interface. The small difference between the lines indicates that the absolute asperity height is not as important as the distribution of heights.

CONCLUSIONS

In modeling the behavior of a single fracture with an asperity model, it has been shown that accounting for the deformation of the half-spaces defining the fracture leads to greater reductions in aperture than would be calculated if only the deformation of the asperities were considered. In addition, the spatial geometry of the asperities becomes important leading to differential deformation of the fracture surfaces that can result in significant changes in void geometry. This change in aperture geometry with stress has particularly important implications for fluid flow calculations.

In previous work it was demonstrated that the spatial geometry of the asperities and their dimension are important parameters in determining fracture stiffness (Hopkins et al., 1987). For a constant contact area, small, dispersed contact points form a stiffer interface than large or clustered contact areas. Results discussed here show that the distribution of asperity heights affects both the shape

and magnitude of the stress-stiffness curve. The more nearly equal the heights, the stiffer the fracture is. The distribution of heights is found to be more important than the absolute height. Finally, the analytical model presented here has been shown to yield values for specific stiffness that are consistent with those observed in the laboratory for single fractures in natural rock.

REFERENCES

- Bandis, S.C., A.C. Lumsden and N.R. Barton, Fundamentals of rock joint deformation, *Int. J. Rock Mech. Min. Sci. Geomech. Abstr.*, 20, 249-268, 1983.
- Brown, S.R. and C.H. Scholz, Closure of random elastic surfaces in contact, *J. Geophys. Res.*, 90, 5531-5545, 1985.
- Brown, S.R. and C.H. Scholz, Closure of rock joints, *J. Geophys. Res.*, 91, 4939-4948, 1986.
- Engelder, T. and C.H. Scholz, Fluid flow along very smooth joints at effective pressures up to 200 megapascals, in *Mechanical behavior of crustal rocks*, *Am. Geophys. Union Monogr.*, vol. 24, pp. 147-152, AGU, Washington D.C., 1981.
- Gale, J.E., Comparison of coupled fracture deformation and fluid flow models with direct measurements of fracture pore structure and stress-flow properties, in *Rock Mechanics: Proc. of the 28th U.S. Symp.*, edited by I.W. Farmer, J.J.K. Daemen, C.S. Desai, C.E. Glass, and S.P. Neuman, pp. 251-261, A.A. Balkema, Rotterdam, 1987.
- Gangi, Anthony F., Variation of whole and fractured porous rock permeability with confining pressure, *Int. J. Rock Mech. Min. Sci.*, 15, 249-257, 1978.
- Goodman, R.E., *Methods of geological engineering in discontinuous rocks*, 172p., West Publishing, New York, 1976.
- Greenwood, J.A. and J.H. Williamson, Contact of nominally flat surfaces, *Proc. R. Soc., London, Ser. A.*, 295, 300-319, 1966.
- Greenwood, J.A. and J.H. Tripp, The contact of two nominally flat rough surfaces, *Proc. Inst. Mech. Engr.*, 185, 625-633, 1971.
- Hopkins, D.L., N.G.W. Cook and L.R. Myer, Fracture stiffness and aperture as a function of applied stress and contact geometry, in *Rock Mechanics: Proc. of the 28th U.S. Symp.*, edited by I.W. Farmer, J.J.K. Daemen, C.S. Desai, C.E. Glass, and S.P. Neuman, pp. 251-261, A.A. Balkema, Rotterdam, 1987.
- Iwai, K., Fundamental studies of fluid flow through a single fracture, Ph.D. thesis, Univ. of Calif., Berkeley, 1976.
- Pyrak-Nolte, L.J., L.R. Myer, N.G.W. Cook and P.A. Witherspoon, Hydraulic and mechanical properties of natural fractures in low permeability rock, in *Proc. of the Sixth International Congress on Rock Mechanics*, edited by G. Herget and S. Vongpaisal, A.A. Balkema, Rotterdam, 1987.
- Raven, K.B. and J.E. Gale, Water flow in a natural rock fracture as a function of stress and sample size, *Int. J. Rock Mech. Min. Sci. Geomech. Abstr.*, 22, 251-261, 1985.
- Snow, D.T., A parallel plate model of fractured permeable media, Ph.D. thesis, Univ. of Calif., Berkeley, 1965.

Witherspoon, P.A., J.S.Y. Wang, K. Iwai, and J.E. Gale, Validity of cubic law for fluid flow in a deformable rock fracture, *Water Resour. Res.*, 16, 1016-1024, 1980.

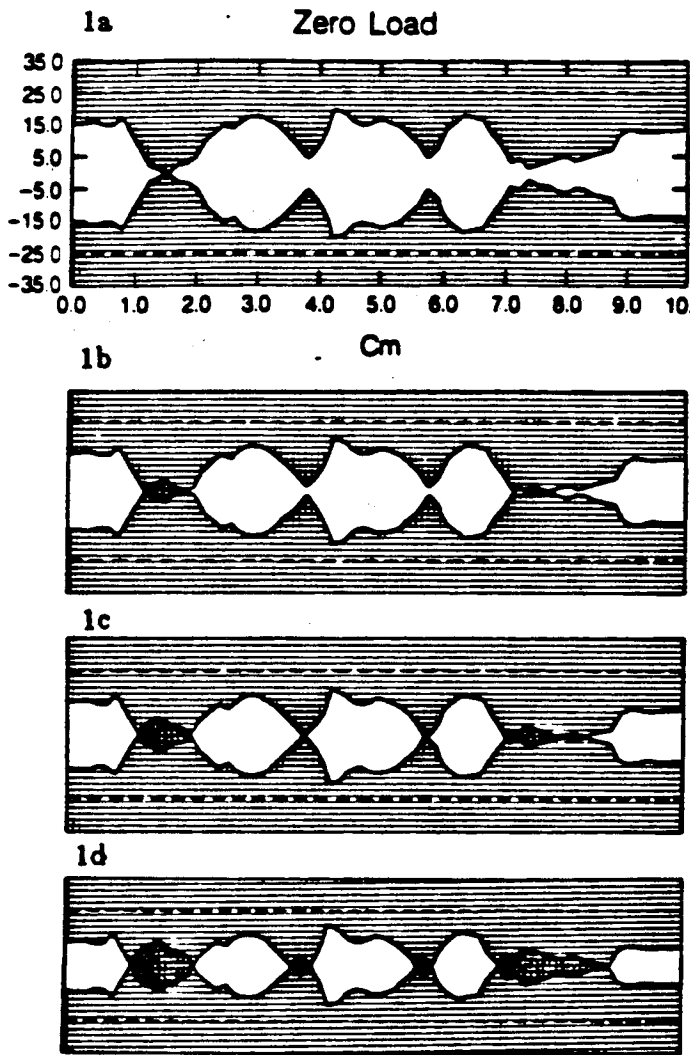


Figure 1. Schematic diagram of the change in aperture with increasing stress for a cross-section through an idealized fracture assuming a simple interpenetration model. The reference lines have come together 13%, 23%, and 32% in Figures 1b, 1c, and 1d, respectively.

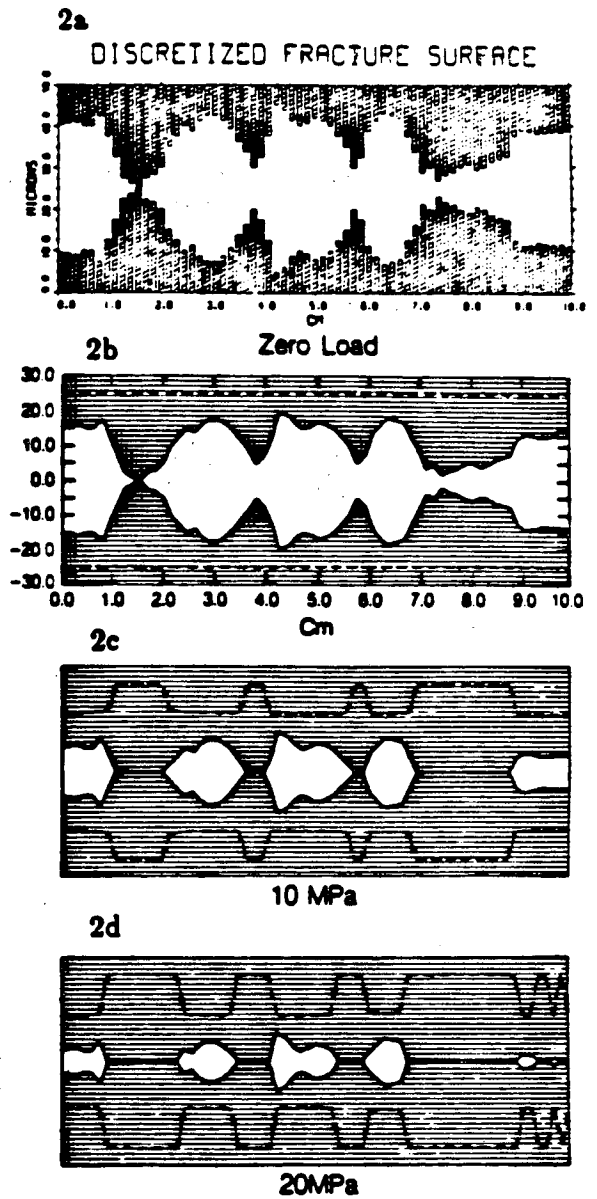


Figure 2. Calculated change in aperture with increasing stress using the model described in Section 2 for the same idealized fracture pictured in Figure 1a. The reference lines have come together 17% and 26% in Figures 2c and 2d, respectively.

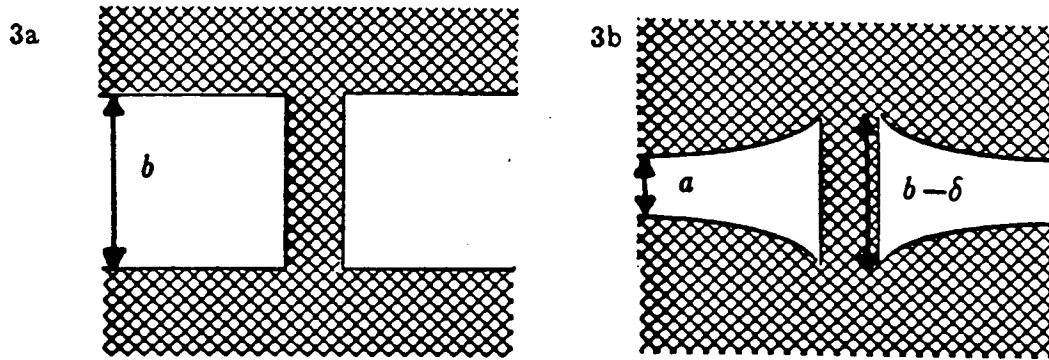


Figure 3. Cross-section of aperture for a single asperity between parallel plates under zero load (a) and after a load is applied (b).

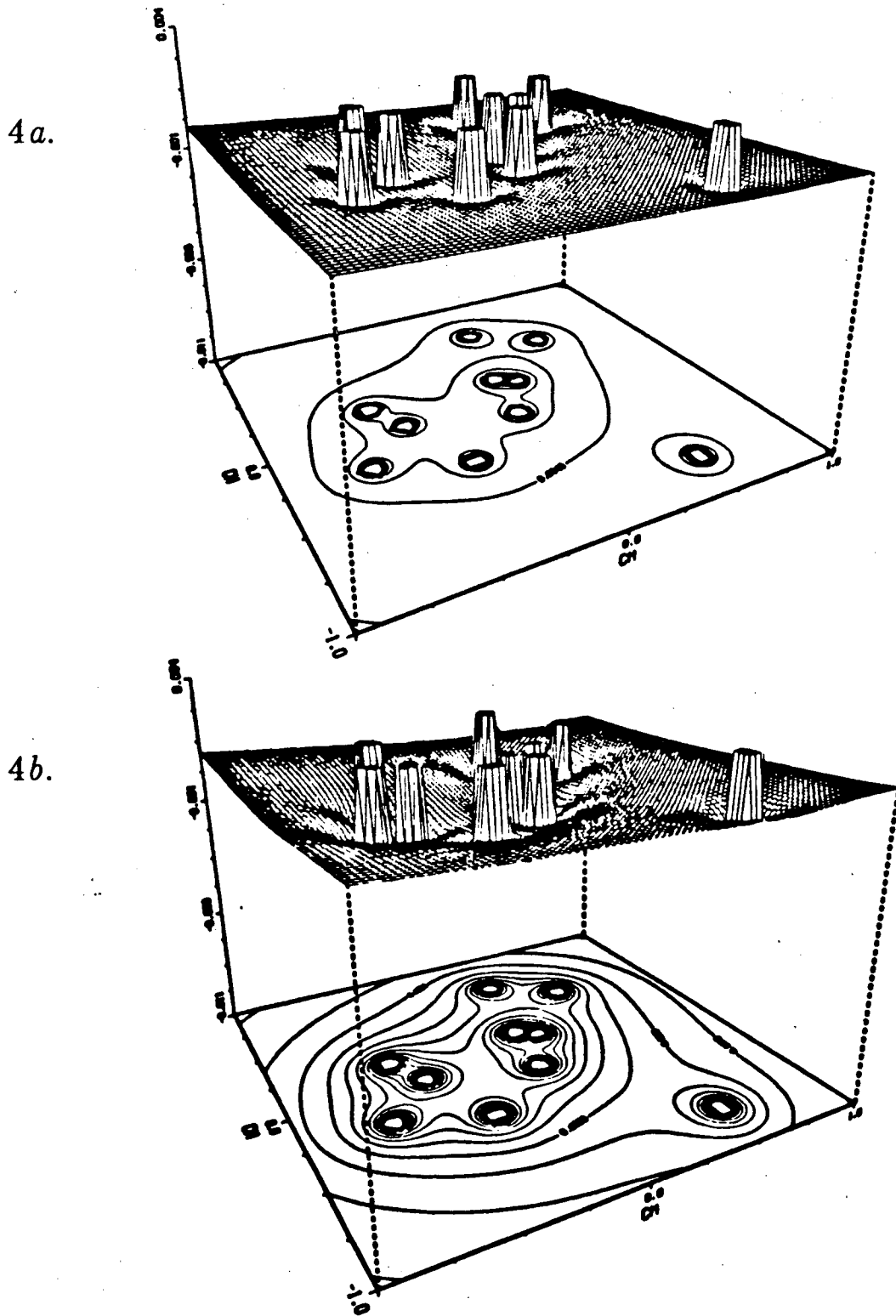


Figure 4. Aperture contours and the displacement of the fracture surface at two stress levels. Under low stress (16.6 MPa), the aperture is relatively uniform (4a). At higher stresses (50 MPa), the asperities begin to indent the fracture surfaces creating high aperture pockets and steep gradients as indicated in 4b.

DISC LOCATIONS (25% MAXIMUM CONTACT AREA)

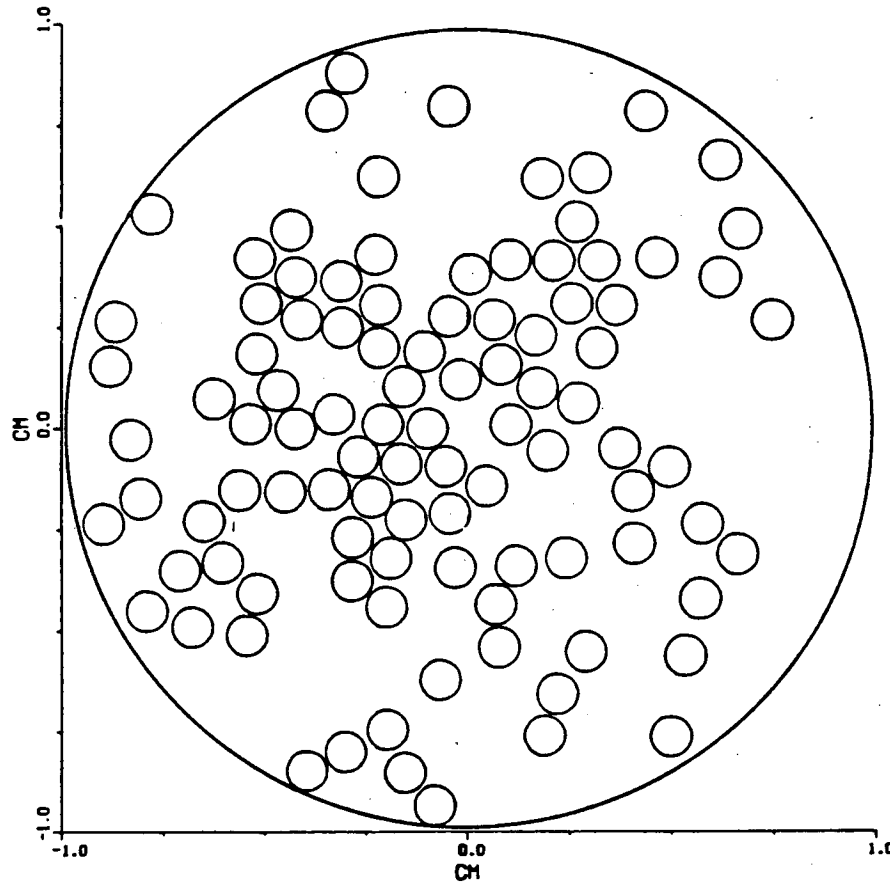


Figure 5. Spatial orientation of disks used to generate the curves of stress vs. specific stiffness plotted in Figure 6. Disk diameter is 1mm.

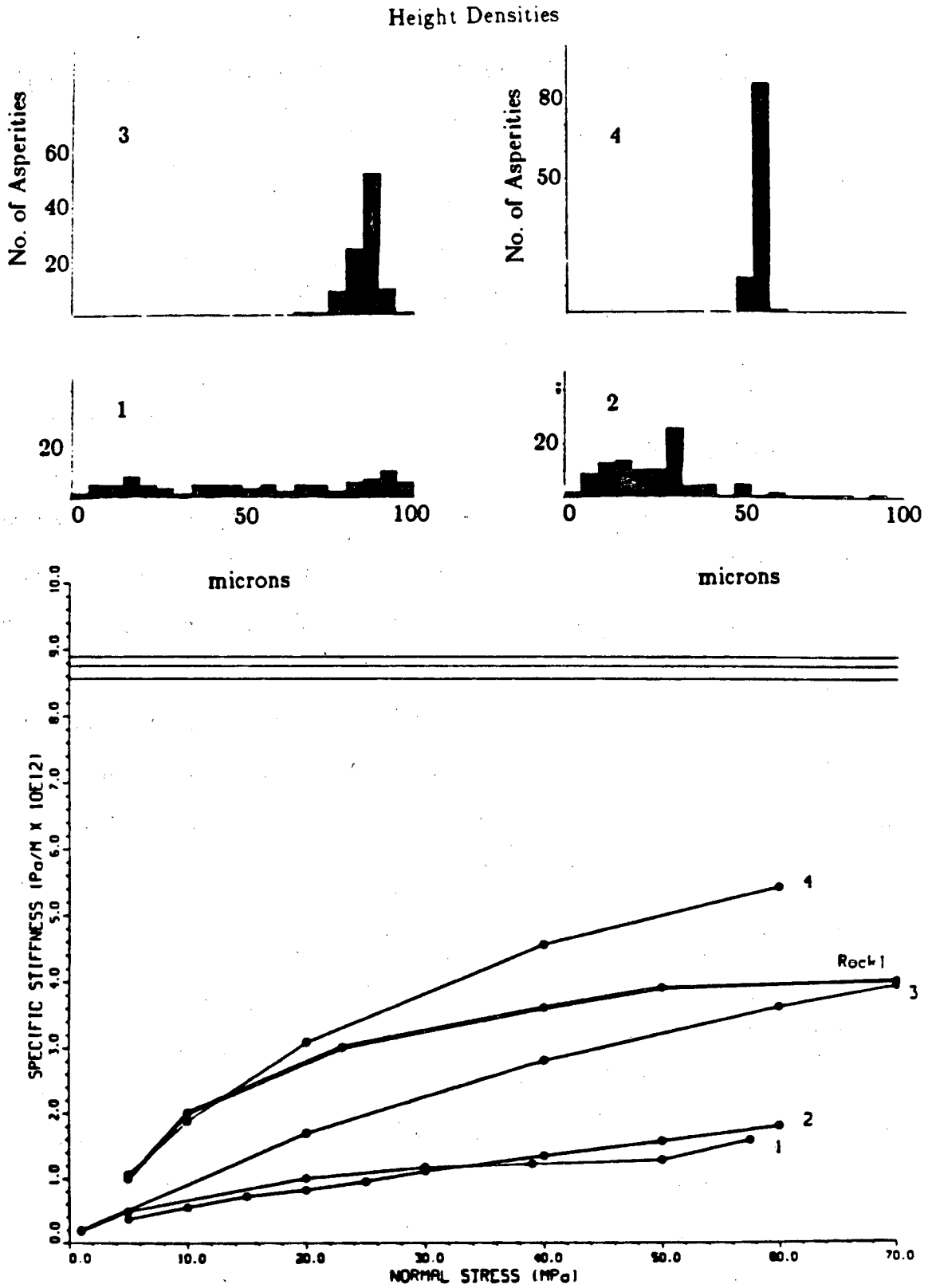


Figure 6. Curves (1-4) of stress vs. specific stiffness for the spatial geometry shown in Figure 5 and different height distributions (plotted as histograms). The bold line is a curve obtained from laboratory data for a granite core specimen containing a single fracture. Lines 5-7 are the values of stiffness calculated assuming the asperities to be of equal height (heights of 30, 50 and 80 microns, respectively).

Channeling Characteristics of Flow and Solute Transport through a Rough-Surfaced Fracture

*Y. W. Tsang, C. F. Tsang, F. V. Hale,
L. Moreno⁺, and I. Neretnieks⁺*

INTRODUCTION

There are experimental evidences (both on the laboratory scale and in the field) that fluid flow in a single fracture does not occur evenly in a fracture plane, but that majority of the flow takes place in a limited number of preferred paths. We present here our investigations of flow in two dimensions, corresponding to the physical situation of flow in single fractures. By solving for the flow using the Laplace equation in two-dimensions, we would like to understand the flow characteristics in single fractures and to identify the key parameters that control the channeling flow pattern, thus affording a way to interpret single fracture field and laboratory experiments which exhibit channeling behavior.

METHOD AND RESULTS

Here we outline the numerical model to calculate the fluid flow and solute transport through a single fracture with variable apertures. The fracture plane is partitioned by grids with different aperture values assigned to each square enclosed by grid lines. The spatially varying apertures in the single fractures are generated using geostatistical method, based on a given aperture density distribution and a specified spatial

⁺ Department of Chemical Engineering Royal Institute Of Technology S-100 44 Stockholm, Sweden

correlation length. Figure 1 shows two realizations of statistically generated apertures with identical mean and variance of the log-normal aperture density distribution. Figure 1a differs from Figure 1b only in the spatial correlation length of the apertures. The correlation length is expressed in terms of a fraction of the linear extent of the square generated region, it is 0.1 in Figure 1a and 0.4 in Figure 1b. The variation of the apertures is represented by the different shading of the mesh, the darker the shading, the smaller the aperture.

The square region of unit area of Figure 1 therefore represents a single fracture with spatially correlated variable apertures as a flow region. Constant head boundary conditions were assumed for the left and right boundaries, no flow conditions were assumed for the other two boundaries. The local resistance to the fluid flow was assumed to vary inversely as the cube of the local aperture. The fluid potential at each mesh intersection was computed and the steady state flow rates between all adjacent nodes were obtained. The flow rates between the nodes vary over several orders of magnitudes. To display the variation of the large range of flow rates over the entire fracture, the volumetric flow rates are plotted in Figure 2, where the thickness of the lines joining nodes varies as the square root of the flow rate. We have carried out this kind of simulation for many realizations of the aperture variation (Tsang et al., 1987; Moreno et al., 1987). We found that the flow patterns always display the preferred paths of large volumetric flow rates that are formed because of the variation of the apertures within the single fracture plane; and that there is a tendency for all the flow paths of large flow rates to coalesce into a "channel" on the order of one spatial correlation length in width, and the spacing between these large flow rate "channels" also is on the order of the spatial correlation length of the fracture apertures.

Solute transport phenomena are investigated by tracking the particles advected through the fracture. Particles are let in at the left hand (higher constant head) boundary in Figure 1 and collected at the right hand (lower constant head) boundary. A plot

of the number of particles collected at all the outlets on the right hand boundary at different arrival times constitutes the breakthrough curve. In general, the breakthrough curves of tracer transport in two dimensions through these variable-aperture fractures have a fast rise at early times, since the majority of particles take the fast flow paths; then there is a long tail in the breakthrough curve due to a small fraction of particles meandering through the fracture, including in their flowpaths many sections with extremely small volumetric flow rates. Our results show that the dispersion displayed by these breakthrough curves, as measured by the ratio of the difference of 90% and 10% concentration arrival times to the mean arrival time, do not vary significantly with different statistical realizations of apertures nor with different correlation lengths. This follows from the fact that these breakthrough curves involve the residence times of all possible flow paths which originate from the injection line on the left boundary and terminate on the exit line of the right boundary, and both boundaries cover several correlation lengths. So the information contained in the breakthrough curves is an average over several correlation lengths, hence the insensitivity to statistical realization and correlation length value.

On the other hand, the spatial pattern of tracer breakthrough seems to depend very much on the spatial correlation length of the aperture variation in the single fracture. The tracer breakthrough characteristics as a function of space are shown in the contour plot of the number of particles in Figures 3 and 4. The x axis represents the spatial axis of the left hand boundary in Figure 1, which is the boundary for inlets. The y axis represents the spatial axis of the right hand boundary, which is the boundary for outlets. In experimental measurements, information as to the position of the outcoming tracer are represented by the y coordinate of the tracer concentration in Figures 3 and 4. The position from which the outcoming tracer originates is contained in the x coordinates; this information can be obtained experimentally only when different tracers (e.g., different dyes) are introduced at different locations at the input boundary.

The contours denote the particle number that enter or exit the single fracture. These figures show that the fast flow paths for tracer transport tend to coalesce into "channels" with width and spacing on the order of one spatial correlation length. A comparison of Figure 3 with Figure 4 shows the difference of flow pattern between the cases with correlation 0.1 and 0.4. This kind of plot of measurable data may be a possible means to estimate the spatial correlation lengths of the system. More work is needed to develop this further.

CONCLUSION

The variable-aperture character of a fracture causes its fluid flow and tracer transport properties to be quite different from those derivable from the parallel-plate model of the fracture. To understand the character of fracture flow and transport requires new measurements and analysis methods. In this report, the channeling of fluid flow and tracer transport in a single fracture has been demonstrated. Based on our calculations in two-dimensions here, we recommend point injection measurements such as Figures 3 and 4 which probe the spatial correlation length of the aperture heterogeneities in the single fracture. Our calculations also show that if one employs line injection and line collection of tracers, where the measurement line lengths cover a few correlation lengths, then the resultant breakthrough curves tends to be more stable and not so sensitive to the local heterogeneities, and therefore may be analyzed to elucidate the dispersivity of the system.

REFERENCES

- Tsang, Y. W., C. F. Tsang, F. V. Hale, L. Moreno and I. Neretnieks, Channeling characteristics of flow and solute transport through a rough-surfaced fracture, LBL Report 23195, 1987.

Moreno, L., Y. W. Tsang, C. F. Tsang, F. V. Hale and I. Neretnieks, Flow and tracer transport in a single fracture: a stochastic model and its relation to some field observation, submitted to Water Resources Research, 1987.

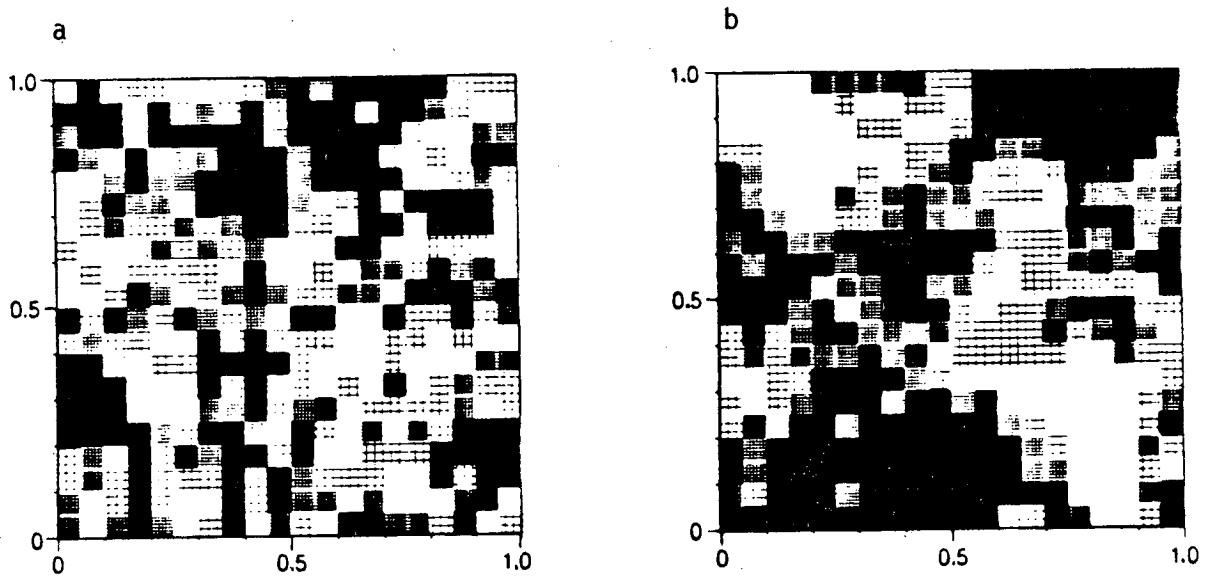


Figure 1. Statistically generated apertures in the plane of a single fracture of linear dimension 1.0, with a spatial correlation length of 0.1 (a) and 0.4 (b) respectively.

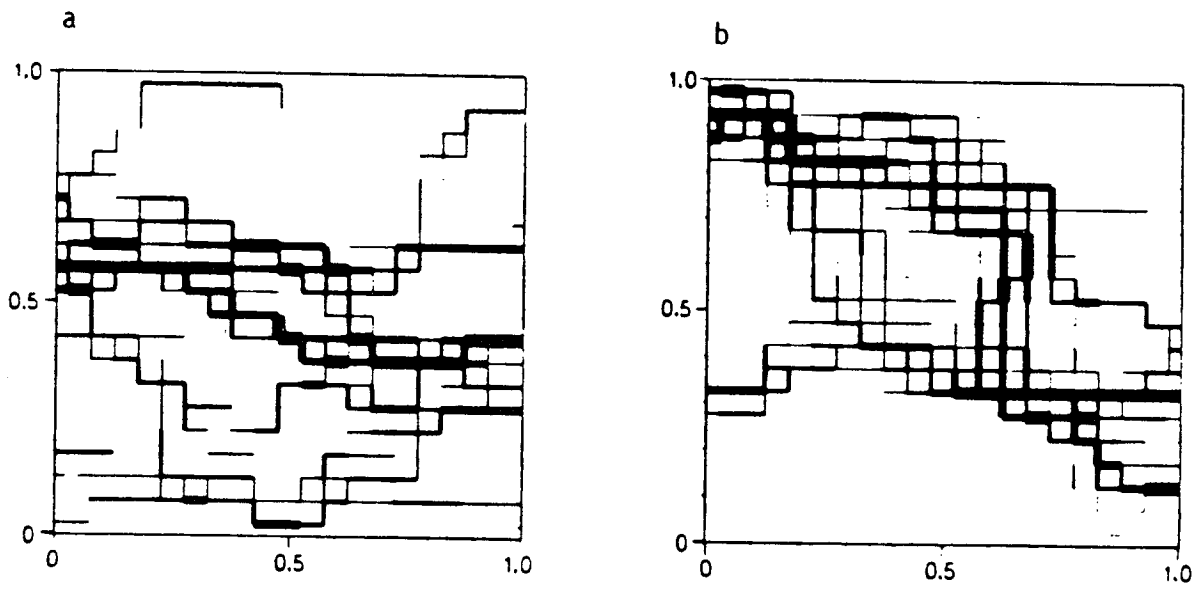
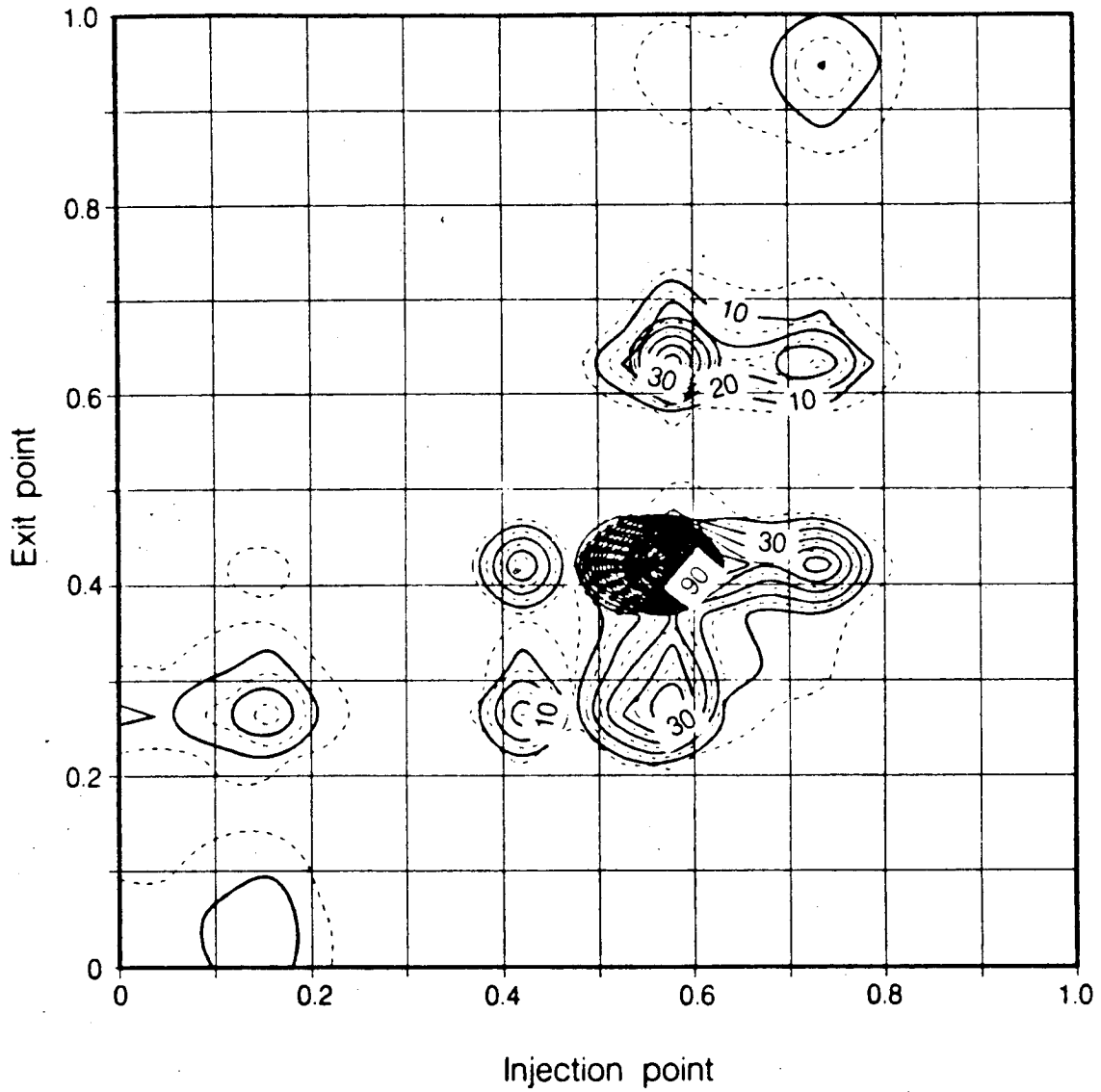


Figure 2. Fluid flow rates for the fractures with aperture variation as shown in Figure 1. The thickness of the lines is proportional to the square root of the flowrate. Cases (a) and (b) correspond to spatial correlation length of 0.1 and 0.4 respectively.

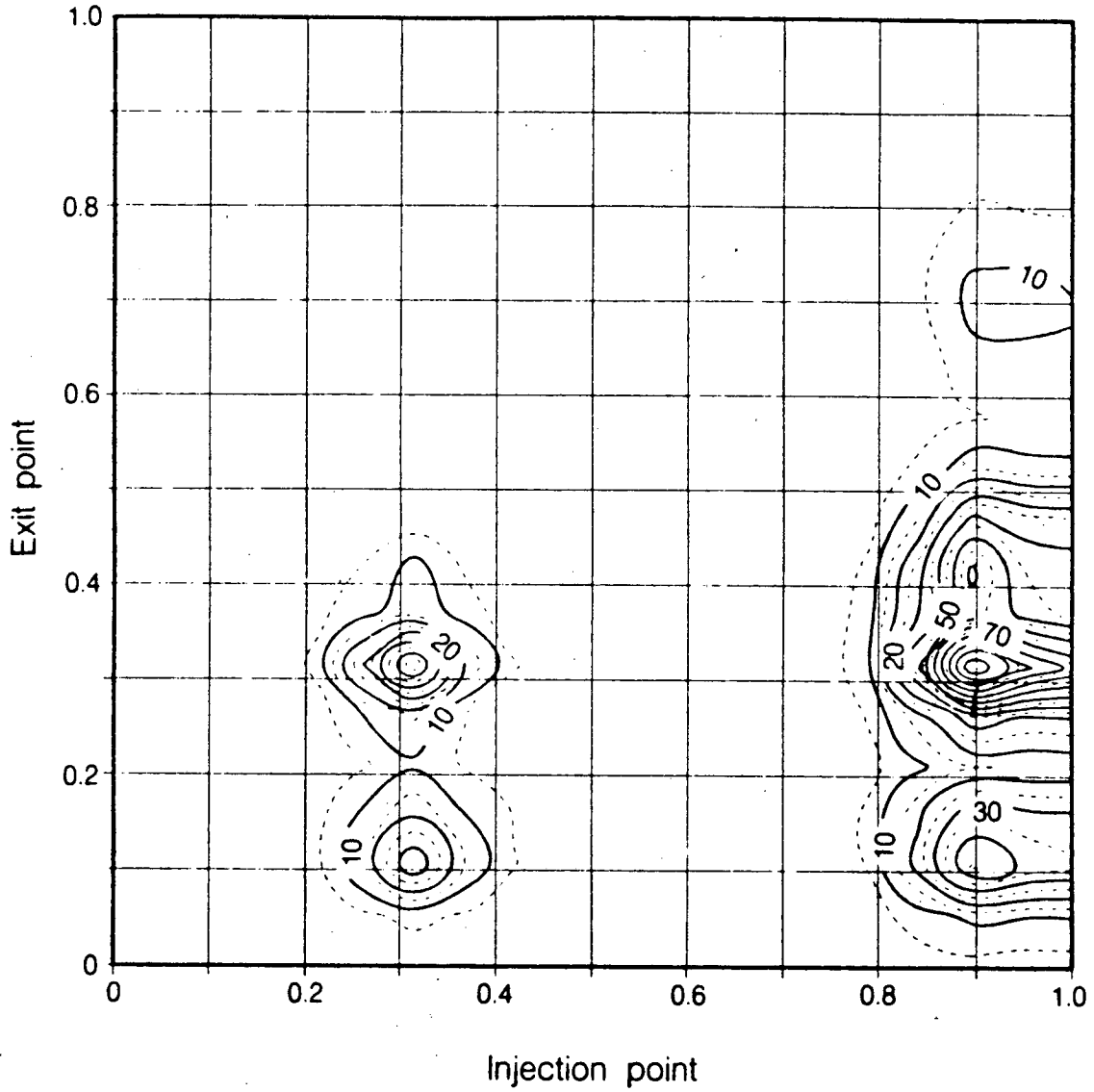
Transfer matrix
run 513



XBL 875-9677

Figure 3. Contours of particle number as a function of tracer entrance location and collection location, for a fracture with aperture variation as shown in Figure 1a.

Transfer matrix
run 544



XBL 875-9680

Figure 4. Contours of particle number as a function of tracer entrance location and collection location, for a fracture with aperture variation as shown in Figure 1b.

Tracer Transport in Fractured Media—a Variable-Aperture Channel Approach

Y. W. Tsang and C. F. Tsang

INTRODUCTION

There are field evidences that fluid flow in fractured crystalline rock mass is very unevenly distributed and takes place in selected preferred paths. This is the flow channeling phenomenon, which seems to be present in both three-dimensions for a network of fractures and in two-dimensions in a single fracture. We have developed (Tsang and Tsang, 1987) a theoretical approach to treat the fluid flow as through a system of statistically equivalent one-dimensional flow channels. Each channel has variable apertures along its length which conform to a given aperture density distribution and a spatial correlation length. By including only the essential physics of flow through a tight medium in this conceptual model, we seek to analyze flow and transport data in two and three dimensions in a highly heterogeneous medium by a system of independent one-dimensional channels, thus simplifying the computation effort enormously. In this report, we shall apply the one-dimensional channel model to the two-dimensional flow and tracer transport in a single fracture. Based on the insight gained, we shall discuss the implications of flow channeling to field measurements and data interpretations.

Interpretation of 2-D Tracer Transport by the Channel Model

Results are presented in the previous article in this report for flow and transport in two-dimensions in a single fracture with spatially correlated variable apertures. The flow through such a heterogeneous system is obtained by solving the Laplace equation for the fluid potentials within the fracture, and the tracer breakthrough is obtained by tracking particles in the steady state flow field. To analyze the two-dimensional results with the one-dimensional variable-aperture channel approach involves:

- (1) determination of the apertures on the particle flow paths from the two-dimensional simulation. Figure 1 shows a typical normalized aperture density distribution for all the apertures in a fracture (broken curve), and for the subset of apertures specifically along the particle flow paths (solid curve). The figure illustrates clearly that the smallest apertures are avoided in two-dimensional flow through a fracture.
- (2) employing the aperture density distribution that characterizes the apertures on the particle flow paths, derived from the previous step, to generate one-dimensional statistically equivalent channels. A breakthrough curve is then derived from the residence times of the set of channels.
- (3) comparing the breakthrough curve derived from the channel model to that of the two-dimensional simulation as shown in Figure 2. The solid curve shows the results for the average of the two-dimensional simulations for eight realizations of aperture variations. The long-dash broken curve is for the average of the one-dimensional channel model calculations using the aperture density distributions as derived in step (2). The horizontal bars give the limits of the spread of values for eight realizations. We also construct a system of constant-aperture channels using the aperture density distribution from step (2). The resultant breakthrough is shown as the short-dash broken curve in Figure 2. Finally, if the entire fracture has only one constant aperture, then the plot in Figure 2 would be a step with

tracer concentration equal to 0 before $t/t_m=1$ and 100% thereafter, implying a piston flow with zero dispersivity. The resultant breakthrough through of such a parallel plate representation of a single fracture is shown as the dot-and-dash curve in the figure.

Figure 2 is plotted with time on the horizontal axis normalized to the mean residence time t_m in order to compare the dispersivity predicted from different models. The actual values of mean residence times from the different models are presented in Table 1. The second column gives the expected values obtained by dividing total fracture volume by the calculated total flow rates in two-dimensions. The third column gives the mean particle residence times from the breakthrough curves derived from particle tracking in two-dimensions. These agree within a few percent of the values in column 2. The fourth column gives the mean residence time from the breakthrough curves derived from the one-dimensional variable aperture channel model. We note that the mean residence times are within a factor of two of those derived from the actual two-dimensional transport. The last column gives the mean residence times obtained from the breakthrough curves derived from a system of constant aperture channels. The mean residence times in this last column are typically two to three orders of magnitude smaller than those predicted from both the two-dimensional and one-dimensional variable-aperture channel representations. This is easy to understand since in the constant-aperture channel representation, the larger the aperture, the shorter the residence time, therefore the average is heavily weighted by the residence times of the largest constant aperture channels.

The qualitative agreement between the results from the one-dimensional variable-aperture channel model and the two-dimensional simulations in both Figure 2 and Table 1 is good. Calculations (Tsang et al., 1987) show that if in tracking the particles in the two-dimensional simulations we group the particles in quartiles according to their residence times within the fracture, and if the aperture parameters of the fastest

quartile of particles are used to generate the variable-aperture channels, then the resultant breakthrough curves agree even better with those from two-dimensional simulations. This paved the way (Tsang et al., 1987) for an inverse calculation to be carried out, in which we determine the aperture parameters which characterize the most conductive flow channels from the two-dimensional fracture breakthrough data.

CONCLUSIONS

In analyzing tracer breakthrough data from transport in a two-dimensional single fracture in terms of statistically equivalent one-dimensional channels, we could back out the coefficient of variance for the aperture distribution along the most conductive flow channels (Tsang et al., 1987). Furthermore, in the variable-aperture channel model the mean residence time, t_m , from tracer measurements reflects the mean aperture of the actual flow channels.

The breakthrough data referred to in this report are comprised of a sum of measurements over a line covering a few correlation lengths. Channeling, by its very definition, implies that flow is very uneven spatially and there may be large areas where the flow and transport is zero. No existing theoretical approach can predict deterministically the tracer flow paths and the tracer breakthrough curve at one particular observation point. Point measurements are hard to interpret in heterogeneous systems. However, for tracer transport which sums over data from multiple-point measurements spanning a few correlation lengths, many channels will be involved and we may be able to use the present model to predict the total tracer breakthrough curve. This underlines the usefulness and importance of making tracer measurements with line tracer injection and line observation of tracer emergence.

REFERENCES

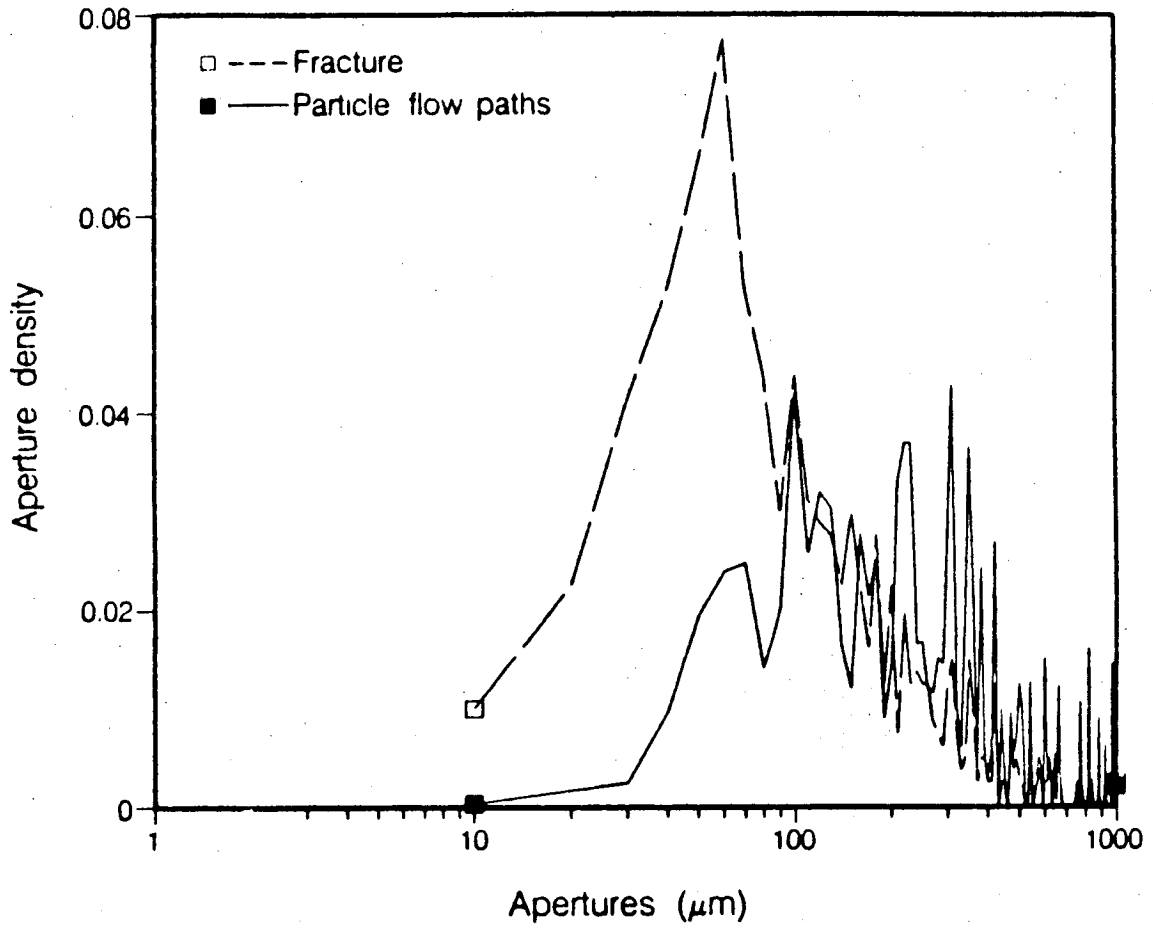
Tsang, Y. W. and C. F. Tsang, Channel model of flow through fractured media, *Water Resources Research*, Vol. 23, No. 3, p. 467-479, 1987.

Tsang, Y. W., C. F. Tsang, I. Neretnieks, L. Moreno, Flow and tracer transport in fractured media, a variable-aperture channel model and its properties, submitted to *Water Resources Research*, 1987.

Table 1. Mean residence times calculated from (a) fracture volume divided by total calculated flow rate, (b) mean particle travel times from 2-D calculations, (c) mean residence times from a system of statistically equivalent 1-D variable-aperture channels and (d) mean residence times from a system of constant-aperture channels.

Run	Mean Residence Time (arbitrary units)			
	Fracture Volume	2-D	Variable-Aperture	Constant-Aperture
	2-D Flow Rate	Particle Tracking	1-D Channels	1-D Channels
511	0.59	0.59	0.82	0.004
512	1.46	1.49	1.64	0.012
513	0.35	0.34	0.39	0.007
514	0.33	0.33	0.41	0.006
541	0.07	0.07	0.06	0.0005
542	2.29	2.30	3.10	0.007
543	0.86	0.85	1.15	0.0047
544	0.30	0.30	0.35	0.003

Realization 541



XBL 875-9685

Figure 1. The aperture density distributions for apertures along particle paths and over the entire fracture

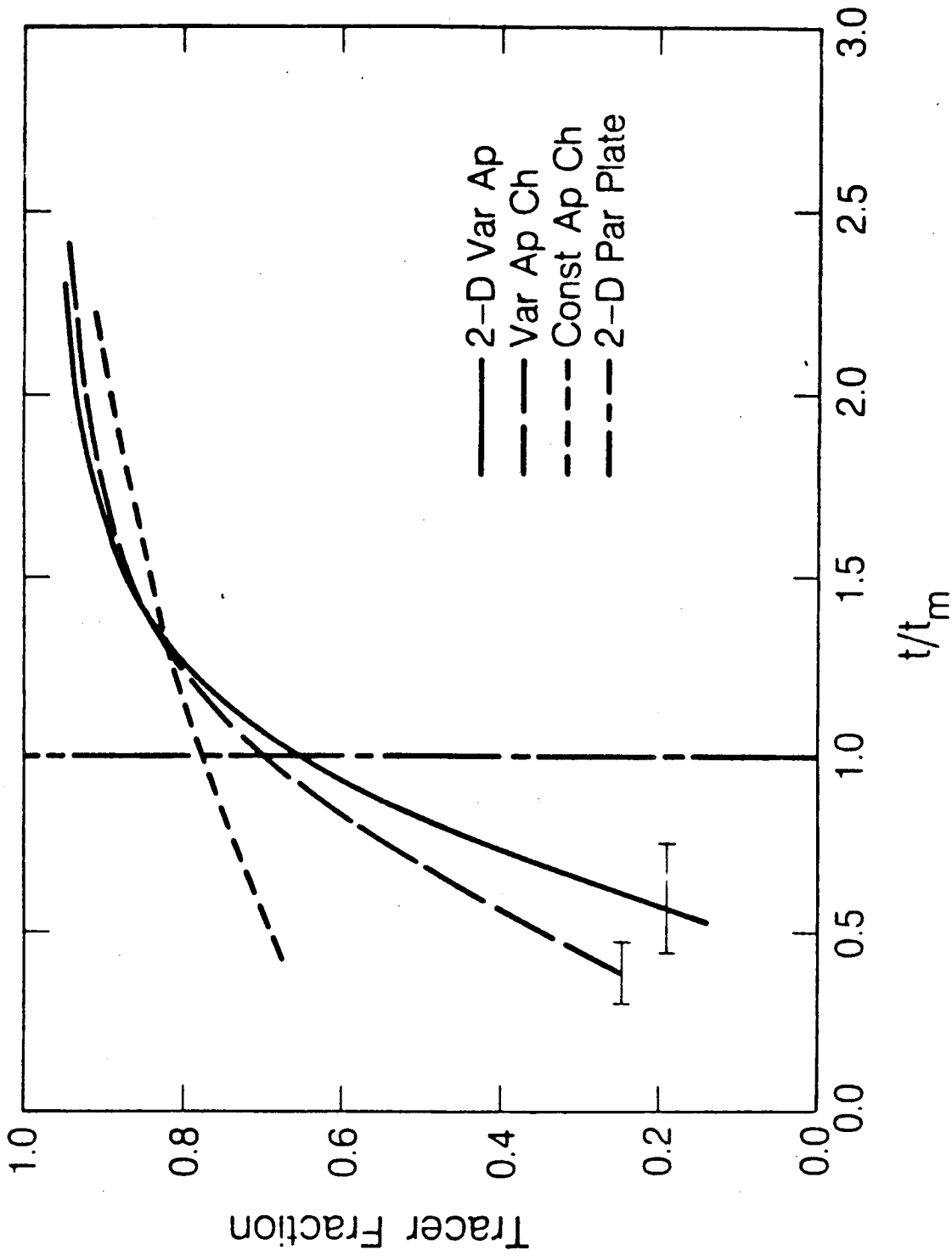


Figure 2. Tracer breakthrough curves from two-dimensional calculation, one-dimension variable-aperture channel calculation, constant-aperture channel calculation, and parallel-plate fracture calculation. Horizontal bars give limits of values from different realizations.

A Scheme for Calculating Flow in Fractures Using Numerical Grid Generation in Three-Dimensional Domains of Complex Shapes

J. C. S. Long, P. A. Witherspoon and K. Muralidhar

The science of fracture hydrology is a relatively new field. It is a separate endeavor from classical porous media ground water hydrology because analysis techniques developed for porous media do not work well for fractured rock. Basic research is needed to understand how the features of fractures control flow in the rock. To that end, we are interested in how the features of individual fractures control flow.

Fractures in general have rough sides and these sides are held apart through the contact of asperities on the surfaces. The area of contact, "contact area", is irregular as is the aperture of the fracture where it is open. Thus from the point of view of fluid mechanics, a fracture is an irregular three-dimensional channel with irregularly spaced and sized obstacles.

To characterize the geometry of such a channel is a problem in itself. On going research is focussed on the quantification of void geometry in a fracture. Several laboratory and analytical techniques are under investigation. Casts of the fracture can be made by injecting a low melting point metal into the fracture (Pyrak-Nolte et al., 1987). The fracture can then be taken apart and both sides photographed. In such a photo, the contact area shows up as the color of the rock and the open area show up as

the color of the metal. Both photographs and profile data can be used in a conditional geostatistical simulation which provides an estimate of the aperture as a function of location in the fracture plane. Alternatively, it may be possible to quantify the geometry of the fracture directly using parallax photography. This task has been concerned with how we can proceed to analyze flow through the channel once the geometry is defined.

The problem of fluid flow in an irregular geometry can be solved theoretically only if a numerical approach is adopted. Further, any such scheme must have a definite capability to handle boundary shapes which do not coincide with coordinate lines. In the present work, a three-dimensional grid generation procedure is described, which maps the interior of a complex region onto the interior of a rectangular parallelepiped. This also guarantees that the boundaries of the transformed region represent constant values in terms of the new system of coordinates. The flow computation is performed in the newly defined region, and an inverse transformation rule extracts values of flow velocities and pressure in the geometry of interest. This two-step procedure of grid generation followed by flow calculation is described in detail in the final report for this task (Muralidhar and Long, 1987).

Mesh generation is useful to the numerical solution of partial differential equations in a fracture because the profile of the flow boundary is usually different from that of any of the fundamental coordinate systems. This leads to interpolation errors in boundary conditions which in turn could significantly deteriorate the overall accuracy. There are alternative methods, such as the finite element method (FEM), where boundary shape can be included in the formulation of the physical problem, through the use of higher order elements. Whether FEM results in more or less algebraic complexity than the approach presented here remains as yet unresolved. Considerable gain in accuracy can be accrued through grid generation by selectively relocating nodal points to represent critical portions of the flow region while keeping the total number of

nodes fixed. A skewed mesh also causes a larger truncation error compared to an orthogonal system. The mesh generation procedure described in this report provides a systematic way to reduce the skewness both in the interior of the physical space, as well as the manner in which the grid line intersects the boundary.

In this work, the emphasis is on grid generation which can, (1) be accomplished via differential equations, (2) handle complex boundary shapes, and (3) impose a pre-determined degree of orthogonality on the grid lines. The formulation is presented in three dimensions, suitable for flow analysis in a single rock fracture. It is general enough to be extended to include other mesh properties such as concentration of nodes near a point or line, where severe gradients in the field variable are likely to occur. The governing equations for grid transformation are written with respect to the Cartesian coordinates and the solution for the grid points in the physical space constitutes a transformation law. This procedure falls in the class of techniques which employ boundary transformation to accommodate complex domains. The mapping function is implicit in the differential equations required for the transformation and has only a point wise definition. The rectangular geometry which arises after transformation can be advantageously used for performing computation of the physical problem. This is because the regular boundary shapes permit easy application of boundary conditions. Further, the nodal points in this space are placed at equal intervals, making discretization rules algebraically simple. The whole process of transformation is accommodated in the mathematical model by viewing it as a change of coordinates.

The actual differential equations chosen to define the mapping function depend ultimately on the physical problem prevailing on the flow domain. The interest in this study is restricted to low Reynolds number steady flow in rock fractures, and the respective equations and boundary conditions are known to form an elliptic problem. The grid generated from such a system of equations has built-in smoothing properties, as is observed in related diffusion-dominated problems. Little modification is required

to extend this to time-dependent cases. However, in high speed flows, it is necessary to permit the formation of boundary layers, and special treatment is usually required.

The oldest and the simplest method of transforming a given shape to another convenient one is Conformal Mapping (Churchill, 1960), arising from complex variable theory. If an analytical mapping function can be found for the boundary shape at hand, then the grid is generated with little effort, and is naturally orthogonal everywhere in the domain. Further, in many linear problems the governing equations are fully preserved. However, the analytical procedure cannot be generalized and is definitely limited to two-dimensional regions. A related type of mapping based on algebraic formulas and which can be extended to three dimensions has been described by Eisman (1985). It has been found to be useful in the aeronautics industry, where smooth aerofoil shapes are frequently encountered. The approach utilizing differential equations (as opposed to algebraic expressions) is quite recent, and a summary of the procedure involved has been provided by Thompson et al. (1982). The motivation to use differential equations comes from Conformal Mapping Theory, where the real and the imaginary parts of the mapping function must be harmonic, i.e., satisfy Laplace equation. Thompson et al. (1982) also describe the use of Poisson equations for grid generation, where, by a proper choice of source terms, the desired grid control can be accomplished. Brackbill and Saltzman (1982) have extended this minimization principle to include various measures of grid quality, such as orthogonality and concentration as constraints. The variational method appears to be the most general of all techniques and has been used in our work.

Grid generation viewed as a numerical procedure for coordinate transformation has been recently used in the solution of two-dimensional continuum problems in both fluid and solid mechanics. Altus and Bar-Yoseph (1983) have studied stress distribution in orthotropic, laminated composites using this method. Projan, Rieger and Beer (1981) have studied free convective movement of a fluid in the gap between eccentric

cylinders, by mapping it into a rectangular strip. Goldman and Kao (1981) have described their experience with this technique, applied to heat conduction problems in multiply-connected domains. Napolitano and Orlandi (1985) have published results of a comparison study of laminar flow in a complex geometry, using different numerical schemes. Those employing coordinate transformation are seen to be the most accurate simulations.

The final report (Muralidhar and Long, 1987) consists of two parts. First, the equations governing grid generation in three dimensions, including a method to improve orthogonality of the generated coordinates are fully derived. These equations are valid for both simply and multiply connected domains. It is usually simpler to solve for the flow field in a multiply-connected domain where the "holes" overlap the coordinate lines, rather than convert it to one which is simply connected, by use of branch surfaces. This approach could however fail, if the stiffness matrix to be inverted is singular due to these holes in the matrix structure. Secondly, the equations and boundary conditions governing flow are presented in both Cartesian and the transformed coordinates in both two dimensions and three dimensions. The numerical procedure for the solution of these equations is developed in each case and this is followed by results of selected test cases.

REFERENCES

- Altus, E. and Bar-Yoseph, P., 1983, "A 3-D Finite Difference Solution for Orthotropic Laminated Composites Using Curvilinear Coordinates," *Computers and Structures*, Vol. 17, pp. 573-577.
- Brackbill, M. V. and Saltzman, J. S., 1982, "Adaptive Zoning for Singular Problems in Two Dimensions," *Journal of Computational Physics*, Vol. 46, pp. 342-368.
- Churchill, R. V., 1960, *Complex Variables and Applications*, McGraw Hill, New York.
- Eisman, P. R., 1985, "Grid Generation for Fluid Mechanics Computations," *Ann. Rev. Fluid Mechanics*, Vol. 17, pp. 487-522.
- Goldman, A. and Kao, Y. C., 1981, "Numerical Solution to a Two-Dimensional Conduction Problem Using Rectangular and Cylindrical Body-Fitted Coordinate Systems," *Journal of Heat Transfer*, Vol. 103, pp. 753-758.
- Muralidhar, K. and Long, J. C. S., 1987, "A Scheme for Calculating Flow in Fractures Using Numerical Grid Generation in Three-Dimensional Domains of Complex Shapes," LBL Report, LBL-24453.
- Napolitano, M. and Orlandi, P., 1985, "Laminar Flow in a Complex Geometry: A Comparison," *Int. J. Numerical Methods in Fluids*, Vol. 5, pp. 667-683.
- Projan, V., Reiger, H. and Beer, H., 1981, "Numerical Analysis of Laminar Natural Convection between Concentric and Eccentric Cylinders," *Numer. Heat Transfer*, Vol. 4, pp. 131-146.
- Pyrak-Nolte, L. J., Myer, L., Cook, N. G. W. and Witherspoon, P. A., 1987, "Hydraulic and Mechanical Properties of Natural Fractures in Low Permeability Rock," presented at 6th International Congress on Rock Mechanics, held in Montreal, Canada, 30 August, 1987.
- Thompson, J. F., Warsi, Z. U. A. and Mastin, C. W., 1982, "Boundary-Fitted Coordinate Systems for Numerical Solution of Partial Differential Equations - A Review," *J. Computational Physics*, Vol. 47, pp. 1-108.

Thompson, J. F., Ed., 1982, *Numerical Grid Generation*, Elsevier Science Publishing Co., New York.

Studies Relating to the Stress Corrosion of Minerals in Radioactive Waste Repositories

J.A. Apps and A. Meike

Introduction

Pressure solution is a widely observed phenomenon in nature and is the principal means through which water saturated rocks compact and deform at temperatures below 400 °C, [Tada and Siever (1987); Elliott (1973)]. Pressure solution is often a controlling mechanism for slip along faults (e.g., see Lehner and Battaille, 1984) and for the formation of slickenslides commonly observed on fault faces. The actual mechanisms involved are not clearly understood, and differing hypotheses have been advanced over the years to explain field observations, c.f., Weyl (1959), Ostapenko (1968), Elliott (1973), Rutter (1976), Lehner and Battaille (1984), and Tada et al. (1987).

Recent high voltage electron microscopic studies of the micromechanics of deformation in limestone (Meike, 1986) have provided convincing evidence of several processes that have not been adequately recognized in past studies, but which may be of widespread applicability to many rock types and mineral phases. Meike observed that localized stress had induced stress corrosion cracking in the constituent calcite crystals of the limestone, and that this cracking had propagated through concurrent dissolution at the crack tips. The dissolved calcite had precipitated elsewhere in the rock, mainly in voids and distensional cracks. Of note was the tendency for phyllosilicates to grow in the voids of the developing cracks.

N. G. W. Cook (personal communication, 1986) also concluded from independent arguments relating to the deformation of rocks, that localized stresses could exceed that necessary to induce dislocations in individual crystal grains. Furthermore, cracks in certain orientations in a stress field could induce exceedingly high localized stresses at their tips, which would also cause defect formation.

Preliminary calculations using normalized deformation maps from Ashby (1972) indicate that for those minerals where appropriate data is available, all will be subject to crystal dislocations under the stresses and temperatures expected in the near field of all three potential high-level repository sites. Field observations showing manifestations of pressure solution phenomena are presently known only at the Nevada Test Site, where slickensiding on faults, is observed to have affected secondary zeolites (Carlos, 1985). Although no pressure solution phenomena have been described in Permian evaporites of the Palo Duro Basin, owing to the lack of observed faulting, studies by Urai (1983) on polycrystalline, carnallite and bischofite and by Baes et al. (1983) indicate that pressure solution is a dominant deformation mechanism operating in evaporite minerals. In basalts of the Pasco Basin, field studies of fault plane mineralogy and the occurrence of pressure solution phenomena have not been made. However, the high regional stresses and the metastable condition of the glass suggest that a form of pressure solution is highly likely in the near field region of the repository.

After excavation of a repository, localized stresses surrounding waste container wells, and even drifts and crosscuts, would, when resaturated and subjected to elevated temperatures due to the decay of radionuclides in the waste, induce pressure solution along cracks and fractures in the host rock. This will lead to supersaturation with respect to both primary and secondary minerals. Local recrystallization and precipitation of secondary minerals will occur in voids

and adjacent rock pores with potentially dramatic changes in rock porosity and permeability. The secondary minerals in the Pasco Basin or the Nevada Test Site host rocks would be clays and zeolites. Both mineral classes are potential hosts for a variety of toxic radioelements.

Information to quantify the pressure solution mechanism is sparse. Laboratory studies between 200–350 °C (de Boer et al., 1977; Sprunt and Nur, 1977) show that pressure solution can be very rapid and lead to significant changes in porosity and permeability of unconsolidated sands within weeks. Calculations with assumed empirical activation energies at repository temperatures suggest that pressure solution phenomena would be significant for the expected repository temperatures and host rock mineralogies at all three potential repository sites.

Pressure solution is a phenomenological process. The objectives of the present research are to elucidate the mechanisms involved, and establish their importance or otherwise in modifying the hydrologic, geochemical and mechanical properties of the near field host rocks. From our review of the literature, and knowledge of geochemistry and rock mechanics, we hypothesize that pressure solution occurs as follows:

1. High localized stresses induce the formation of crystal defects at the asperities of mineral grains, and at the tips of microfractures.
2. The resulting high defect densities will enhance dissolution kinetics leading to supersaturation with respect to the affected minerals.
3. Dissolved chemical constituents will migrate away from asperities or crack tips into adjacent voids where precipitation may occur, or advecting fluid may carry them away after mixing and dilution. Diffusion of dissolved mineral constituents away from asperities may be retarded by visco-electric forces in the aqueous surface boundary layer (Rutter, 1976; Tada et al., 1987), or it may be enhanced through some surface

diffusion phenomenon (Jensen and Radke, 1986), or diffusion may also take place through a layer of water thick enough to be only slightly affected by interfacial forces (Lehner and Bataille, 1984).

We are conducting a research program to resolve the major uncertainties. This program includes:

- (1) An experimental study to measure enhanced dissolution kinetics due to stress-induced defect formation in selected minerals.
- (2) Studies to evaluate the stresses required to induce defect formation, using a high voltage transmission electron microscope (HVEM).
- (3) HVEM and high resolution electron microscopy (HREM) of naturally deformed chert to clarify the micromechanical details of stress-induced dissolution and reprecipitation in silica.
- (4) A critical review of the literature to determine the rate-controlling mechanisms involved in the dissolution and transport of chemical constituents away from stressed asperities.

Progress during FY 1987

1. Experimental Study to Measure Enhanced Dissolution Kinetics in Minerals Due to Stress

After discussions with Professor Neville Cook, Hans-Rudolph Wenk both of the University of California, Berkeley, and the late Dr. Hugh Heard, LLNL, a design for a pressure system to measure the dissolution rate of radially stressed slotted single crystals of selected minerals as a function of temperature, confining pressure and "pore" pressure was finalized. The Laboratory solicited bids from all potential fabricators, and selected Coretest Laboratories, Mountain View, California, as the only bidder who came within budget and met all specifications.

The equipment was fabricated and delivered in August, 1987. A conceptual description of the equipment is described in last years' annual report (Apps 1987).

Modification of the pressure vessel, installation of the furnace and fabrication of the internal cell holding the single slotted crystal and interfacing with a HP data acquisition system and microcomputer remain to be completed before experiments can begin. Details of the planned procedures are given in last year's annual report (Apps 1987).

2. Evaluation of Stresses Required to Induce Defect Formation

The dislocation activation stress (DAS), i.e., the minimum stress required to induce dislocations, must be known to predict deformation due to stress-related heterogeneous dissolution. DAS is specific to a mineral slip system. The critical resolved shear stress (CRSS), usually measured by bulk methods, is accurate enough to predict textures and other homogeneous deformation phenomena, but exceeds the associated DAS by an unknown amount.

The two studies described below aim at a predictive approach to stress-related heterogeneous dissolution. In the first, *in-situ* experiments to measure DAS directly have been developed for two mica minerals, (Meike, 1988), based on successful *in-situ* strain experiments on metals and ceramics. These experiments are difficult, and the physical characteristics of rock-forming minerals limit the direct application of existing experimental procedures. In the second study, a more feasible method was developed to obtain estimates of DAS from static observations of dislocation density gradients. Preliminary experiments were conducted on calcite.

Direct measurements of dislocation activation stresses from HVEM in-situ experiments

The purpose of this investigation is to develop a technique for straining two mica minerals, muscovite ($\text{KAl}_2(\text{Si}_3\text{Al})\text{O}_{10}(\text{OH},\text{F})_2$) and biotite ($\text{K}(\text{Mg}_{0.6-1.8}\text{Fe}_{2.4-1.2})(\text{Si}_3\text{Al})\text{O}_{10}(\text{OH},\text{F})_2$) *in-situ* at the HVEM. These sheet silicates were chosen for some characteristics that facilitate preparation, and for others that hamper preparation but are common in rock-forming minerals. Muscovite and biotite are soft, elastic, relatively easy to prepare and translucent in thick section, but are brittle and cleave easily in thin fragments. Successful experiments will be used to calculate muscovite and biotite (001) DAS (Messerschmidt et al., 1979).

The HVEM permits the use of relatively thick specimens to reduce the tendency to fracture and the surface control of deformation mechanisms. Mica layers 30–60 μm thick were peeled along (001) cleavage planes and narrow strips ($\sim 2 \text{ mm} \times 5 \text{ mm}$) cut with a razor blade. One of the slip directions was aligned with the long axis of the strip. Specimens were attached to pieces of a sliding beryllium-copper alloy cage. The standard tensile straining configuration was modified to a simple shear geometry in order to optimize conditions for (001) slip in the direction aligned with the long axis of the specimen (Meike, 1988). The mica specimens were placed between the two pieces, to permit an attachment method that modifies the stress geometry (Figure 1). An atom milled perforation in the middle of the specimen was the focus of the search for dislocation activation. The straining experiments were videotaped.

The intermediary cage used to modify the straining geometry between a specimen and the tensile straining stage makes possible the use of both the most widely available tensile apparatus and the soundest orientation for the mineral specimen. The option introduces more flexibility for specimen preparation and should reduce barriers to *in-situ* strain experiments on a variety of rock-forming

minerals under more difficult, high temperature conditions. The simple shear geometry offers a preparation alternative to other investigation of deformation including shear induced phase transformations and twinning.

Most observed dislocations originated during sample preparation. In muscovite, dislocation segments between pin points ($>20 \mu\text{m}$) were too long to activate within the limits of the strain stage, even near the atom milled stress raiser. However, (010) and (001) dislocations may have been activated in the most recent experiments on biotite. The apparent difference between biotite (001) DAS and muscovite (001) DAS may only reflect the development of a better technique. However, the results are consistent with arguments that the chemical variation in the octahedral layer of biotite may allow dislocations to activate with greater ease than in muscovite (Bell and Wilson, 1986).

Estimating dislocation activation stresses from stress gradients in calcite

The purpose of these experiments is to determine the DAS from a gradient in dislocation density by creating a predictable stress gradient in single crystals of calcite.

Cones (9.25° $1/2$ angle) were cut from large crystals of Iceland spar parallel to (0001), and one end ground parallel to (0001). The cones were fitted with cylindrical indium jackets with conical interiors (9.25° $1/2$ angle), and placed in cylindrical silver jackets sealed with tungsten carbide discs (Figure 2).

All experiments were conducted in a 10 Kb triaxial gas apparatus built by S. Kirby for the Rock Mechanics Laboratory at USGS, Menlo Park. The calcite cones were heated to experimental temperature (50° , 100° , 150°C). The confining medium, argon gas, was raised to 1 kbar before the uniaxial load was applied parallel to (0001). The actual strain rate differs from the nominal rate (10^{-5}) by a only few percent for strong specimens and therefore must have

differed very little for a weak calcite specimen at the low experimental stresses. The specimens were unloaded immediately after the strain gauge measured an initial permanent deformation.

Deformed cones were sectioned vertically through the center. TEM mounts (3 mm dia.) were taken along the cone axis of each thin section and thinned. Observation with the HVEM permitted the use of thicker parts of the specimen for more accurate dislocation density estimates. Multiple orientations of the sample were used to determine dislocation Burgers vectors and to avoid the systematic omission of low contrast dislocations.

A strain gradient was achieved in preliminary experiments. The smaller end of each cone deformed permanently while the larger end has retained its original shape. Dense concentrations of dislocations ($\sim 10^{10} \text{ cm}^{-2}$) are observed at the small ends of the cones. In general, the dislocation density decreases as the cross-sectional area perpendicular to the cone axis increases. The presence of very densely spaced dislocations support the observation that a strain gauge offers only a very crude approximation of microscopic deformation.

3. Examination of Stress-Related Dissolution in Deformed Cherts

A transmission HVEM and HREM investigation was conducted on a drastically modified chert fold from the Marin headlands, California. This study permits examination of a natural case of stress related dissolution in a low temperature SiO_2 rich system and is a basis for comparison of field deformation mechanisms with those to be observed in the experimental investigation of radially stressed slotted cylinders of quartz (Apps, 1987). It also offers the opportunity to examine the solution cleavage mechanism, microstructures associated with heterogeneous diffusive mass transfer in a partially amorphous or microcrystalline material, and to review the role of dislocations, which require crystalline material

to exist.

The aim of the electron microscope investigation is to identify the phases and their distribution with respect to the solution cleavage surface, and to characterize the grain boundaries. Thin sections were selected from areas and orientations that represented fold features in 3-dimensions (Figure 3). Copper grids were epoxied to key areas, excised from the rest of the thin section and ion milled to approximately 300 angstroms. Hand specimens, thin sections and TEM foil were mapped in detail to permit identification of areas representative of heterogeneous diffusive mass transfer process during electron microscopy. Transmission electron microscopy was conducted at a 1.5 MeV Kratos high voltage electron microscope, which permits greater flexibility in the choice of site and orientation in the specimen analyses than lower voltage systems. High resolution and dark field techniques were used extensively to determine the presence of second phases and perturbations of the crystal structures along grain boundaries.

The non-cylindroidal fold exhibits soft sediment deformation, bedding parallel mineral segregation, two distinct phases of brittle fracture with secondary quartz filling, and cleavage perpendicular to bedding. The deformation complexity survives to the submicroscopic scale. Representative microstructures from deformed quartz veins, bedding parallel opaque layers and the chert matrix were documented.

The presence of dislocation microstructures in a large secondary vein filling supports thin section evidence of a subsequent episode of deformation. The heterogeneous distribution of dislocations within and between the crystals suggests that the secondary quartz was deformed under conditions between brittle and ductile styles of deformation. An opaque layer parallel to the bedding consists primarily of fine grained phyllosilicates. Large equant phyllosilicate plates

were observed in addition to the lath-shaped cross-sections. Although magnetic minerals are distributed irregularly through the rock, they are primarily associated with the phyllosilicates. Their heterogeneous distribution caused variable electron beam stability, and astigmatism in some of the images. The bright field/dark field image pairs typical of the chert matrix, adjacent to the phyllosilicate-bearing opaque layer, permitted identification of fine interlocking grains of quartz and chalcedony. Pods of quartz, often portions of radiolaria or quartz-replaced foraminifera tests within the anastomosing phyllosilicate layers, are typical pressure solution effects. The quartz crystals within the foraminifera indent each other in another common pressure solution configuration. In one high resolution image, quartz lattice fringes from a quartz pod terminate at a sharply defined, high angle grain boundary. In another of quartz grains surrounding a pore, a small grain also indents a larger grain at an abrupt high angle boundary. No evidence of an amorphous or second phase has been observed along either the tightly interlocked or more open types of grain boundary. Previous work on carbonates (Meike and Wenk, 1988) demonstrated that the evidence for the mechanism of heterogeneous diffusive mass transfer can be confined to a very restricted area. Further high resolution and standard electron microscopy is needed to clarify scope and magnitude of the mass transfer process.

4. Review of Intergranular Transport

As noted in the introduction, the literature is replete with conflicting hypotheses regarding the transfer of molecular material from the loci of dissolution to pores or voids in a rock. While it is generally understood that diffusive transfer occurs along intergranular boundaries in a chemical potential gradient, it is not clear how thick the intergranular boundaries are, or how they affect the diffusion of molecular species. This must be clarified, as estimates of the

molecular diffusion coefficient in the interlayer boundary vary from about $10^{-9} \text{ m}^2 \cdot \text{sec}^{-1}$ (Lehner, and Bataille, 1984) to as low as $10^{-16} \text{ m}^2 \cdot \text{sec}^{-1}$ (Breen et al. 1983); a variation of seven orders of magnitude. This raises the question whether surface dissolution at the mineral asperities or diffusive transport is the rate controlling step in pressure solution. Because the activation energy for surface dissolution is usually high compared with that involved in aqueous diffusive transport (Nigrini 1968), pressure solution may be either diffusion controlled or surface rate controlled, depending on the relative magnitudes of the surface rate or diffusion coefficients at a given temperature and whether or not the diffusion process occurs in an unmodified aqueous phase.

A literature review, which is still in progress, reveals that interfacial forces between minerals are complex and poorly understood (e.g., see Ninham 1980) they consist of electrostatic, coulombic, Van der Waals and hydration forces, which, through interaction with the aqueous phase, could stabilize the interfacial distance at varying values depending upon the nature of the participating solid, the concentration of dissolved species in the aqueous phase, temperature and pressure. The pressure needed to bring two curved muscovite mica plates into contact (Isrealachvelli and Adams 1977) is about 10^7 times less than the 4000 bars which Van Olphen (1963) estimates is needed to remove the last monolayer of water from a smectite. Tada et al. (1987) have reviewed estimates of the so-called disjoining pressure necessary to squeeze out a water layer from between two plane silica plates. They estimate the pressure required to displace the last monolayer of water to be 2200 bars. Based on their findings, the interfacial distance between quartz grains would be between 4 and greater than 10 nm in typical repository environments. Although a number of details relating to interfacial forces and their impact on interlayer spacing remain to be clarified, it is clear that silica and smectite surfaces will be separated from each other by a

significant layer of aqueous phase.

Field observations by Heald (1956) show that the extent of compaction due to pressure solution in St. Peter's Sandstone, is markedly affected by the presence of clays. This led Heald (*loc. cit.*) to conclude that the interlamellar spacing of smectite clays could act as conduits for the transport of ionic and molecular species. Instead of a single intergranular layer, a film of clay 0.01 mm thick could provide up to 5000 layers, thereby greatly enhancing the potential for migration of dissolved species from the loci of high stress conditions.

It seemed appropriate to review intermolecular diffusion interlamellar diffusion in smectites as an approximation of a multilayer interface. Several papers have described the diffusion of water molecules in montmorillonites. Olejnik and White (1971) used neutron spectroscopy techniques to measure the self diffusion coefficient of water in montmorillonites and vermiculites. They found that the self diffusion coefficient of water differed little from that of pure water, and even at only 0.4 nm from the surface, it was still only ten times less than in the bulk phase. The interlamellar translational diffusion of the ionic and molecular species has not been investigated and further review of the literature in this area will be required. It appears to be very variable, depending on the size and charge density of the species involved. Recent work by Jensen and Radke (1986) has shown that the effective diffusivity of cesium in bulk smectite gel consists of two components, the ionic diffusivity in the aqueous phase and a surface diffusivity, the surface diffusivity being a significant component of the total diffusivity. Their work suggests that the interlamellar diffusion of some cations may be comparable if not greater than that of water molecules. In contrast, it is known that some large anions, e.g., I^- are sterically hindered in migrating through narrow pores of the order of 5 nm.

The present review concludes tentatively that intergranular distances in smectites and silica are between 0 and 5 nm. Diffusion of these species in these spaces may be highly variable. The presence of clay films may greatly increase alter the diffusive flux. There is no direct evidence that molecular diffusion coefficients in intergranular spaces will be as low as suggested by Rutter (1976) or Tada et al. (1987), at least between smectites and silica.

Anticipated Research During FY 1988

The principal activities during FY 1988 will consist of the following:

1. Completion of the review of interlayer diffusion of ionic and molecular species.
2. Completion of the experimental equipment to measure the dissolution of minerals under stress and initiation of experiments.
3. Completion of a report on pressure solution phenomena in Marin Headlands chert.

HVEM and HREM studies will continue, but will no longer be part of this project.

This project will terminate during FY 1988. Funding will be solicited elsewhere for continuation of fundamental generic studies relative to the stress corrosion of minerals.

Acknowledgements

The assistance of the late Dr. Hugh Heard in designing the pressure dissolution equipment and cone experiments is gratefully acknowledged. The cone experiments could be conducted thanks to R. Coe, S. Kirby, J. Pinkston, T. Teague and K. Yi. Special thanks for the *in-situ* HVTEM experiments are due to

D. Ackland, L. Callup, M. Moore, W. Smith, D. Howitt, T. Marela, W. Quan, S. Schaffer, and J. Tanger IV. Use of the HVEM and the Siemens 102 HREM at National Center for Electron Microscopy (NCEM) is gratefully acknowledged. The tireless efforts of P. Chakraborty in reviewing literature and assisting in the preparation of a report on pressure solution mechanisms is much appreciated. This work was supported under U.S. Department of Energy Contract No. DE-AC03-76SF00098.

References

- Apps, J.A., 1987. Pressure solution geochemistry, in *Earth Science Division, Annual Report 1986*. Lawrence Berkeley Laboratory Report, LBL-22090, p. 129-133.
- Ashby, M.F., 1972. A first report on deformation mechanism maps, *Acta Metallurgica*, v. 20, p. 887-897.
- Baes, C.F., Jr., Gilpatrick, L.O., Kitts, F.G., Bronstein, H.R., and Shor, A.J., 1983. The effect of water in salt repositories; Final report. Oak Ridge National Laboratory Report ORNL-5950, 62 p.
- Bell, I.A., and C.J. Wilson, 1988. Deformation of biotite and muscovite: TEM microstructure and deformation model, *Tectonophysics*, v. 78, p. 201-228.
- Breen, C., Adams, J.M. and Riekel, C. 1983. Hydrogen exchange in interlamellar water in the 23.3-angstrom Na⁺ montmorillonite: Pyridine/water intercalate. II. Activation Energies. *Journal of Colloid and Interface Science*, v. 94, p. 380-389.
- Carlos, B.A. 1985. Minerals in fractures of the unsaturated zone from drill core USW G-4, Yucca Mountain, Nye County, Nevada. Los Alamos National Laboratory Report LA-10415-MS, 55 p.
- DeBoer, R.B., Nagtegaal, P.J.C. and Duyvis, E.M., Pressure solution experiments on quartz sand, *Geochimica et Cosmochimica Acta*, v. 41, p. 257-264.
- Elliot, D., 1973. Diffusion flow laws in metamorphic rocks, *Geological Society of America Bulletin*, v. 84, p. 2645-2664.

- Heald, M.T., 1956. Cementation of Simpson and St. Peter sandstones in parts of Oklahoma, Arkansas, and Missouri, *Journal of Geology*, v. 64, p. 16-30.
- Isrealachvelli, J.N. and Adams, G.E., 1977. Measurement of Forces between two mica surfaces in aqueous electrolyte solutions in the range 0-100 nm, *Journal of Chemical Society, Faraday Transactions*, v. 74, p. 975-1001.
- Jensen, D.J. and Radke, C.J. Cation diffusion through compacted sodium montmorillonite at elevated temperature, *Journal of Soil Science*.
- Lehner, F.K., and Bataille, J., 1984. Nonequilibrium thermodynamics of pressure solution. Report No. 25, Division of Engineering, Brown University, Providence, R.I. 52 p.
- Meike, A., 1986. A study of deformation-enhanced dissolution in theory, experiment and nature, based on microstructural evidence (Doctoral Thesis). University of California, Berkeley, California, 166 p.
- Meike, A., Specimen cage modification for TEM in-situ shearing, *Proceedings of the Materials Research Society 1988 Fall Meeting*, (in press).
- Meike, A. and Wenk, H.R., 1988. A TEM study of microstructures associated with solution cleavage in limestone, submitted to *Tectonophysics*.
- Messerschmidt, U. and Appel, F., 1979. Method of evaluating geometrical-statistical parameters of the interaction between dislocations and point obstacles from electron micrographs, *Kristall und Technik*, v. 14, p. 1331-1337.
- Nigrini, A., 1969. Prediction of ionic fluxes in rock alteration processes at elevated temperatures (Doctoral Thesis), Northwestern University (University Microfilms 70-131).
- Ninham, B.W. 1980. Long-range vs. short range forces. The present state of play. *Journal of Physical Chemistry*, v. 84, p. 1423-1430.
- Olejník, S. and White, J.W., 1972. Thin layers of water in vermiculites and montmorillonites—modification of water diffusion, *Nature (Physical Science)*, v. 236, p. 15-16.
- Ostapenko, G.T. 1968. Recrystallization of minerals under stress, *Geochemistry International*, v. 5, p. 183-186.
- Rutter, E.H., 1976. The kinetics of rock deformation by pressure solution. *Philosophical Transactions of the Royal Society of London, Series A*, v. 283, p.

203-219.

- Tada, R. and Siever, R., 1987. Pressure solution during diagenesis: A review, *Annual Reviews of Earth and Planetary Science* (in press).
- Tada, R., Maliva, R. and Siever, R. 1987. A new mechanism for pressure solution in porous quartzose sandstone. *Geochimica et Cosmochimica Acta*, v. 51, p. 2295-2301.
- Sprunt, E.S., and Nur, A. 1977. Destruction of porosity through pressure solution. *Geophysics* v. 42, p. 726-741.
- Urai, J.L. 1983. Deformation of wet salt rocks (Doctoral Thesis), University of Utrecht, Holland, 221 p.
- Van Olphen, H., 1963. An introduction to clay colloid chemistry: Interscience, London, 301 p.
- Weyl, P.K., 1959. Pressure solution and the force of crystallization—A phenomenological theory, *Journal of Geophysical Research*, v. 64, 2001-2025.

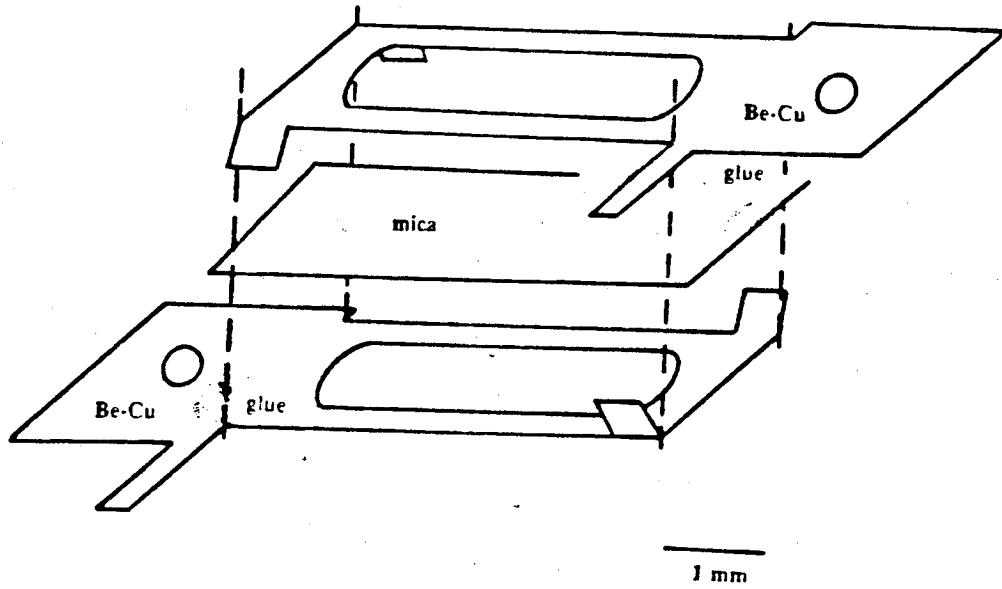


Figure 1. Sliding beryllium-copper cage, modified for the observation of defect formation in stressed mica.

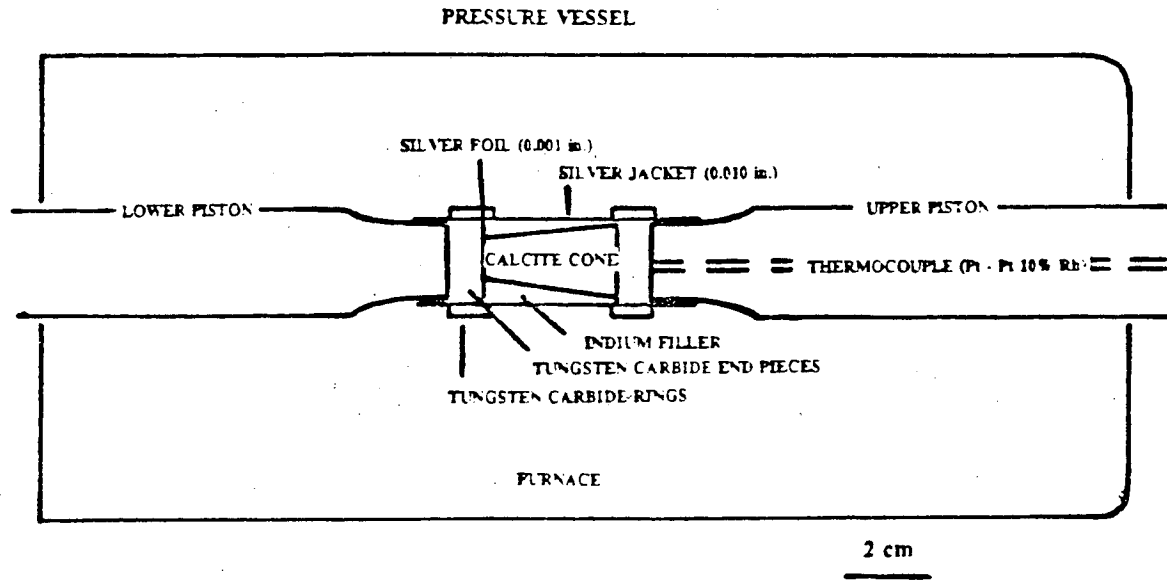


Figure 2. Experimental configuration of apparatus to stress oriented cones of Iceland spar.

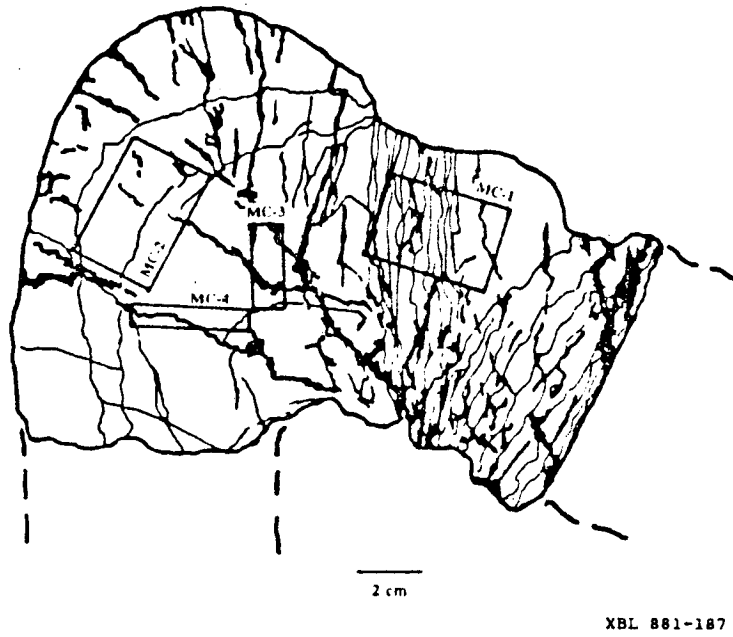


Figure 3. Sample locations for HVEM and HREM studies of a modified chert fold from the Marin Headlands, California.

Investigation of Seismic Imaging Techniques for Fracture Characterization

E.L. Majer and T.V. McEvilly

Introduction

The goal of this work is to develop seismic methods to characterize fracture properties. This includes both field techniques and the development of new modeling codes. The emphasis has been on using tomography to map the fracture distribution between boreholes and underground workings. In order to achieve this goal it is first necessary to understand how fractures effect the velocity and amplitude of the seismic waves, i.e., to understand the physics of the process. This is being done by Myer and Cook under a separate task of this project. The next step is to integrate "the physics" learned in the laboratory work into modeling codes to determine the sensitivity of the technique and possible applications. With controlled field experiments it is then possible to extrapolate the laboratory work to full size field applications. The work to date funded by this project has been mainly directed towards the code development and theoretical work. The controlled field experiments and the full sized field work are being funded by other parts of the DOE nuclear waste program. There is a small component of field work in this project but it is very small compared to the code development.

The code development during the last year has been in two areas. The first code developed is a 2-D ray tracing program. This provides the capability to model lateraly varying layered structures. The program was further developed

by V. Cerveny during his stay at LBL. The program name is Beam87. A full description of the program by V. Cerveny follows. The second program, also developed by V. Cerveny with help from D. Gajewski and I. Psencik, of the University of Alberta is also a ray tracing program, but for full 3-D anisotropic media. The work is still continuing on this program and will be finished during the upcoming year. Only a brief description of the program is given here.

Description of Program Package Beam87

The Beam87 package provides numerical modeling of high-frequency seismic body wave fields generated by a point source in a 2-D laterally varying layered structure by the gaussian beam summation method (or by the ray method). The Beam87 package is comprised of several different programs that together make up the total code set. The first program of the package Beam87 is the ray tracing program RT. This program performs the complete ray tracing, i.e. the ray tracing, dynamic ray tracing and spreading-free amplitude computations.

Program RT is the first program of the program package Beam87 which is designed for the numerical modeling of high-frequency seismic body wave fields in 2-D laterally varying layered structures by the gaussian beam method and by the ray method. In the program RT, initial value or two-point or interval ray tracing is performed. Along known rays, the dynamic ray tracing is performed and the whole ray propagator matrix is determined. After this, the spreading-free amplitudes (radial, transverse and vertical components) are computed. Various results of computations along the rays and/or at endpoints of rays in the region of interest along the earth surface are then stored in two different files lu1 and lu2. These files are used in the succeeding programs of Beam87. It would be, of course, possible to use the files lu1 and/or lu2 even in other applications. The model is 2-D, laterally inhomogeneous, with curved interfaces. Interfaces are

specified by points read from the input data. They are approximated by cubic spline interpolation. Each interface crosses the whole model from its left border to the right border. The interfaces may have corner points and may be fictitious in certain parts. Various interfaces may also partially coincide. Thus models with vanishing layers, block structures, fractures, isolated bodies may be handled by the program. Within individual layers, the velocity may vary both vertically and horizontally. The medium may be slightly dissipative. Optionally, also a model with a thin transition layer replacing selected structural interface of the first order may be considered. Velocity distribution inside such a thin layer is not specified in the program RT, but only in the succeeding program GB. The thin layer must be of a constant vertical thickness.

The source may be situated at any point of the medium, with exception of layers of zero thickness, i.e., it cannot be situated between two coinciding interfaces. The radiation pattern of the source is not specified in the program RT, but only in the succeeding program GB of the program package Beam87. all the direct and primary reflected waves P and S, including the converted waves at the point of reflection, can be generated automatically. Multiple reflections and converted waves of arbitrary type are optionally generated manually. The refracted waves are considered as special cases of reflected waves with compound ray elements.

Three types of the ray tracing may be performed in the program RT:

a) Initial value ray tracing. The initial value ray tracing does not yield a regular system of endpoints along the earths surface. In principle, the initial value ray tracing may be used in the gaussian beam summation procedure, but the system of endpoints must be sufficiently dense in the regions close to the receivers. In some situations, however, the initial value ray tracing does not guarantee a sufficiently dense system of endpoints of rays in certain regions, and

the summation of gaussian beams does not yield satisfactory results.

b) Two-point ray tracing. The two-point ray tracing yields a fully regular system of endpoints along the profile (with a specified constant distance between individual endpoints). It usually yields very stable results in the combination with the gaussian beam summation procedure, and is highly recommended. For iterations to a considered grid point, method of halving intervals, regula falsi or the combination of both methods may be used. The efficiency of the two-point ray tracing would be considerably increased by the paraxial ray approximation methods, but this has not yet been included.

c) Interval ray tracing. The interval ray tracing is a modification of initial value ray tracing which yields a sufficiently dense system of endpoints. In regions where the initial value ray tracing does not give a sufficiently dense system of endpoints, some sort of two-point ray tracing is used to increase the density of rays.

Special care is devoted to certain singular situations in the ray field. Certain branches of the program seek rays of refracted waves, which are close to the rays of head waves, rays of reflected and refracted waves in vicinities of shadow boundaries, etc. In case that a ray which does not come to the earth's surface is obtained during the shooting, the corresponding boundary ray separating the illuminated region, the region is sought. As soon as the boundary ray is found the iterations to the receivers in the illuminated region are performed in the above described way. The program works in single precision, so that the determination of all rays is impossible in certain situations. The spreading-free amplitudes are evaluated by standard high-frequency formulae. They have a reduced meaning: the ray centered components of the vectorial amplitudes are unit at the point source. The radiation patterns are taken into account only in the succeeding program GB. For all elementary waves under consideration, the radial and

vertical components of the vectorial amplitudes are computed and stored at the endpoints of the rays. For monotypic S-waves, transverse components are also automatically computed. Elements of the ray propagator matrix and several other quantities are determined by solving the dynamic ray tracing system along the known ray by a modified Euler's method.

Slight absorption may be considered. In this case, a global absorption factor t times (quantity obtained as a time integral of $1/q$ along a ray, where q is a quality factor) is also evaluated. The quality factor distribution in the model may be related to the distribution of corresponding velocity, or is constant in individual layers, see below. Program RT is supplemented by the program SMOOTH for the preparation of data for the velocity model, which is included in the program package Beam87. Program package Beam87 also includes program GB for the computation of the frequency response by the gaussian beam method or by the ray method, program SYNT is designed to compute the body wave synthetic seismograms (using the file generated by GB), program RAYPLOT to plot rays, travel-times and amplitudes or spreading-free amplitudes, program BPLOT to plot gaussian beam synthetic seismograms (using the files generated by SYNT), and finally program POLAR to plot particle motion diagrams (using the files generated by SYNT). An auxiliary program SORT is designed to change the succession of records in the file lu2 generated by RT to obtain a monotonous succession in the increasing (or decreasing) ray parameters. This program must be used only if the interval ray tracing is performed in RT. For the initial value ray tracing and for the two-point ray tracing the succession is monotonic automatically and the program Sort is not necessary. The plotting programs require calcomp routines plot, number, symbol, and factor. No other special calcomp routines are required.

In the present version of the program RT, there are three possibilities of the approximation of the velocity distribution inside individual layers: 1) bicubic spline interpolation (identical to that used in seis83), 2) linear interpolation between isovelocity interfaces, 3) piece-wise bilinear interpolation. approximations 1) and 3) are convenient for modeling specific features within layers. The approximation 2) is convenient especially when there is no detailed information about the velocity distribution within a layer. Note that the approximation 2) needs a minimum of input data. also note that this approximation introduces second order interfaces (with continuous velocity, but discontinuous gradient).

Description of Program ANRAY

Program ANRAY is designed for ray, travel time, and in the near future, amplitude computations in 3-D general anisotropic and isotropic laterally varying layered media. The program enables computation of rays specified by initial angles at the source or by specifying source and profile on the surface of the model passing through the epicenter on which the rays should terminate. Spreading-free amplitudes may be computed along the rays. The program also allows vertical profiles along the boundary of the model. This enables simulation of crosshole and VSP applications. The model is a system of layers separated by curved non-intersecting interfaces. The interfaces are specified by points on a rectangular grid covering the model cross-section. The material inside of the layers may be either isotropic or anisotropic. All 21 elastic parameters and density may vary spatially within the anisotropic layers while the P- and S-wave velocities and density may also vary.

Application Examples

Beam87

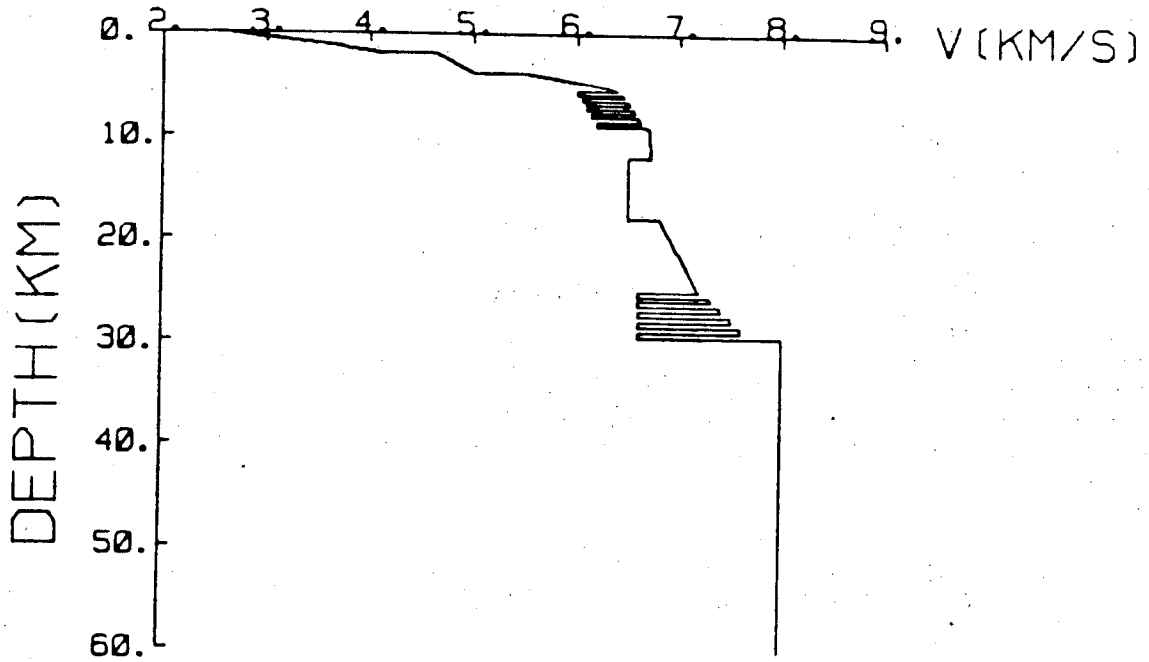
As an example, for the complex crustal structure shown in Figure 1, the calculated synthetic seismograms are shown in Figure 2, 3 and 4. The model consists of two sedimentary layers with high velocity gradients. In the upper crust a stack of 10 alternating high and low velocity layers is introduced, each 200m thick with a velocity contrast of 0.4 km/s. The middle crust from 12 to 18 km depth shows a pronounced velocity inversion. The lower crust-upper mantle transition again is a zone of alternating high and low velocity zones, 500 m thick with a velocity contrast of 0.6 to 1.0 km/s. In Figure 2 the synthetic seismograms are shown for offsets from 20 to 175 km, representing a standard crustal refraction profile. Figure 3 shows the offset from 0 to 25 km. In Figure 4 the offset from 0 to 10 km, corresponding to a standard shotgather of a near-vertical-incident seismic reflection survey. In all calculations the source was an explosion at a depth of 20 m. All traces are normalized to the maximum amplitude.

ANRAY

Shown in Figure 5 is an application of ANRAY. The model used was one that we could check against other modeling results in 2-D. For this reason we used a ray path that is often used by other seismologists. The path is along a profile that starts at Berkeley and ends in the Atlantic Ocean. The path includes the complex structure of the Western U.S., the more stable continental interior, and the intermediate regions of the Atlantic. The lower half of Figure 5 shows the path of the rays in cross section, i.e., the usual convention. The top half of Figure 5 shows the path of the rays in plan view. In this view it becomes very clear that the rays do not travel in the plane but in and out of the plane. This is a very important point when doing tomography in anisotropic media. One

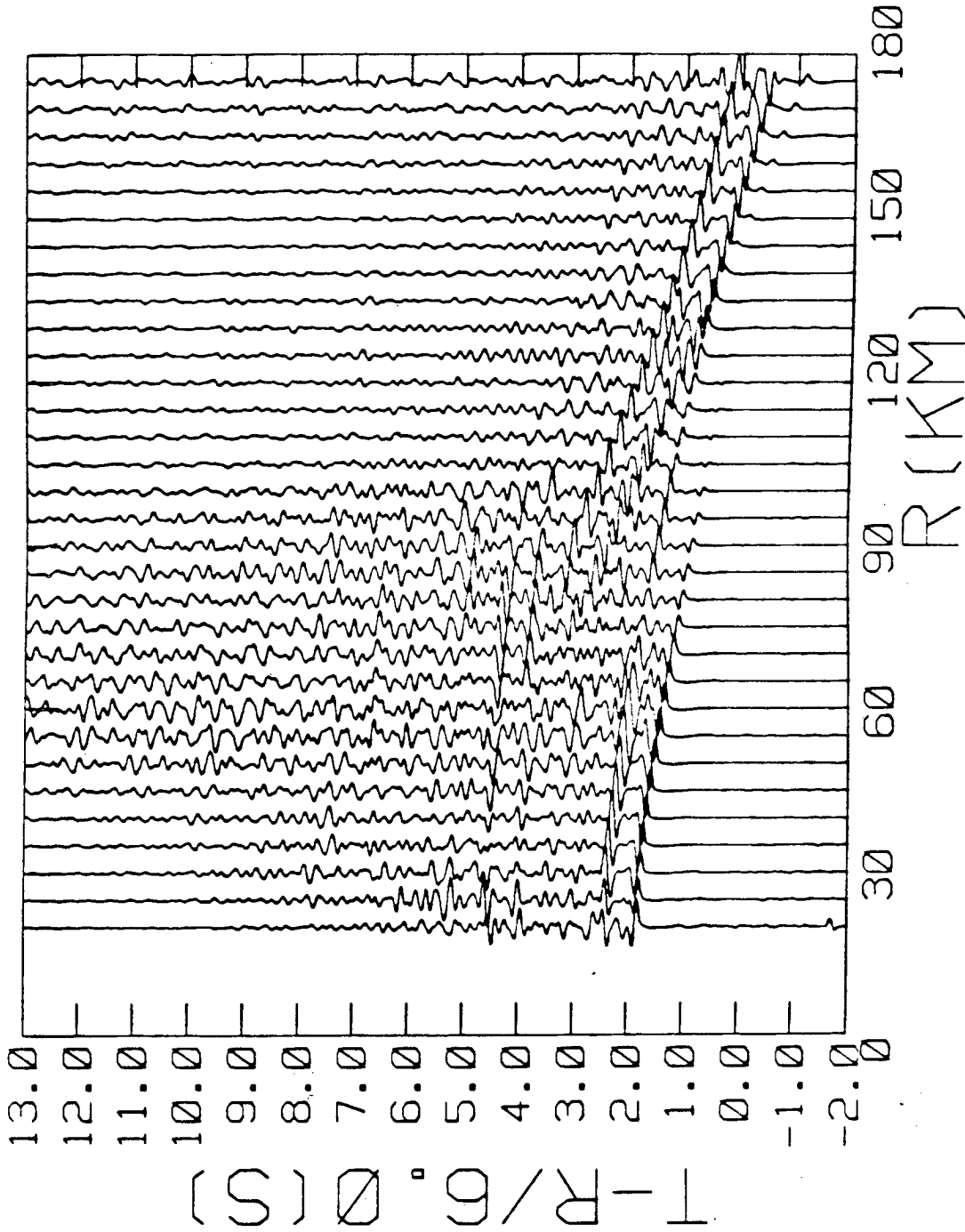
assumes that the rays are all confined to a single plane when obtaining a tomographic image. This program provides the capability to check for this assumption and to provide the correct ray paths.

P-VELOCITY STRUCTURE



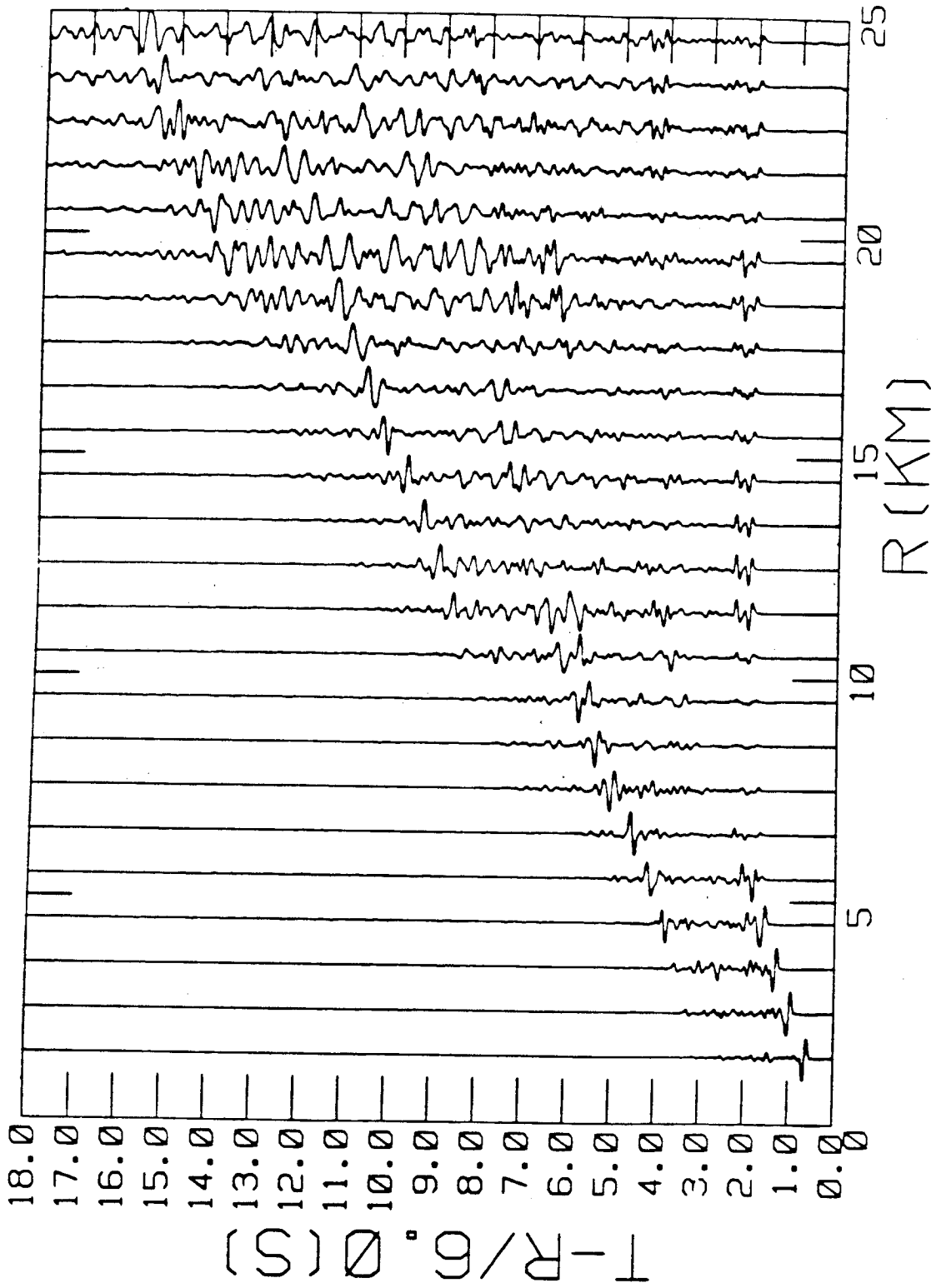
XBL 871-247

Figure 1. P-wave velocity-depth function used to calculate the synthetic seismograms shown in Figures 2, 3 and 4. The S-wave velocities were assumed to be $V_p/1.732$. A constant velocity-density relation with $\text{Rho} = 1.67 + 0.174 \cdot V_p$ was used. The Q-factor varied with depth, being 200 for P-waves and 100 for S-waves in the upper 5 km, 400 for both P- and S-waves in the upper and middle crust to the bottom of the low velocity zone, and 1000 below.



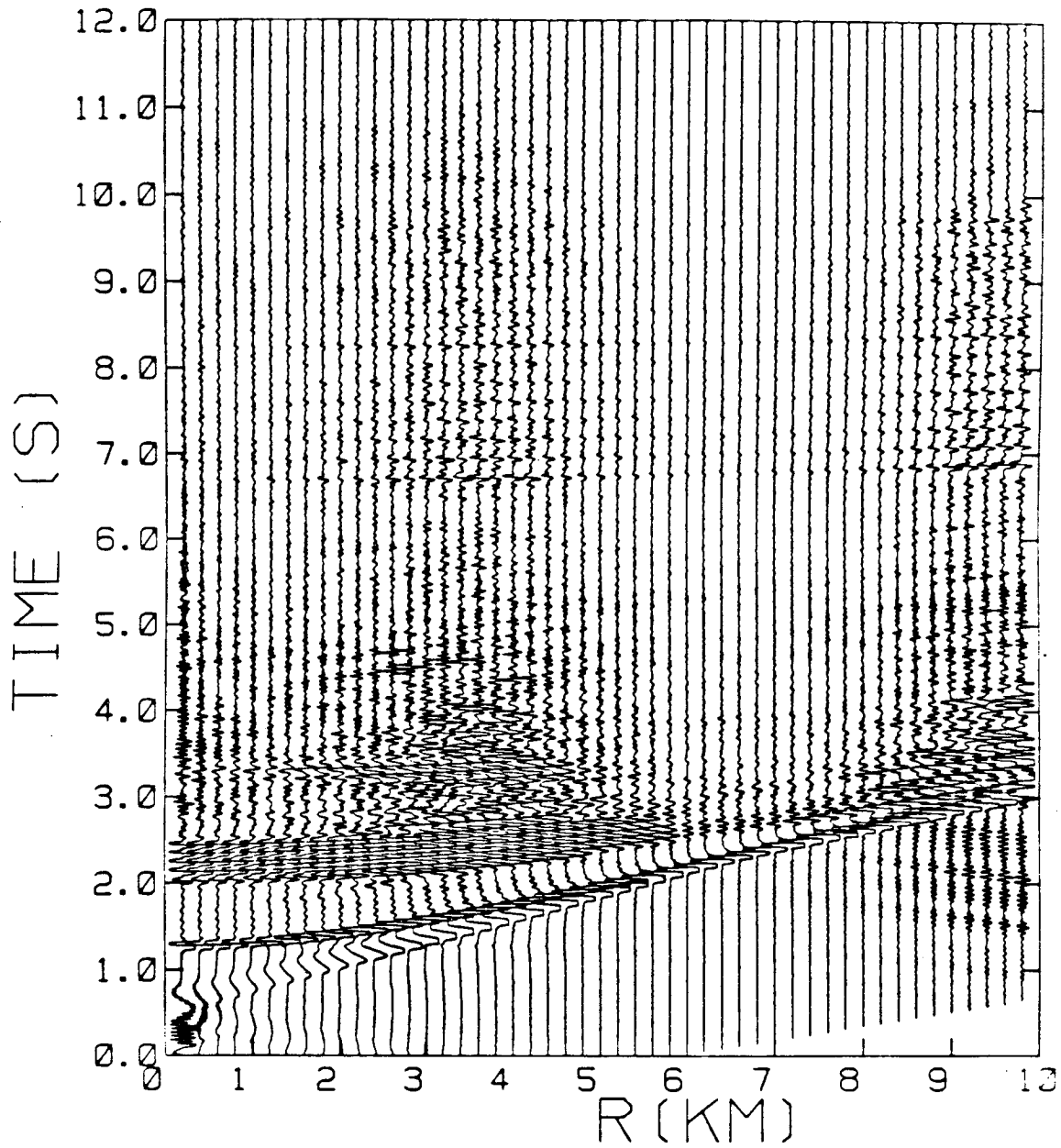
XBL 871-248

Figure 2. Seismograms in the distance range from 20 to 175 km, calculated using Kind's program. The velocity-depth function was divided into 84 layers. Only phases with velocities greater than 4.9 km/s are considered. Times are reduced by 6.0 km/s.



XBL 871-249

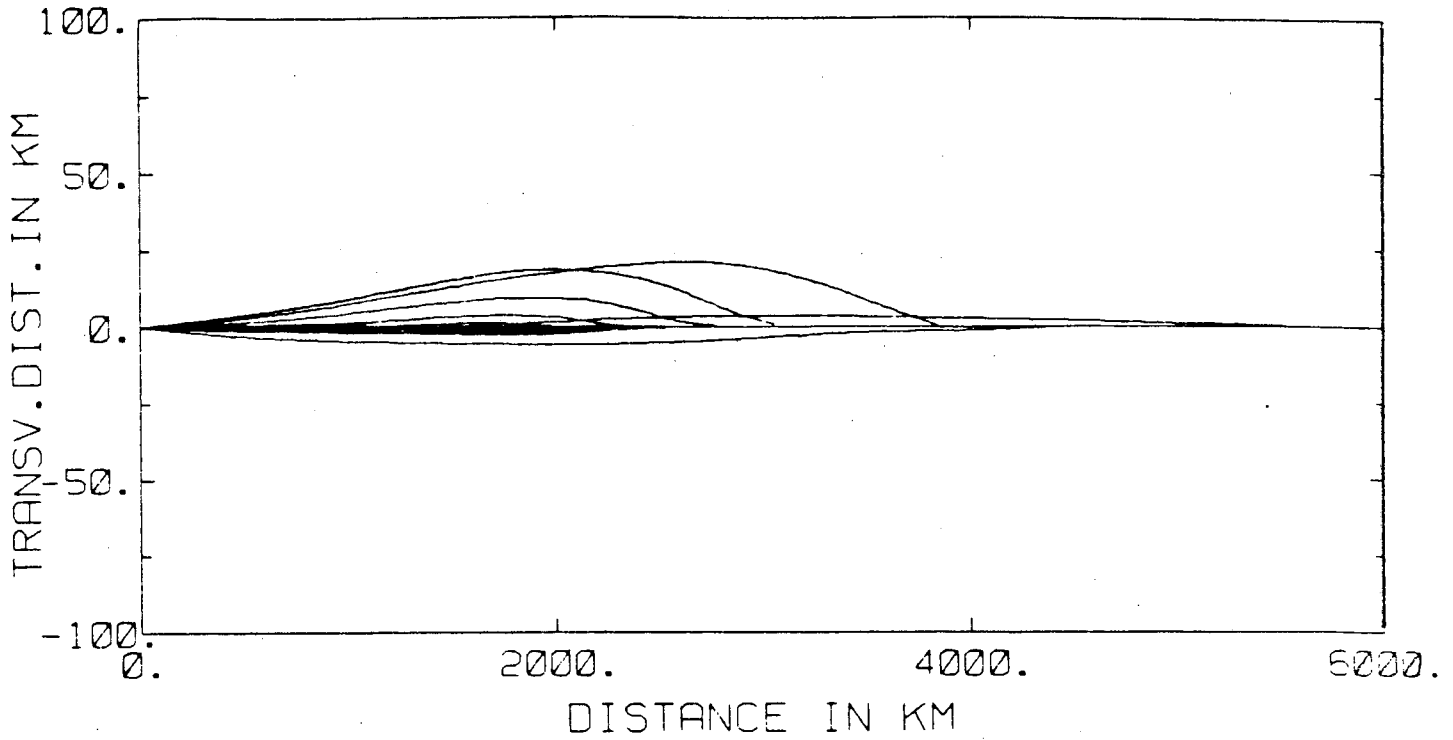
Figure 3. Seismograms in the distance range from 1.5 to 24.5 km, calculated using Kind's program. As for Figure 2 again 84 layers were used, but all phases with velocities greater than 1.0 km/s are included. Times are reduced by 6.0 km/s.



XBL 871-250

Figure 4. Seismograms in the distance range of 0.2 to 9.8 km, calculated using Sandmeier and Wenzel's program. 37 layers were used and the phase velocities greater 4 km/s were considered. The amplitudes of the first arrivals and the first reflection are clipped to enhance the later arrivals.

MANTLE P WAVES
HORIZONTAL PLANE



MANTLE P WAVES
VERTICAL PLANE

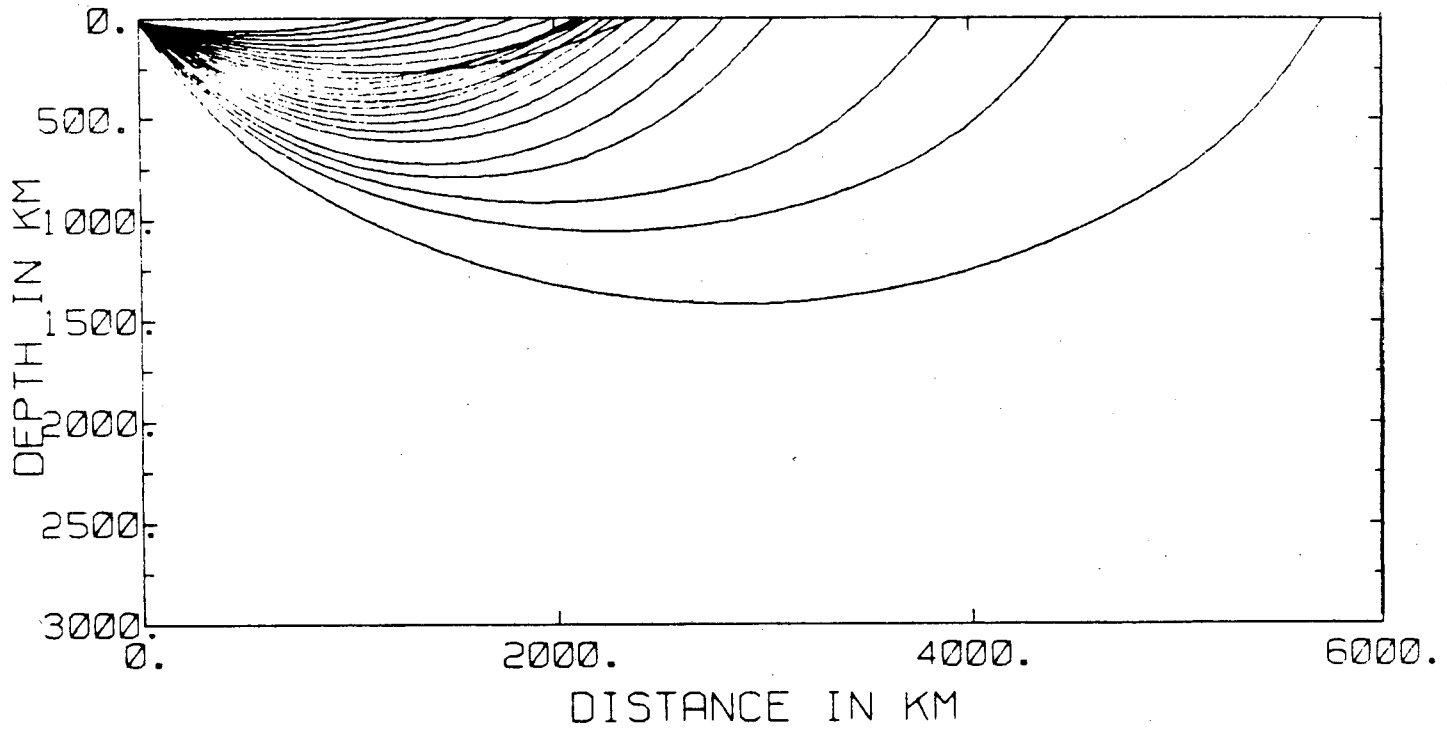


Figure 5. Projections of ray paths on a horizontal plane (upper) and on a vertical (lower) plane for a 3-D velocity model. Distances are measured on the surface of the earth and an earth flattening transform has been applied to the depth coordinate.

Wellbore Breakout and Applications

Ziqiong Zheng and Neville G. W. Cook

Introduction

Borehole breakouts--that is, the fractures and spalling that occur adjacent to boreholes drilled in rock subjected to stress--have been studied for more than two decades. It has been shown that under conditions where the magnitudes of the stresses in the rock are of the same order as the strength of the rock, portions of the borehole wall will fracture and spall. This results in an elongation of the borehole cross section in the direction of the minimum stress orthogonal to the borehole axis [*Leeman, 1960, Cox, 1970; Bell and Gough, 1979, 1982; Hickman et al., 1985; Plumb and Hickman, 1985; Zoback et al., 1985*].

Using an approach based on the micromechanics of rocks, we seek a consistent explanation of how breakouts occur and why they are stable in the absence of external support. Near the surface of a borehole the loading is essentially biaxial (with a high tangential stress and a stress parallel to the borehole axis), and failure is likely to occur by extensile splitting parallel to the free surface. Here we use a criterion appropriate to extensile splitting in compression [*Kemeny and Cook, 1987*]. Away from the boundary of the borehole, where the radial stress provides increasing confinement, any failure that takes place will result from shear fracture; a Mohr-Coulomb shear-failure criterion is used in our research for the stability of the regions away from the borehole boundary. A numerical technique is developed to model the spalling, growth, and stabilization of breakouts on the basis of the above micromechanics arguments for an elastic, isotropic, homogeneous

material. The process of breakout formation consist of progressive spalling of thin slabs near the borehole wall and show that this process can lead to a stable shape of the breakout cross section for an elastic brittle material. Stress distributions around the final breakout cross sections are compared with a Mohr-Coulomb failure criterion to show that the elastic stress distribution around the breakout is stable, so that the analysis based on the assumption that the material is elastic is valid. The stable breakout cross sections have distinct pointed ends that, we conclude, play a very important role in the stabilization of breakouts. Different loading histories can lead to different breakout shapes and sizes with different degrees of stability, even though the states of stress in the rock away from the borehole are the same. Unique relations between breakout size (i.e., the depth and angle) and applied stress magnitudes do not exist; therefore, obtaining in situ stress magnitudes from observed breakouts is very difficult. In Fiscal Year 1986 a numerical technique based on the fictitious force method was used to study the breakout process. It has since been found that the displacement discontinuity method [Crouch and Starfield, 1983] provides a more accurate solution. Results of a re-evaluation of the breakout problem based on this more accurate method are presented below.

Recent Numerical Models and Results of Breakout

The locations and the size of the initial spalling of rock around the boundaries of the borehole can be calculated from the Kirsch's solution for stress distributions around a circular hole and from a splitting criterion. With the removal of the first layer of spalled rock, a new free surface is created and the cross-sectional shape of the borehole is changed; therefore, the stress distribution around the borehole is also changed. In general, the concentration of the tangential stress in the rock adjacent to the elongated portion of the new cross section will be even greater than it was around the initially circular cross section because of the higher aspect ratio, but the extent of the stress concentration zone will also be changed. A numerical model using displacement discontinuity method has been

developed to calculate the stresses and strains around the newly created borehole geometry. After the first spall, the newly exposed rock will be subjected to essentially biaxial conditions and should fail again by splitting in a class II fashion. The new free surface diminishes the radial stress in the rock adjacent to it, so that another extensile fracture should form subparallel to the circumference of the new cross section. Wellbore breakout is assumed to be the result of a series of such episodes of spalling by extensile splitting.

The numerical model used in this report can model sequence of changes in cross section by successive episodes of spalling. The stress condition is assumed to be plane strain, and the rock is assumed to be linear elastic, isotropic, and homogeneous up to the point of failure. The elements are chosen to be thin to simulate the thin slabs that spall from the boundary. Initially, the boundary element analysis is used to determine the tangential stress around a circular borehole for values of the rock mass stresses of interest. The rock plane strain strength Q is used as the failure criterion in the absence of confining stress on the boundary. A thin annular arc of rock is removed that extends into the rock mass a short distance of the borehole radius, where the tangential stress in this portion of borehole circumference exceeds the strength of the rock. The new stress distribution in the rock around the elongated cross section resulting from the previous removal of a thin layer of rock is calculated by boundary element analysis using the cross section produced by the first spall. Another thin layer of rock of the same thickness is then removed everywhere on the circumference of the cross section where the tangential stress exceeds Q . The same procedure is repeated, and the final cross section of the borehole is obtained by allowing a succession of such episodes until the tangential stress is everywhere less than the strength of the rock on the boundary.

The stability of a breakout cross section formed according to the above analysis is verified in two ways. First, the tangential stress everywhere on the boundary of the final breakout cross section has to be less than the biaxial compressive, or tensile, strength of the

rock, depending on whether the tangential stress is compressive or tensile; i.e., no further spalling or tensile fractures can take place under the criterion. Second, in the rock away from the boundary, failure by extensile splitting should not occur, because this mode of fracture is strongly inhibited by confining stress, but shear failure may occur in response to the high stresses around the breakout. Therefore, the distribution of elastic stresses everywhere in the rock outside the borehole boundary is compared with the Mohr-Coulomb shear failure criterion; the stress parallel to the borehole axis is assumed to be the intermediate principal stress. If the elastic stresses everywhere in the rock are less than those necessary to create failure, either by the extensile splitting criterion or by a Mohr-Coulomb criterion, the breakout cross section generated should indeed be stable.

Figure 1 illustrates a complete series of episodes by which a stable breakout cross section develops from an initially circular hole, as determined by the numerical solution. Notice that the breakout section is smooth except the position where the breakout section join with the original circular section. The breakout cross section shapes created by the fictitious force method, however, have turning points due to the inaccuracy of the method, on the breakout section. Figure 2 shows the changes in the principal stresses at critical points situated about 0.1 of the borehole radius into the rock from the circumference of the changing borehole cross section. The numbers on the abscissa correspond to the successive episodes of spalling represented by the cross sections in . Figure 2a divides the borehole cross section into three sections on the basis of the nature of changes in the principal stresses in each section. Section I consists of points not directly in front of any broken-out part of the borehole. Section III consists of all the points on the line directly in front of the breakout tip, and section II contains points not in sections I and III. It is clear from Figure 2 that both principal stresses in section I diminishes as the breakout propagates. The final mean stress in section II is slightly less, but the stress difference is much less than those before the breakout. In section III, the mean stress values increase

almost linearly as breakout progresses, but the stress difference decreases very rapidly by the end of the breakout process, so that the stability of breakout is insured.

An examination of the complete state of stress around a breakout with a Mohr-Coulomb failure criterion contributes to an understanding of why breakout is a stabilizing process. Figure 3 shows a Mohr-Coulomb failure criterion with internal friction angle of 35 degrees, a compressive strength of 75 MPa, and Mohr circles for states of stress at a point a small distance away from the breakout tip before and after the breakout. Figure 4 shows detailed contours of the maximum shear stress (half the difference between the principal stresses) and the mean stress (half the sum of the principal stresses) in the rock around a stable breakout cross section that corresponds to the final episode in Figure 2. Contours of maximum shear stress obtained from photoelastic experimental studies show the same pattern as that in Figure 4. The numbers in the right column show the shear stresses required to cause a failure that would correspond to the mean stress values in the left column when using the Mohr-Coulomb criterion shown in Figure 3. It can be seen that the mean stresses are sufficiently high that the rock in this region is far from failure in terms of a Mohr-Coulomb criterion.

Relation of Breakout to Stress Measurement

Searching for possibilities of using wellbore breakout to not only predict the directions of the in situ stresses, but also in the magnitudes, we performed numerical simulations of breakouts using the methodology described above for a wide range of stress conditions, as shown in Figure 5. The region labeled "non-breakout zone," bounded by the almost circular arc, represents conditions under which the tangential stress everywhere on the circular borehole boundary is less than that necessary to produce any spalling, as determined by equation (2); therefore, breakout should not occur for a homogeneous, isotropic, and elastic material. Breakout shapes shown in figure 5, the outer shapes where

two shapes are at the same point, are determined by applying the stresses first to the rock mass and then excavating the borehole. To some extent, this represents what happens when an actual borehole is drilled, although the full stress concentrations around the hole build up progressively as the hole is drilled beyond the plane of the cross section.

In laboratory tests of borehole breakouts, it is easier to increase the stresses in a specimen of rock with a pre-drilled borehole [*Haimson and Herrick, 1985; Mastin, 1984; Ewy, 1987*] than to drill into prestressed rock. To model this gradual increases in stress around a pre-existing hole, the methodology used is similar to that described above. Stable breakout cross sections produced by gradually increasing the stresses around a pre-existing hole are shown in Figure 5 as the inner breakout cross sections for some of the same ratios of the final principal stresses and ratios of the difference of these stresses to rock strength as were used for the outer breakouts. There is a remarkable difference between the stable breakout cross sections produced when a hole is drilled into a rock mass under pre-existing stress and those produced when stresses are applied to a rock mass in which a hole has already been drilled. The amount of breakout needed to develop a stable cross section in the former case is much larger than in the latter although the final stress values are the same. This tells us that breakouts are not only controlled by the final stress magnitudes but also controlled by the stress history. In practice, it is difficult to determine what kind of stress path the rock has been subjected to. Another very important result from our analysis is that the breakout depth is controlled predominantly by the initial breakout angle, which can be determined from the Kirsch's solution for the stresses around a circular opening using an appropriate failure criterion. This initial breakout angle can be the same for different combinations of stress magnitudes. As shown in figure 5, one pair of breakout angles and depths can correspond to stresses of different magnitudes. That is, in situ stresses can't be determined solely from the sizes of breakouts.

Hydraulic fracturing, a powerful and useful technique for stress measurements inside a borehole, was developed from the famous Kirsch's solution for the distribution of stresses around a circular opening. The stresses around a borehole with breakout, however, differ from the Kirsch's solution. This may affect stress measurements done by the hydraulic fracturing and hence the applicability of the technique in boreholes with breakout is.

To examine the effect of breakout on hydraulic fracturing, we conducted theoretical and numerical analyses of the following aspects: i) In the absence of internal pressure on the borehole wall, how is the stress field around a borehole, in which breakout has taken place, redistributed and changed from that given by the Kirsch's solution? ii) With internal pressure only, how is the induced tangential stress on a borehole boundary with breakout different from that on a circular borehole boundary? iii) When the above two aspects are combined, how does the breakout affect the hydraulic fracturing measurement?

We began with a theoretical study of the tangential stresses induced on the boundary of an elliptical opening by a far field stress and applied internal pressure. Explicit solutions for boundary tangential stresses induced by far field stress have been given by Jaeger and Cook (1979):

$$\sigma_t = p \frac{2ab + (a^2 - b^2)\cos 2\beta - (a + b)^2 \cos 2(\beta - \eta)}{a^2 + b^2 - (a^2 - b^2)\cos 2\eta}$$

where β ----- the angle between the direction of p and x axis

p ----- the far field stress

$a = C \cosh \xi_0$ ----- long axis

$b = C \sinh \xi_0$ ----- short axis

and the relation between Cartesian and elliptic coordinates is given by

$$x = C \cosh \xi \cos \eta$$

$$y = C \sinh \xi \sin \eta$$

The boundary tangential stress induced by any kind of internal pressure, however, has a much more complicated form (Timoshenko and Goodier 1951). Since our interest is on the stresses at the ends of the short and long axes, respectively, a much simpler solution of these stresses can be reached by applying the principle of superposition. The boundary tangential stresses are:

$$\sigma_t = p_i \left(1 - 2 \frac{b}{a}\right) \text{ ----- at the ends of the short axis}$$

$$\sigma_t = p_i \left(1 - 2 \frac{a}{b}\right) \text{ ----- at the ends of the long axis}$$

where p_i is the internal pressure. In the case of a circular opening, $a = b$ and hence $\sigma_t = -p_i$. In the case of ellipse, $a > b$ so that $|\sigma_t| < |p_i|$. The tensile tangential stress induced by the internal pressure has indeed become smaller value than the internal pressure itself.

The boundary stress distribution on the cross section of a borehole with breakout was calculated using the boundary element method (displacement discontinuity). First of all, we used extensile splitting along the borehole boundary as the mode of failure for breakout. Breakouts for different combinations of far field stress and rock strength were generated as shown in figure 5. A tensile strength for rock is chosen and used as the criterion for the formation of tensile fractures around a breakout boundary, especially at those locations where hydraulic fractures are expected. Stress changes at critical locations due to the progress of the breakout are monitored. Different values of internal pressure are then applied to the stable breakout borehole boundary and the tangential stresses on the borehole boundary are calculated by the numerical analysis. The numerical results show the following features. i). The stress concentrations in front of breakout tips increase as the borehole diameter elongates, and the boundary tangential stress at points 90 degrees from

the breakout is less compressive as compared to that at same points on a circular borehole boundary. The compressive tangential stress at these points decreases continuously until it becomes high enough to generate a tensile fracture at these points. ii). The tensile boundary tangential stress induced by the internal pressure is not equal to and everywhere the same as in the case of a circular opening. Instead, the tensile stress induced at boundary close to breakout has greater value than the internal pressure (and is overcome by the high compressive stress concentration induced by far field stress). On the other hand, the tensile tangential stress at points where hydraulic fractures are expected has lower value than the internal pressure. This behavior is the same as the boundary stresses on an ellipse and described above.

From comparisons of the theoretical "break down" pressures which should be measured in a circular borehole with those obtained from numerical results on a wellbore breakout, our conclusions are as follows. For large borehole breakouts where tensile fractures have already been generated at the locations of hydraulic fractures, obviously only the "shut in" pressure, which is equal to the minimum stress orthogonal to borehole axis, can be measured. For moderate and small breakouts where no tensile fractures are generated, however, the effect of breakout on hydraulic fracturing measurements is not significant. This is because that the elongation of one diameter of borehole cross section not only reduces the boundary compressive tangential stress induced by the far field stress, but also reduces the tensile tangential stress induced by the internal pressure applied on the wall of the borehole. The two reductions in boundary stress compensate one another so that the measurement of break down pressure is not affected significantly by modest breakout shapes. In practice, of course, it would be difficult to set packers for hydraulic fracturing in holes with extensive breakouts.

Conclusions

Micromechanical models based on linear elastic fracture mechanics have been used as the mechanism of failure by extensile splitting subparallel to the circumference of a borehole near the ends of a diameter in the direction of the minimum principal stress orthogonal to the borehole axis. Utilizing failure criteria based on this model, a methodology has been developed to generate stable breakout cross sections in elastic brittle rock by means of numerical simulation. This work denied the possibility of using the breakout phenomena to determine in situ stress magnitudes because of the strong dependence of the breakout on the stress history and of the breakout depth on the initial breakout angle, which can be generated for different stress values. There is no unique relationship between the breakout size and in situ stresses. Figure 6 is a plot of breakout angle vs. breakout depth for all combinations of stress and strength for the breakouts generated in a prestressed rock (see Figure 5). Each curve corresponds to a particular stress ratio. The near-superimposition of the four curves indicates a strong dependence of breakout depth on the breakout angle.

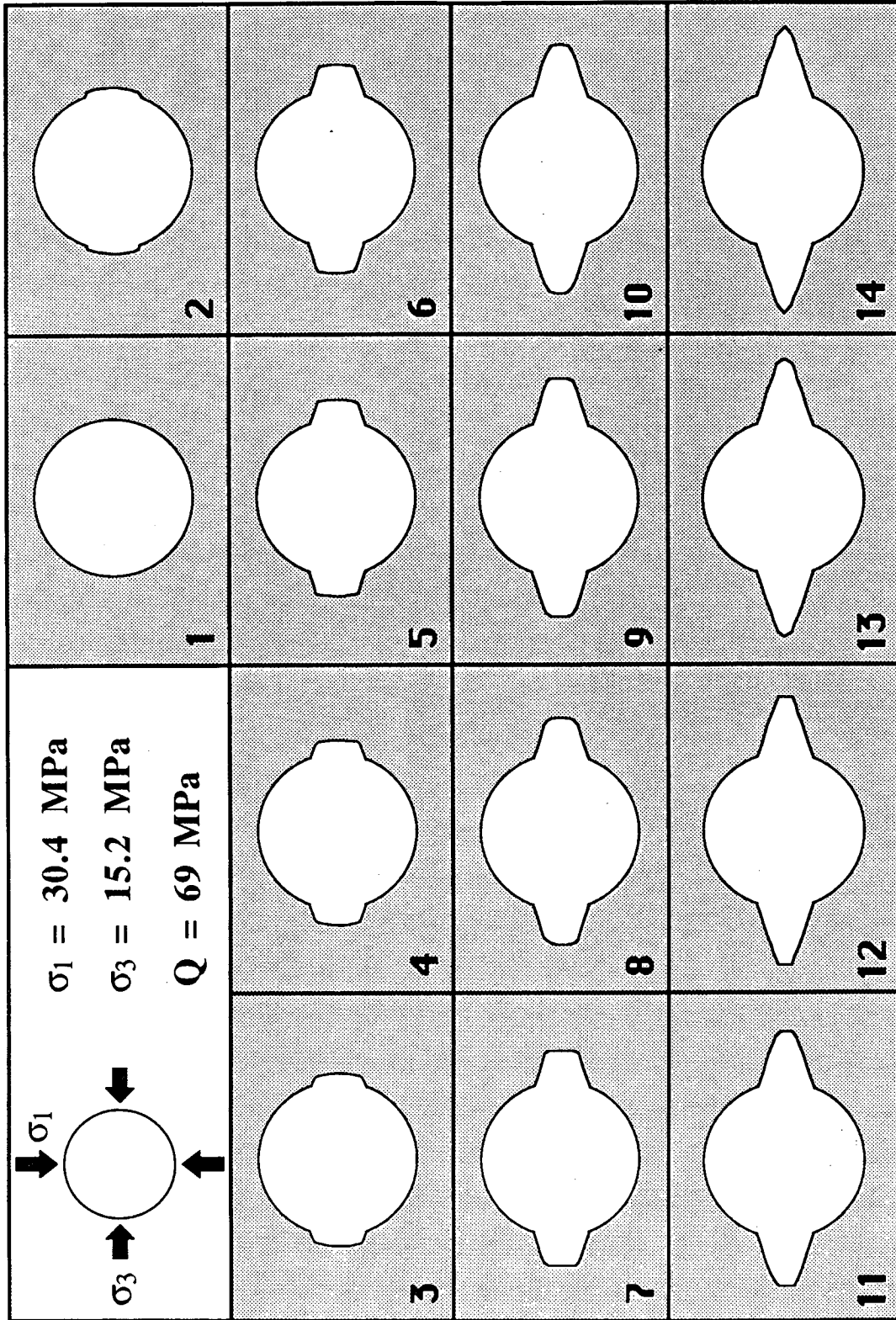
From comparisons of the theoretical "break down" pressures which should be measured in a circular borehole with those obtained from numerical results on a borehole breakout, our conclusions are: For large borehole breakouts where tensile fractures have already been generated at the locations of hydraulic fractures, obviously only the "shut in" pressure, which equals to the minimum stress orthogonal to borehole axis, can be measured. For moderate and small breakouts where no tensile fractures are generated, however, the effect of breakout on hydraulic fracturing measurements is not significant. This is because that the elongation of one diameter of borehole cross section not only reduces the boundary compressive tangential stress induced by the far field stress, but also reduces the tensile tangential stress induced by the internal pressure applied on the wall of the borehole. The two reductions in boundary stress compensate one another so that the

measurement of break down pressure is not affected significantly by modest breakout shapes. In practice, it would be difficult to set packers for hydraulic fracturing in holes with extensive breakouts anyway.

References

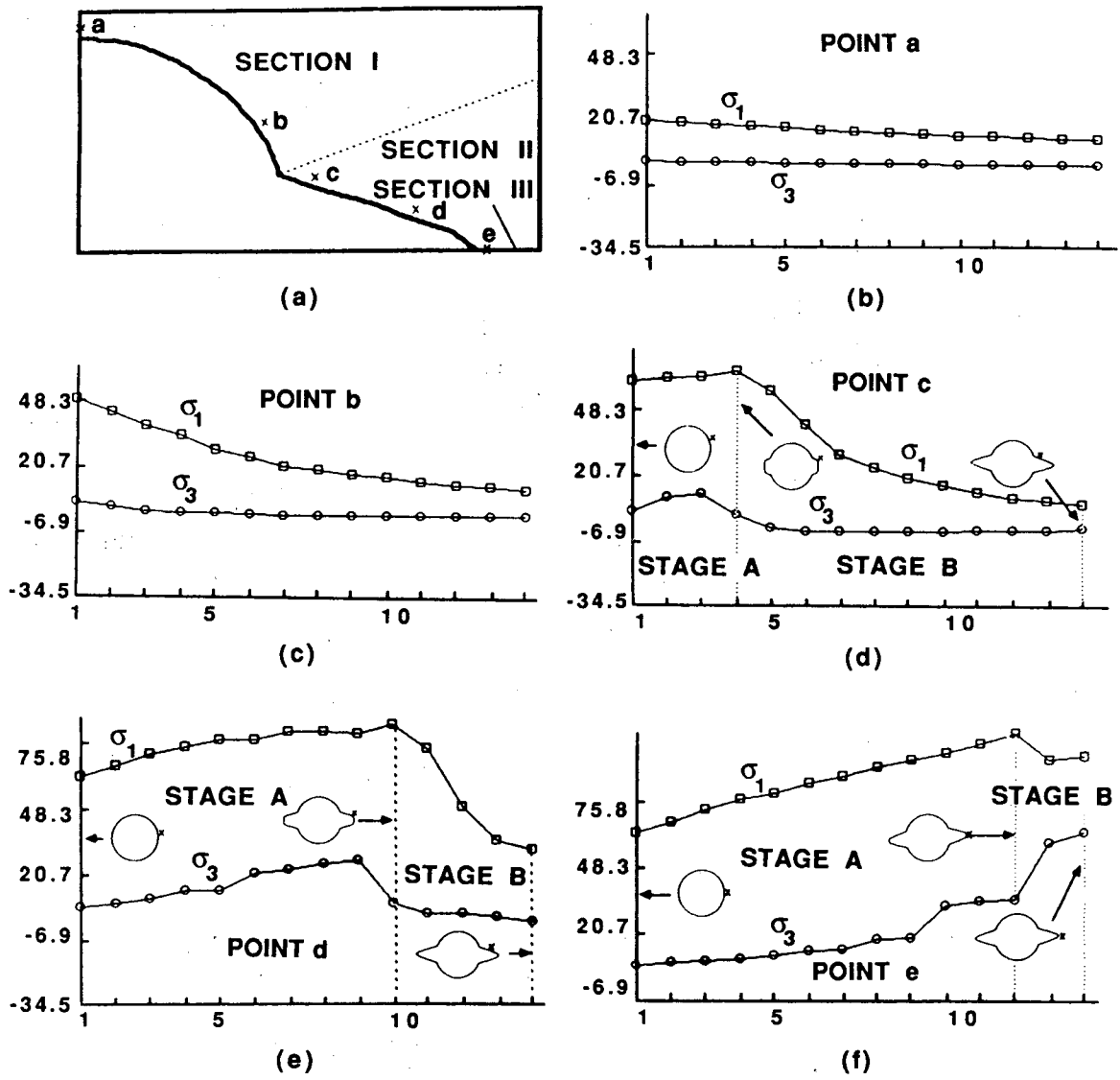
- Bell, J.S. & D.I. Gough 1979. Northeast-southwest compressive stress in Alberta: Evidence from oil wells. *Earth Planet. Sci. Lett.* 45:475-482.
- Brace, W. F. , B. W. Paulding, and C. Sholtz, Dilatancy in the fracture of crystalline rocks. *J. Geophys. Res.*, 71(16), 3939-3953, 1966.
- Cox, J.W. 1970. The high resolution dipmeter reveals dip-related borehole and deformation characteristics. 11th annual Logging Symposiums, Soc. of Prof. Well Log. Anal., Calgary, Alberta.
- Crouch, S.L. and A.M. Starfield 1983. *Boundary Element Methods in Solid Mechanics*. London, George Allen & Unwin.
- Ewy, R., Kemeny, J., Zheng, Z. & N.G.W. Cook 1987. Generation and Analysis of Stable Excavation Shapes Under High Rock Stresses. 6th Congr. I.S.R.M., Montreal, 875-882.
- Gay, N.C., Fracture growth around openings in large blocks of rock subjected to uniaxial compression, *Int. J. Rock Mech. Min. Sci.*, 13, 231-243, 1976.
- Gough, D.I. & J.S. Bell 1982. Stress orientations from borehole wall fractures with examples from Colorado, east Texas, and northern Canada. *Canadian J. Earth Sci.* 19:1358-1370.
- Haimson, B.C. & C.G. Herrick 1985. In situ stress evaluation from borehole breakouts experimental studies. 26th U.S. Symp. on Rock Mech., 1207-1218.
- Hickman, S.H., J.H. Healy & M.S. Zoback 1985. In situ stress, natural fracture distribution, and borehole elongation in the Auburn geothermal well, Auburn, New York. *J. Geophys. Res.* 90, B7:5497-5512.
- Horii, H., and S. Nemat-Nasser, Compression-induced microcrack growth in brittle solids: Axial splitting and shear failure, *J. Geophys. Res.*, 90(B4), 3105-3125, 1985.
- Jaeger, J.C. & N.G.W. Cook 1979. *Fundamentals of Rock Mechanics*. 3rd ed., Chapman and Hall, London.
- Kim, K., Dischler, S.A., Aggson, J.R. & M.P. Hardy 1986. Characterization of the state of in situ stress by hydraulic fracturing for a nuclear waste repository in Basalt. Rockwell International RHO-BW-SA-551.
- Leeman, E.R. 1960. The Measurement of the stress in the ground surrounding mining excavations. *Papers and discussions*, 1958-59:331-356.
- Mastin, L. 1984. The development of borehole breakouts in sandstone. M.S. Thesis, Stanford University, Stanford.
- Plumb, R.A. & S.H. Hickman 1985. Stress-induced borehole elongation: A comparison between the four-arm dipmeter and the borehole televiewer in the Auburn Geothermal well. *J. Geophys. Res.* 90, B7:5513-5521.
- Timoshenko, S.P. & J.N. Goodier 1970. *Theory of Elasticity*. 3rd ed., McGraw-Hill Book Company, New York.
- Wawersik, W.R., and W.F. Brace, Post-failure behavior of a granite and diabase, *Rock Mechanics*, 3, 61-85, 1971.

Wawersik, W.R., and C. Fairhurst, A study of brittle rock fracture in laboratory compression experiments, Int. J. Rock Mech. Min. Sci., 7, 561-575, 1970.
Zoback, M.D., Moos, D., Mastin, L., & R.N. Anderson 1985. Well bore breakouts and in situ stress, J. Geophys. Res., 90, B7: 5523-5530.



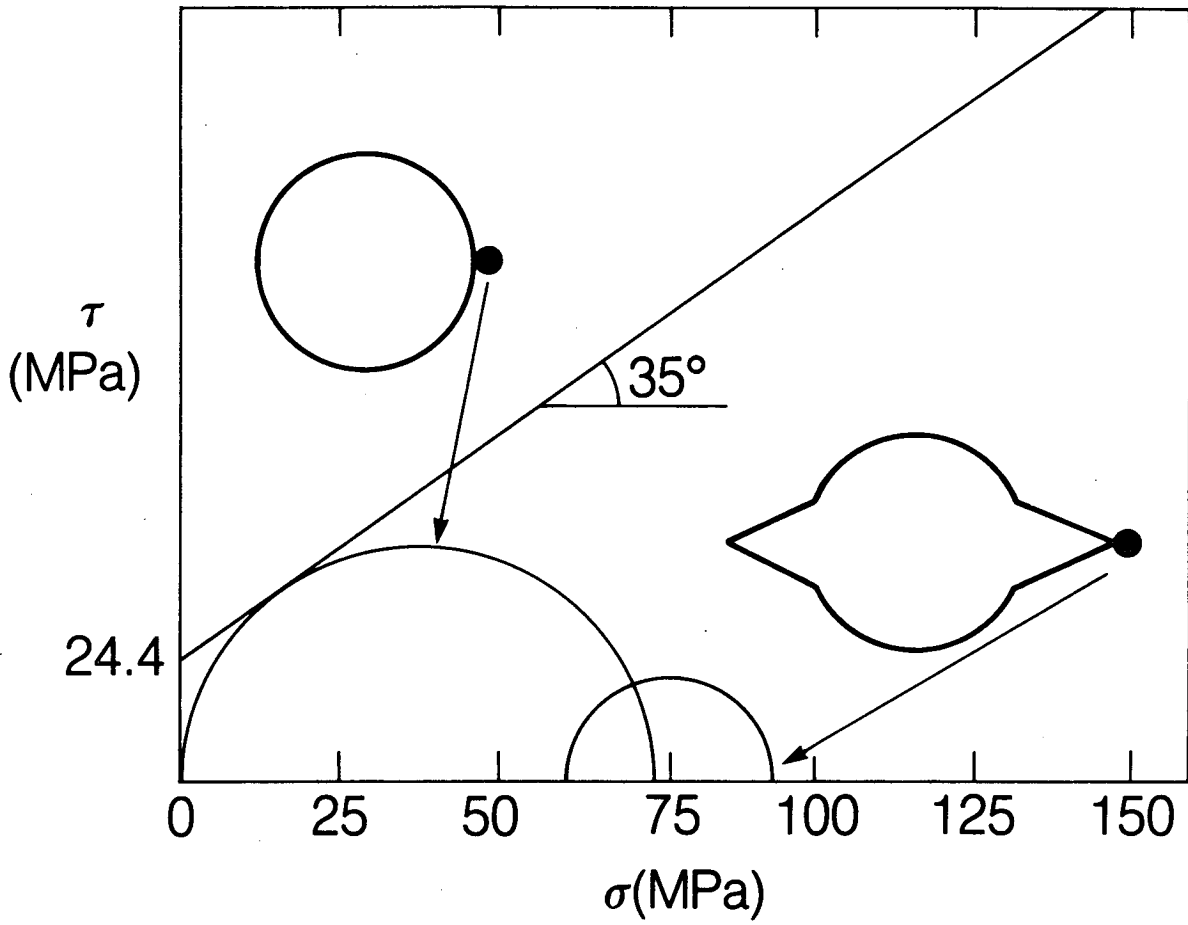
XBL 878-3536

Figure 1. Cross sections through a borehole, illustrating the steps by which a stable breakout cross section evolves. Each episode (1-14) represents an iteration of the boundary element calculation for stress redistribution.



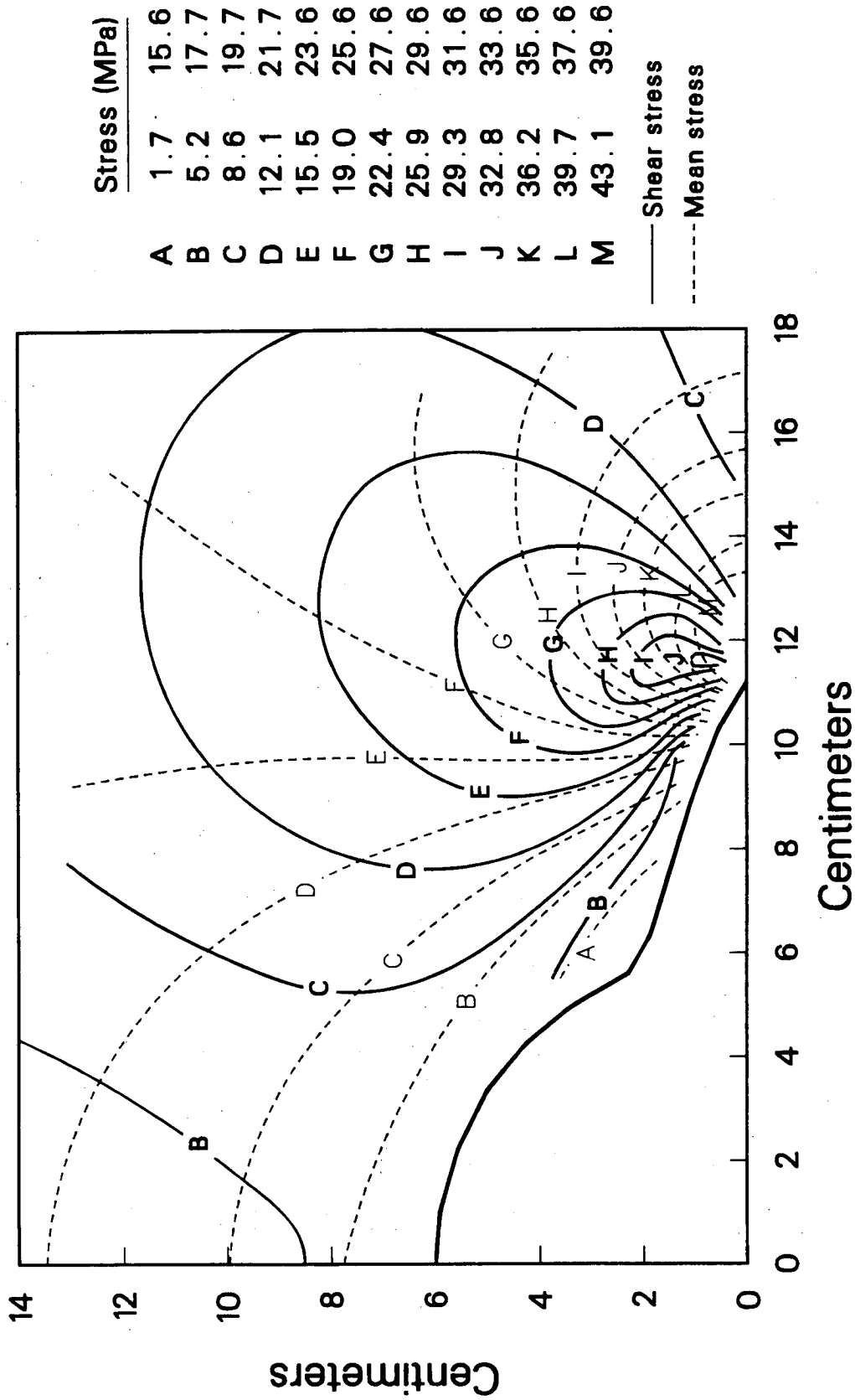
XBL 879-3953

Figure 2. Changes in the principal stresses at selected positions around a borehole as the section changes from circular to a stable breakout shape. Episode numbers are as illustrated in Figure 1.



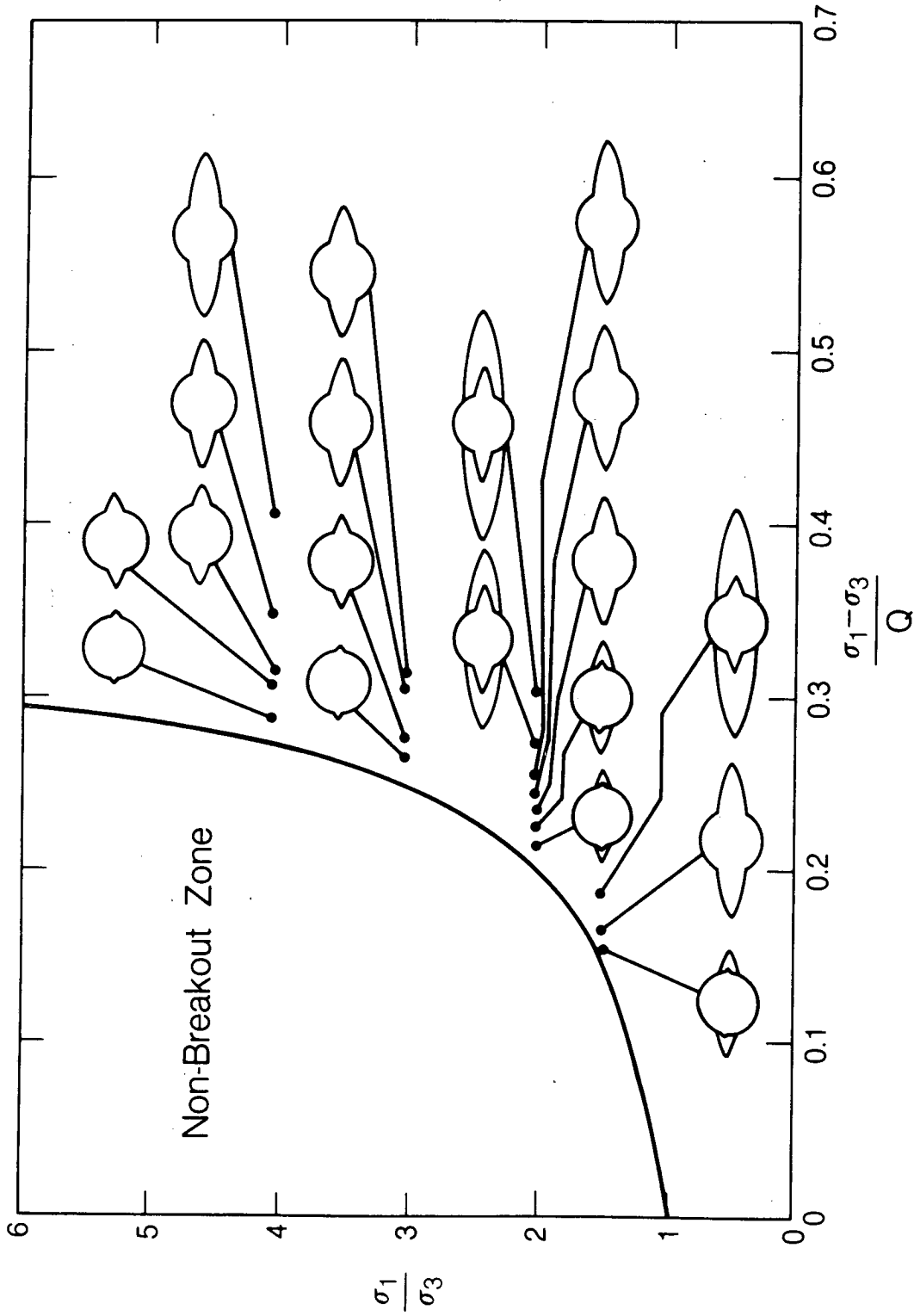
XBL 8710-11197

Figure 3. Maximum stress concentration before and after breakout compared with a Mohr-Coulomb criterion (assumed internal friction angle $\phi = 35^\circ$, and compressive strength C_0 is equal to 75 MPa).



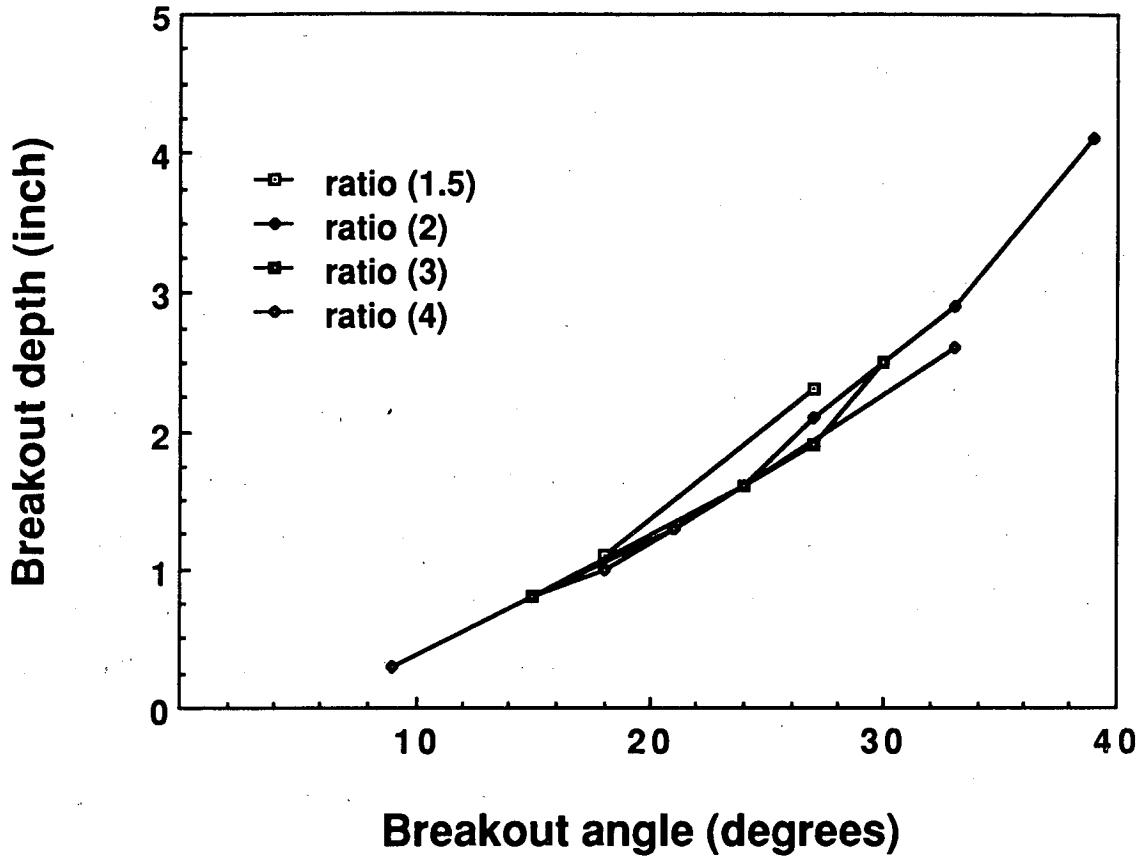
XCG 8611-12257 A

Figure 4. Contours of maximum shear stress and mean stress around the stable breakout shape shown in Figures 1 and 2.



XBL 8611-9251

Figure 5. Simulated stable breakout cross sections for different values of field stress in relation to the biaxial compressive strength. The larger breakouts are for the cases in which a hole is created instantly in rock under pre-existing stress. The smaller breakouts are for the cases in which stress is gradually increased around a pre-existing hole.



XBL 879-3954

Figure 6. Breakout angle vs. breakout depth for all combinations of stress and strength for breakouts generated in a pre-stressed rock (see Figure 5). Each curve corresponds to a particular constant stress ratio, as shown at the top left.

Deformation, Fracture and Failure Around Single Underground Openings

Russell T. Ewy, Neville G. W. Cook & Larry R. Myer

Introduction

The fracture and progressive failure of rock around underground excavations is of considerable importance to the safety and stability of mining stopes and tunnels, civil engineering structures, and underground nuclear waste repositories. Brittle fracture is the most common mode of failure observed around underground excavations, especially under high stress conditions (Maury 1987, Hoek & Brown 1980). It is also difficult to predict and control because the mechanisms are poorly understood. As a result, design of underground excavations still relies heavily on empirical methods. Stress analysis techniques are sometimes combined with laboratory measurements of rock strength and pre-failure and post-failure stress-strain behavior in an effort to predict the zones of rock subject to failure and the resulting deformations. Often the predictions do not match the observations, and the actual mechanism of failure is sometimes different than expected. It is therefore important to study the processes of fracture formation and failure progression around underground openings, and to determine what factors influence and control these processes.

Observations of the fractured zone around highly stressed excavations often reveals numerous fractures aligned parallel to the free surface and parallel to the major principal stress (Cloete et al 1975). These fractures lead to the formation of intact slabs that can detach from the surrounding rock by a buckling process (Fairhurst & Cook 1966). However, observations also indicate that the dominant detachment mechanism may be one

of shearing or 'pseudo-shearing' (Maury 1987), Both modes of fracture are observed in laboratory core tests. This does not mean that core behavior is directly applicable to the strength and failure mechanisms around underground openings, however, for the geometry and loading conditions are quite different. The rock next to an excavation is generally under polyaxial stress in a plane strain condition, but with only one free surface. It is subject to stress and strain gradients, and is loaded by adjacent rock rather than a testing machine. The stress path imposed on the rock during excavation may be quite different than in a typical laboratory test. It is important to determine what effects these differences have on the strength, deformations, and failure mechanisms of the rock, and whether failure in this situation is controlled solely by the stress state.

The most instructive laboratory experiments are therefore those performed on model openings, such as hollow cylinders. Beginning with Adams (1912) and King (1912), several researchers have subjected thick-walled hollow cylinders of rock to axisymmetric loading on the external diameter, most recently Santarelli & Brown (1987), Haimson & Edl (1972) and Daemen & Fairhurst (1971). Gay (1973) used hollow cylinders with both circular and non-circular holes. Hoskins (1969) applied both internal and external pressure, but loaded the samples to complete failure to obtain polyaxial strength data. The application of equal and unequal stresses to large rectangular blocks with pre-drilled circular holes has been investigated by Haimson & Herrick (1985), Kaiser et al (1985) and Mastin (1984). Gay (1976) performed tests on blocks with holes of large eccentricity. Recently, Bandis et al (1987) and Kaiser & Maloney (1987) have drilled circular holes into stressed blocks of artificial rock-like materials.

The aim of our current research is to carefully simulate and observe the deformation, fracture, and failure around underground openings. We are accomplishing this through experiments on thick-walled hollow cylinders of rock with the incorporation of several important features: plane strain loading, the ability to impose different stress paths on the

rock, 'freezing' of the fracture geometry under load using a metal injection technique, and the ability to remove external boundary effects.

Experimental Technique

The rock samples are cored as coaxial hollow cylinders with an inner diameter of 1 inch, an outer diameter of 3.5 inches, and a length of 5.75 to 6 inches. Both the surface of the hole and the outer diameter are lined with rubber sleeves to seal the sample, and it is assembled into a test cell (Figure 1). The sample is constrained to zero axial deformation, as would usually occur underground. In this way the effects of the plane strain loading condition and of the intermediate stress on the strength and failure process can be examined.

Uniform fluid pressure is applied to the outer diameter using a servo-controlled testing machine, and a separate pressure is applied in the hole using a manually operated screw pump capable of measuring precise volume changes. These two independent pressures allow the imposition of various stress paths on the inner surface, such as increasing tangential compression with constant (usually zero) radial pressure, or increasing tangential compression with decreasing radial compression. In this way one can explore the effect of stress path on the strength and failure process.

The apparatus has been designed to provide fluid access directly to the rock, and this is used to fill the pores and any stress-induced fractures with a liquid metal alloy at a constant pressure of about 5 MPa during the experiment. The experiment is performed at 90 degrees C, at which temperature the alloy, commonly called Woods metal, is liquid and resembles mercury. After the failure load is reached the sample is cooled while keeping the stresses constant, thus 'freezing' the stress-induced fractures in the state they exist under load. In this way one can carefully study the processes of fracture formation and

progression around the hole. Because of the scale of the sample, the resulting fractures can also provide insight into the transition from microscale fractures to macroscale fractures.

The samples can be jacketed with a precisely-fit steel ring, if desired, instead of rubber. With the thickness of the steel chosen correctly, the external pressure is effectively transferred to infinity, and the rock will not be subject to any boundary effects from the external diameter.

Observations that can be made from these tests include the elastic and inelastic deformations of the opening, stress level at which yield and rupture occur, types of fractures formed, extent of fractured zone, and stable shape achieved.

Results

Preliminary tests have been performed on Berea sandstone, chosen because it is a well-documented clastic rock, considered to be nearly isotropic. Further tests will be performed shortly on Indiana limestone and possibly other types. Three tests have been performed with Woods metal and one without, all with rubber-jacketed samples. Aluminum specimens were used for calibration.

In all experiments with Woods metal the final loads were 75 Mpa effective pressure on the external boundary and zero effective pressure in the hole. The final loads were 70 MPa external and zero internal for the experiment without Woods metal. In all cases the ultimate failure zone consisted of two diametrically opposite regions, always oriented in the same direction (Figures 2 and 3). The loading is axisymmetric, but the failure is not, as has been noted by other researchers using assumed isotropic materials (Fjaer et. al. 1987, Gay 1973, Daemen & Fairhurst 1971). The preferred failure direction is probably determined by slight anisotropy of the rock.

The failure process itself appears to be one of progressive spalling, in which intact slabs of fairly uniform thickness are successively separated from the surrounding rock by

fractures oriented roughly parallel to the free surface. The exact process of fracture growth and coalescence is not yet clear. It is interesting that brittle spalling behavior occurs in a porous clastic rock such as Berea sandstone. The discrete nature of the fractures and the preferred orientation under axisymmetric load raise doubts about the applicability of continuum theories describing the formation of a strain-softened or plastic zone.

The final stress state would cause a tangential stress of 150 to 160 Mpa on the boundary of the original hole, more than twice the uniaxial strength of this rock. This high strength of the hole wall agrees with the experimental results of Santarelli & Brown (1987), Haimson & Herrick (1985), Mastin (1984) and many others as documented by Guenot (1987). It may be due to size effect, intermediate stress, or the geometry and stress and strain gradients.

In one loading case the external pressure was increased with zero effective internal pressure, once without Woods metal and once with Woods metal. The failure in the sample without Woods metal, which was cored from a different block, encompassed a greater portion of the hole wall and extended deeper into the rock (Figure 2). Both samples exhibited triangular failure regions with distinct pointed tips.

In other cases the effective internal pressure was reduced to zero with constant external pressure, in one case slowly (Figure 3) and in another instantaneously. The deformation of the hole for the slow unloading case is shown in Figure 4. These stress paths are similar to the excavation of an underground opening. Compared to the case of increasing external pressure with Woods metal, these failure zones encompassed a greater portion of the hole wall, but were not as deep. Under microscopic observation the sample unloaded slowly revealed pointed tips in the failure zones, but the sample unloaded instantaneously did not. The failure zones of least depth resulted from the instantaneous pressure drop, possibly indicating an increase in strength with higher strain rate, as has been observed in other laboratory tests.

It thus appears that geometry, stress path, and perhaps strain rate or time do affect the strength, deformation, and failure processes of rock around underground openings. Further research should yield qualitative and quantitative information directly relevant to the design of underground openings. Additional items of importance include the effect of the axial stress magnitude, the influence of pre-existing discontinuities, and possible boundary effects due to the proximity of the outer diameter of the hollow cylinder. This latter issue will be investigated shortly by using steel jackets of appropriate stiffness to ensure that the external pressure acts exactly like a far-field stress.

References

- Adams, F.D. 1912. An experimental contribution to the question of the depth of the zone of flow in the earth's crust. *J. Geol.* 20:97-118.
- Bandis, S.C., J. Lindman & N. Barton 1987. Three-dimensional stress state and fracturing around cavities in overstressed weak rock. *Proceedings Sixth International Congress on Rock Mechanics, Montreal* 2:769-776.
- Cloete, D.R., P.A.G. Collett, N.G.W. Cook, A.J. Jager & A.J.A. White 1975. The nature of the fracture zone in gold mines as revealed by diamond core drilling. *Symposium on Strata Control & Rockburst Problems of the S.A. Goldfields. Association of Mine Managers of South Africa 1972-1973*, p. 107-122. Johannesburg: Chamber of Mines of South Africa.
- Daemen, J.J.K. & C. Fairhurst 1971. Influence of failed rock properties on tunnel stability. *Proceedings 12th U.S. Symp. Rock Mech.*, p. 855-875. New York: AIME.
- Fairhurst, C. & N.G.W. Cook 1966. The phenomenon of rock splitting parallel to a free surface under compressive stress. *Proceedings First International Congress on Rock Mechanics, Lisbon* 1:687-692.
- Fjaer, E., R.K. Bratli, J.T. Malmo, O.J. Lokberg & R.M. Holt 1987. Optical studies of cavity failure in weak sedimentary rocks. *Proceedings Sixth International Congress on Rock Mechanics, Montreal* 2:887-892.
- Gay, N.C. 1973. Fracture growth around openings in thick-walled cylinders of rock subjected to hydrostatic compression. *Int. J. Rock Mech. & Min. Sci.* 10:209-233.
- Gay, N.C. 1976. Fracture growth around openings in large blocks of rock subjected to uniaxial and biaxial compression. *Int. J. Rock Mech. & Min. Sci.* 13:231-243.
- Guenot, A. 1987. Stress and rupture conditions around oil wellbores (in French). *Proceedings Sixth International Congress on Rock Mechanics, Montreal* 1:109-118.
- Haimson, B.C. & J.N. Edl 1972. Hydraulic fracturing of deep wells. *Soc. of Petrol. Engin. Paper no. SPE4061*.
- Haimson, B.C. & C.G. Herrick 1985. In situ stress evaluation from borehole breakouts, experimental studies. *Proceedings 26th U.S. Symposium on Rock Mechanics*, p. 1207-1218. Rotterdam: Balkema.
- Hoek, E. & E.T. Brown 1980. *Underground excavations in rock*. London: Institute of Mining and Metallurgy.
- Hoskins, E.R. 1969. The failure of thick-walled cylinders of isotropic rock. *Int. J. Rock Mech. & Min. Sci.* 6:99-125.

- Kaiser, P.K., A. Guenot & N.R. Morgenstern 1985. Deformation of small tunnels - IV. Behaviour during failure. *Int. J. Rock Mech. & Min. Sci.* 22:141-152.
- Kaiser, P.K. & S. Maloney 1987. Factors influencing the stability of deep boreholes. *Proceedings Sixth International Congress on Rock Mechanics, Montreal* 1:675-680.
- King, L.V. 1912. On the limiting strength of rocks under conditions of stress existing in the earth's interior. *J. Geol.* 20:119-138.
- Mastin, L. 1984. The development of borehole breakouts in sandstone. M.S. thesis, Stanford University.
- Maury, V. 1987. Observations, researches and recent results about failure mechanisms around single galleries. *Proceedings Sixth International Congress on Rock Mechanics, Montreal* 2:1119-1128.
- Santarelli, F.J. & E.T. Brown 1987. Performance of deep wellbores in rock with a confining pressure-dependent elastic modulus. *Proceedings Sixth International Congress on Rock Mechanics, Montreal* 2:1217-1222.

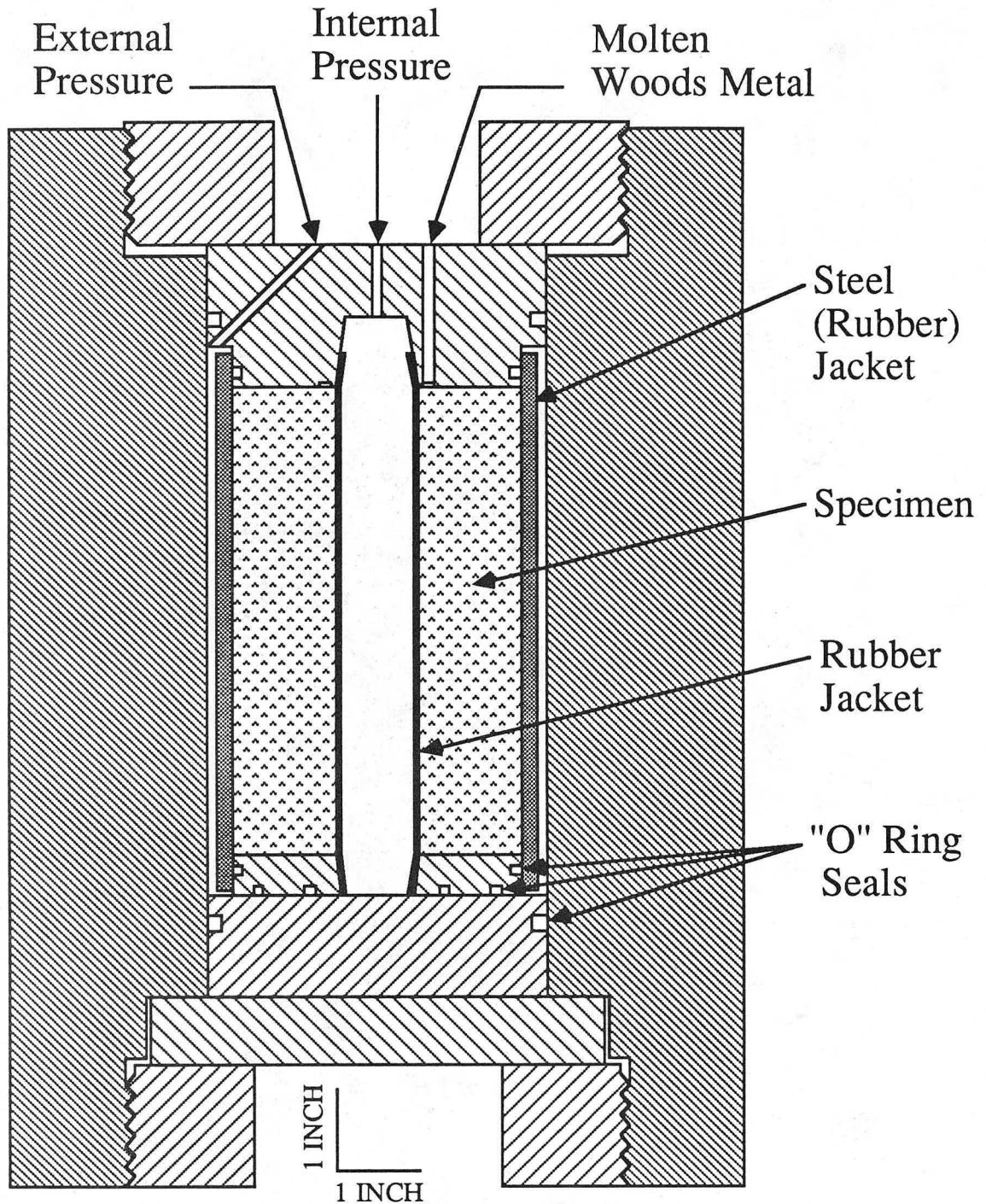
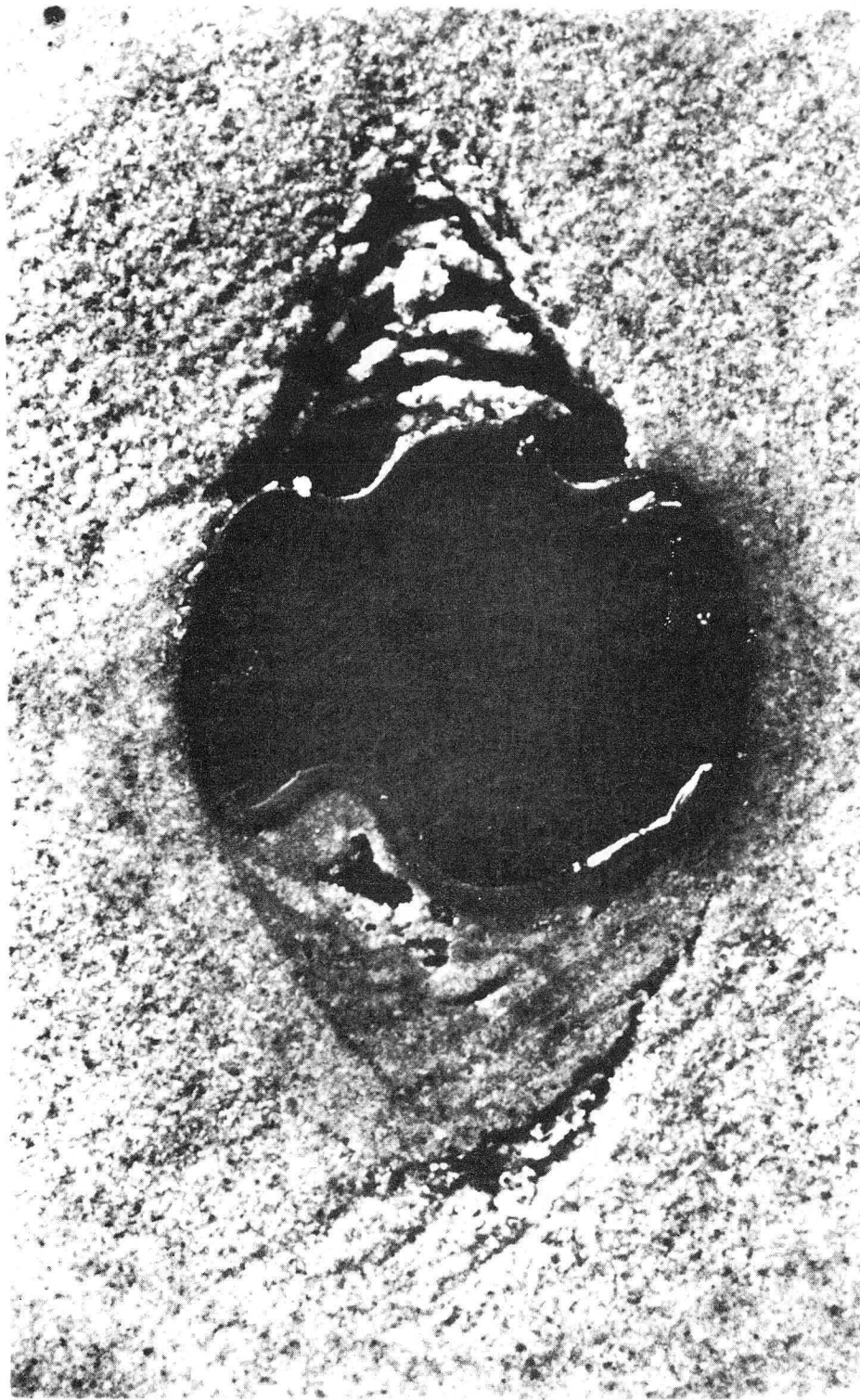
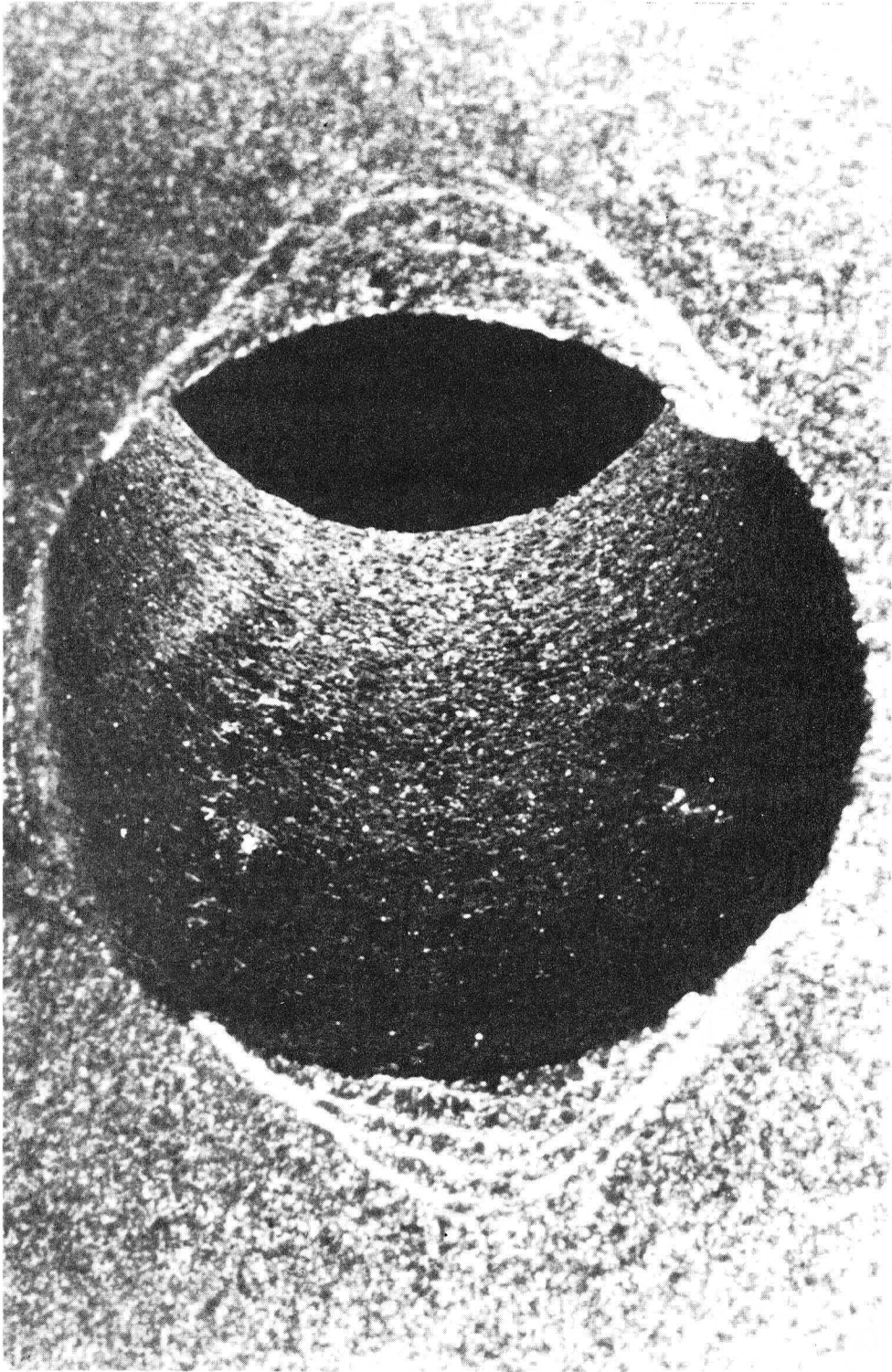


Figure 1. Simplified scale drawing of testing apparatus.



XBB 879-7834

Figure 2. Failure resulting from increasing external pressure with zero internal pressure. The hole and the left-side failure zone were filled with epoxy upon test completion.



XBB 870-9167

Figure 3. Failure resulting from slowly decreasing internal pressure with constant external pressure. Sample was saturated with Woods metal prior to failing, then cooled under load.

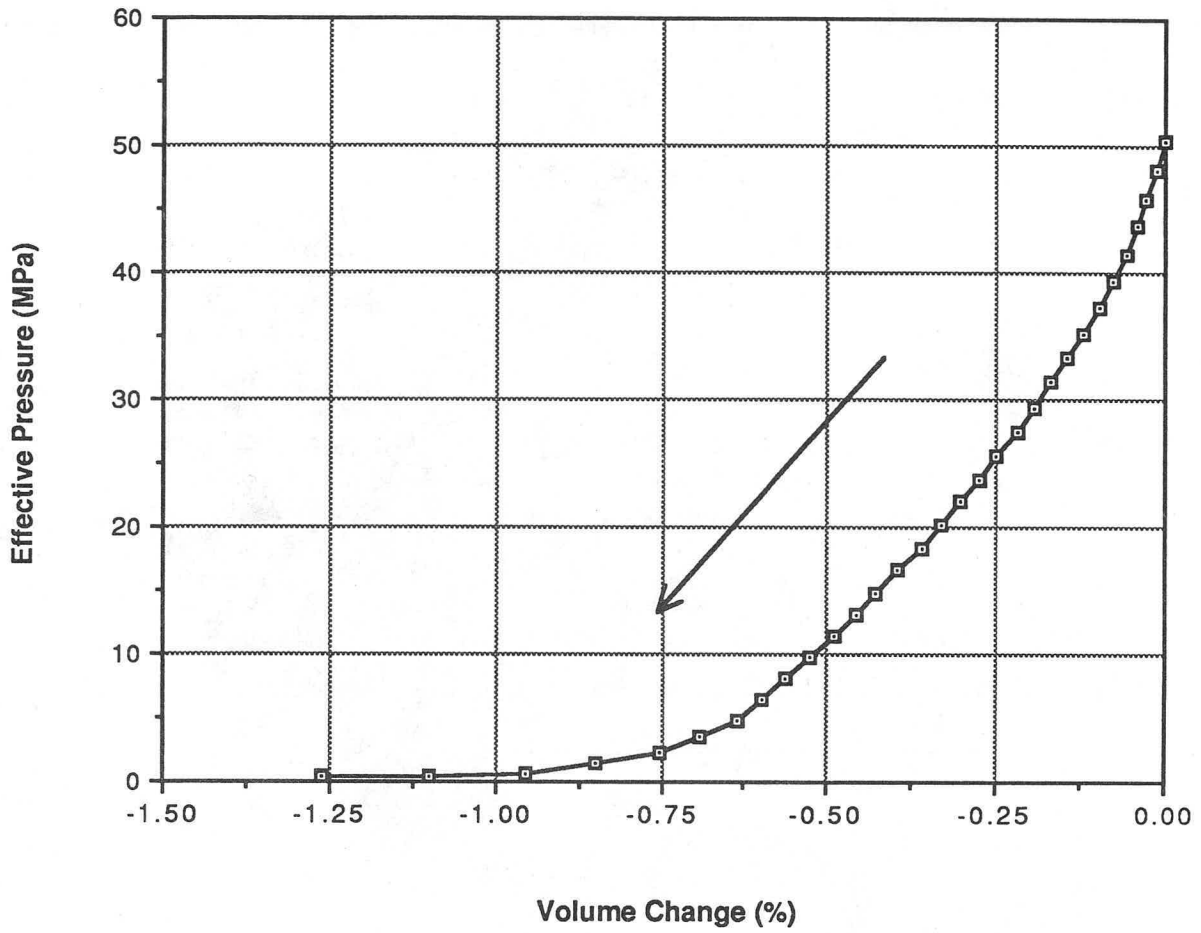


Figure 4. Volume deformation of the hole during release of internal pressure, for the sample shown in Figure 3.

Fracture Mechanics Applied to Faulting and Earthquake Rupture

John M. Kemeny and Neville G. W. Cook

There has been a growing interest in recent years in the geometry and properties of the earthquake source. In the brittle seismogenic region (less than 20 km depth), the earthquake source is often characterized by a growing, cracklike rupture, or the progressive failure of individual asperities or barriers (Das and Aki, 1977). The models usually assume that slip occurs along a planar region, which has been shown to be a fairly accurate description for shallow strike slip earthquakes (Kagan and Knopoff, 1985). One way to characterize the earthquake source is through static earthquake source parameters. These include the seismic moment, stress drop, and strain energy release associated with an unstable rupture. Relationships between these parameters were originally derived for simple source geometries by Knopoff (1958) and Keilis Borok (1959). More recently, Madariaga (1979), Rudnicki and Kanamori (1981), and Rudnicki et al. (1984) and others have looked at relationships between the source parameters for more complicated source geometries. These papers show that the seismic moment can be overestimated and the stress drop can be underestimated, due to the interaction of neighboring slip zones. All of the above results are based on the change in compliance of an elastic body due to the addition of cracks, and show a linear relationship between stress drop and moment, and also the strain energy release is proportional to the stress drop squared. These analyses do not address criteria for the starting and stopping of earthquake rupture, and implicit in these results is the fact that the far field stress is being held constant.

Also related to the earthquake source is the phenomena of slip weakening. Slip weakening describes the stress displacement relationship for a fault undergoing shear, and

in conjunction with the applied boundary conditions, slip weakening gives criteria for the starting and stopping of earthquake rupture, and aseismic slip (Kemeny and Cook, 1987). In particular, slip weakening describes a decreasing strength with increasing displacement, with instability occurring when the slope of the slip weakening curves becomes less than the unloading stiffness of the surrounding ground, and aseismic slip occurring when the opposite is true (Rice, 1983; Li, 1986). The two limits for the unloading stiffness are horizontal for stress controlled boundary conditions and nearly vertical for displacement controlled boundary conditions, with the actual stiffness for field conditions falling somewhere in between. For instance, assuming that the ground surrounding the fault responds as a Maxwell viscoelastic solid, Li and Rice (1983) derive relationships for the unloading stiffness. A method of measuring the stiffness for field conditions was proposed by Stuart (1981). Laboratory measurements of slip weakening by testing precut surfaces in shear under a constant normal stress have been conducted by Jaeger and Cook (1979), Cook (1981), Dieterich (1981), Okubo and Dieterich (1984), and others. Two important parameters with regards to slip weakening are the displacement over which slip weakening occurs, referred to as the critical slip weakening distance (also d_r by Okubo and Dieterich), and the stress drop that occurs from the start of slip weakening to the stress value at which uniform sliding occurs across the sample. Recent laboratory studies have revealed important relationships between the critical slip weakening distance, stress drop, and the roughness of the fault surface (Okubo and Dieterich, 1984), and also relationships with the applied normal stress (Wong, 1986).

Up until now a direct correlation between the static earthquake source parameters and slip weakening has not been made. Slip weakening predicts nonlinear stress displacement relationships for faulting, while the assumptions in the standard stress moment relations assume a linear stress-strain relationship. It has usually been assumed that slip weakening is a result of nonlinear processes occurring at the tips of sharp cracks, due to the singularity in the elastic solution for a sharp crack (Palmer and Rice, 1972). However, it has recently

been shown by Kemeny and Cook (1987) that slip weakening can be the result of the propagation of a cracklike rupture, or the progressive failure of asperities, without regard for the nonlinear processes at the tips of the cracks. Of course, nonlinear processes may be operating at the tips of cracks or the edges of asperities, but the consequences of this will be of lower order when larger scale changes in geometry are occurring, such as the failure of asperities. This is important, because the breaking of asperities or the rupture in a cracklike mode is also associated with the occurrence of a moment, stress drop, and energy release, as described above. Thus the moment and stress drop due to an unstable rupture occur by the same mechanism as that causing slip weakening, and this constrains relationships between the moment, stress drop, and strain energy release due to unstable rupture.

The constraints on the source parameters takes several forms. First of all, the relationship between the moment and stress drop will not be linear as usually assumed, but rather, the stress and moment will depend on each other in a nonlinear fashion, and also depend on parameters such as the fracture energy, G_c . In addition, the relationships between the source parameters will depend strongly on the boundary conditions, in particular, the unloading stiffness of the ground surrounding the fault. This makes it possible to have a large release of energy with almost no seismic moment. These constraints may help to explain some discrepancies between the source parameters, as noted by McGarr et al. (1979) and others.

Theoretical and numerical models have been developed for the mechanical behavior of a fault plane containing asperities, and these models are used to predict relationships between the static source parameters. The asperities are modelled with collinear distributions of cracks in an elastic matrix, where the asperity is the object between cracks. The stress distributions in the asperities, and the criteria for the progressive failure of the asperities, are calculated using the theory of elastic-brittle fracture mechanics (e.g., Rice, 1968). We consider very simple source geometries such as the propagation of a single crack, or the

breaking of a single asperity. These simple formulas allow insight, and the results are derived in closed form. For example, the nonlinear stress-moment relation for a source consisting of a single growing crack is given by:

$$M_0 = \frac{G_c^2 E^2}{\tau^3 \pi (1 - \nu^2) (1 + \nu)}$$

where M_0 is the seismic moment, G_c is the fracture energy, E is Young's modulus, τ is the effective shear stress, and ν is Poisson's ratio.

The results of more complicated configurations of asperities, and statistical distributions such as a fractal distribution of asperities, have also been calculated. Our models take into account the propagation of the cracks or progressive failure of the asperities, and this results in both slip weakening, along with nonlinear relationships between the source parameters. A meaningful way of presenting the results of these models is on a plot of stress drop vs. moment. The traditional relationships between the source parameters plot as a straight line on a stress moment diagram, and thus the use of these diagrams in seismology has not afforded any additional insight. However, in our analysis, the relationship between stress drop and moment is nonlinear, and in conjunction with the applied boundary conditions, the nonlinear stress moment diagram gives information on the starting and stopping of unstable rupture and regions of aseismic slip, and also the moment, stress drop, and energy release due to an unstable rupture. These stress moment diagrams are similar in many respects to the stress-displacement or stress-strain diagrams used in rock mechanics (Jaeger and Cook, 1979). An example of a nonlinear stress-moment diagram for the breaking of a single asperity is shown in Figure 1. Figure 1

shows that during an instability, the stress drop and the seismic moment are related by the linear relationship

$$\tau = k_m M_0$$

where k_m is related to the unloading stiffness of the surrounding ground. Values for the unloading stiffness of the ground surrounding the San Andreas fault have been estimated to be about 0.25 bar/mm.

References

- Cook, N.G.W., 1981, Stiff testing machines, stick slip sliding, and the stability of rock deformation, in *The Mechanical Behavior of Crustal Rocks*, Geophysical Monograph 24, by the American Geophysical Union, Washington, D. C.
- Das, S., and Aki, K., 1977, Fault plane with barriers: a versatile earthquake model: *J. Geophys. Res.*, 82, 5658-5670.
- Dieterich, J. H., 1981, Constitutive properties of faults with simulated gouge, in *The Mechanical Behavior of Crustal Rocks*, Geophysical Monograph 24, edited by N. L. Carter, M. Friedman, J. M. Logan, and D. W. Stearns, pp.103-120, AGU, Washington, D. C.
- Jaeger, J. C. and Cook, N. G. W., 1979, *Fundamentals of Rock Mechanics*, Chapman and Hall, London.
- Kagan, Y. Y., and Knopoff, L., 1985, The two point correlation function of the seismic moment tensor, *Geophys. J. R. astr. Soc.*, 83:637-656.
- Keiles Borok, V., 1959, On estimation of the displacement in an earthquake source and of source dimensions, *Ann. Geofis. (Rome)*, 12:205-214.
- Kemeny, J. M., and Cook, N.G.W., 1987, Crack models for the failure of rock in compression, To appear, *Proceedings of the Second International Conference on Constitutive Laws for Engineering Materials*, Tucson, AZ.
- Knopoff, L., 1958, Energy release in earthquakes: *Geophys. J.*, 1:44-52.
- Li, V. C., 1986, Mechanics of shear rupture applied to earthquake zones, In *Rock Fracture Mechanics*, B. Atkinson ed., Academic Press.
- Li, V. C., and Rice, J. R., 1983, Preseismic rupture progression and great earthquake instabilities at plate boundaries, *J. Geophys. Res.*, 88, 4231-4246.

- Madariaga, R., 1979, On the relation between seismic moment and stress drop in the presence of stress and strength heterogeneity: *J. Geophys. Res.*, 84, 2243-2250.
- McGarr, A., Spottiswoode, M., Gay, N. C., and Ortlepp, W. D., 1979, Observations relevant to seismic driving stress, stress drop, and efficiency, *J. Geophys. Res.*, 84, 2251-2261.
- Okubo, P. G., and Dieterich, J. H., 1984, Effects of physical fault properties on frictional instabilities produced on simulated faults: *J. Geophys. Res.*, 89, 5817-5827.
- Palmer, A. C., and Rice, J. R., 1973, The growth of slip surfaces in the progressive failure of overconsolidated clay: *Proc. R. Soc. London, Ser. A332*, 527-548.
- Rice, J. R., 1968, Mathematical analysis in the mechanics of fracture, in *Fracture: An Advanced Treatise* (H. Liebowitz ed.), 2, 191-311.
- Rice, J.R., 1983, Constitutive relations for fault slip and earthquake instabilities: *PAGEOPH.*, 121, 443-475.
- Rudnicki, J.W., Hirashima, K., and Achenbach, J.D., 1984, Amplification of moment and strain energy release due to interaction of different size fault slip zones, *J. Geophys. Res.*, 89, 5828-5834.
- Rudnicki, J.W., and Kanamori, H., 1981, Effects of fault interaction on moment, stress drop, and strain energy release: *J. Geophys. Res.*, 86, 1785-1793.
- Stuart, W.D., 1981, Stiffness method for anticipating earthquakes, *Bull. Seis. Soc. Am.*, 71, 363-370.
- Wong, T-f., 1986, On the normal stress dependence on the shear fracture energy: In *Earthquake Source Mechanics, Geophysical Monograph 37* (Maurice Ewing 6), American Geophysical Union, Washington, D.C.

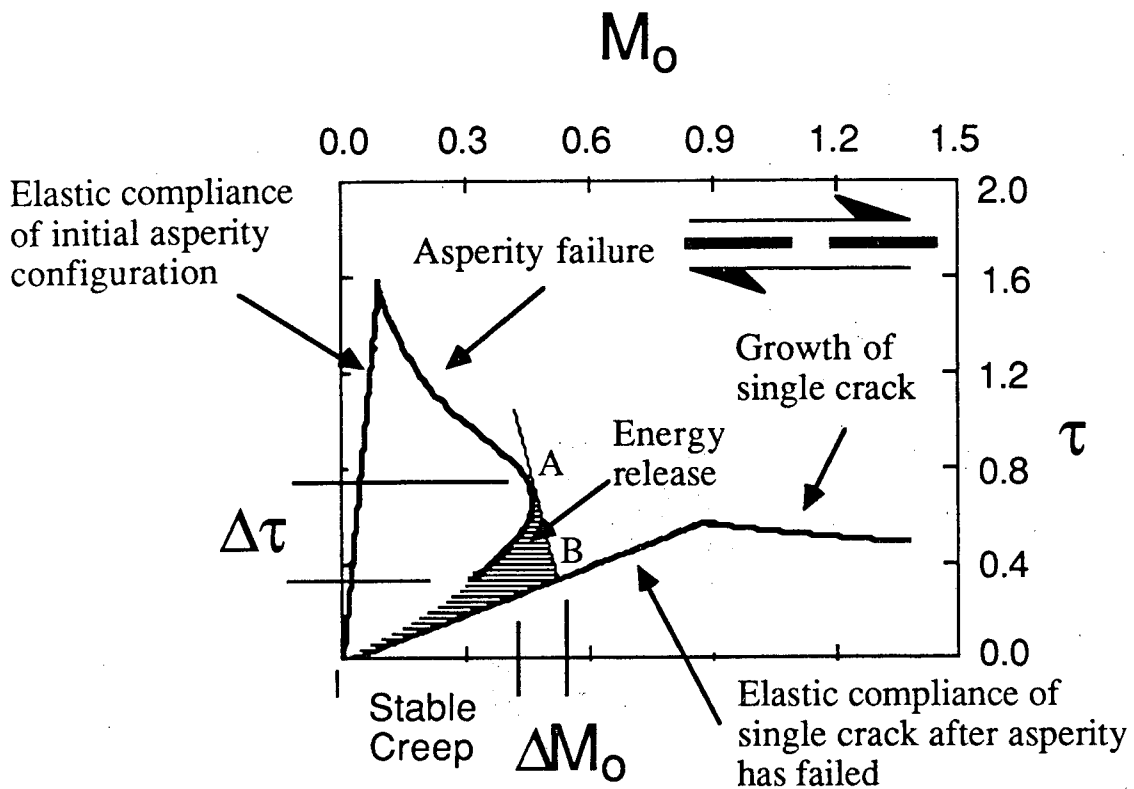


Figure 1. Normalized shear stress - seismic moment diagram for a single asperity represented by the region between two equal sized cracks. Instability occurs when the slope of the stress - moment diagram becomes less than the unloading stiffness of the surrounding ground (point A in the figure). Stability is regained in this case when the asperity completely fails and the geometry becomes that of a single crack (point B). The stress drop, change in moment, and energy release for the instability are shown.

LAWRENCE BERKELEY LABORATORY
TECHNICAL INFORMATION DEPARTMENT
UNIVERSITY OF CALIFORNIA
BERKELEY, CALIFORNIA 94720